A theoretical-experimental study of backup bearings

The pinned vs ball bearing

PhD Thesis

$$(EIv'')'' = q - \rho A\ddot{v}$$

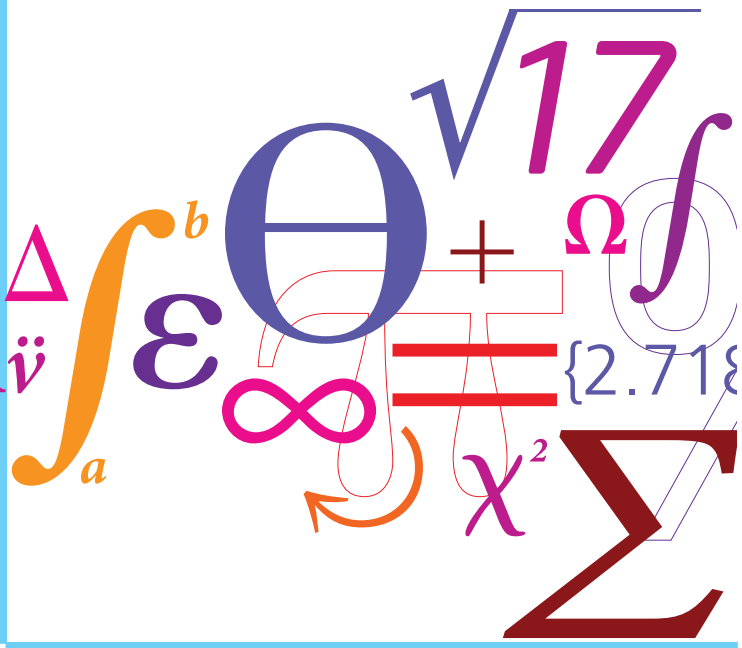

Cesar Augusto Lampe Linhares da Fonseca
DCAMM Special Report No. S228
July 2017

DTU Mechanical Engineering
Department of Mechanical Engineering

A theoretical-experimental study of backup bearings

The pinned vs ball bearing

Cesar Augusto Lampe Linhares da Fonseca

Technical University of Denmark
Kgs. Lyngby, Denmark, 2017

English title of the thesis:
A theoretical-experimental study of backup bearings
– The pinned vs ball bearing

Afhandlingens danske titel:
En teoretisk-eksperimentel undersøgelse af griberlejerne
– Pinnede og kuglelejer

PhD Student:
Cesar Augusto Lampe Linhares da Fonseca
cefonse@mek.dtu.dk
ORCID: 0000-0001-5265-037X

Supervisors:

- **Ilmar Ferreira Santos**, Main supervisor
  ifs@mek.dtu.dk
  ORCID: 0000-0002-8441-5523

  Technical University of Denmark
  Department of Mechanical Engineering
  Section of Solid Mechanics
  Nils Koppels Allé, Building 404
  DK-2800 Kgs. Lyngby
  Denmark
  Phone: +45 45 25 25 25
  Email: info@mek.dtu.dk
  www.mek.dtu.dk

- **Hans Ingo Weber**, Co-supervisor
  hans@puc-rio.br

  Pontifical Catholic University of Rio de Janeiro (PUC-Rio)
  Department of Mechanical Engineering
  Marquês de São Vicente, 225
  22430-060, Rio de Janeiro - RJ
  Brazil
  Phone: +55 (21) 3527-1167

DCAMM Special Report no.: S228
ISBN: 978-87-7475-500-5

Summary (English)

The backup bearing is a mechanical component designed to improve the safety and reliability of Active Magnetic Bearings (AMBs). Rotors levitated by AMBs can be subjected to delevitation and consequently to impacts if a power loss happens because real-time active control is necessary to keep them running. When impacting on a stator surface, the rotor can develop a dangerous behavior caused by the friction force known as the full annular backward whirl. In this situation, the rotor will describe a trajectory around the surface of the bearing at a dominant superharmonic frequency and with large radial forces. Remaining in this condition, it may lead to permanent damage or total failure of the machine. This is why the backup bearing design has to be carefully planned and investigated as to whether it helps to protect the integrity of the machine.

This PhD thesis provides a comprehensive study of two types of backup bearings, which are investigated experimentally and theoretically. The first type is a conventional ball bearing commonly used in industrial applications. The second is an unconventional bearing that, which contains pins inside the clearance for the rotor to impact on. The main objective of this work is to investigate the rotor-to-stator contact dynamics under certain conditions and to explore dynamical phenomena that emerge, so advantages and drawbacks can be stated based on a solid theoretical model validated experimentally.

The mathematical model is discontinuous since the contact forces exist only if the rotor surpasses the boundaries defined by the type of backup bearing. The compliance models proposed by Lankarani and Hunt and Crossley (H&C) are employed to represent this interaction between the rotor and the backup bearing. As a matter of comparison, plots of shaft orbits, of contact force values in time and double-sided frequency spectra are given.

The test rig consists of a horizontal rotor and is able to exchange backup bearings. Thanks to the force transducers, displacement sensors, and an encoder, one is able to characterize the lateral vibration of the rotor, the impact forces and to ascertain that the same conditions are met for each test run. The parameters of the test rig were determined accordingly, so the tests match with the mentioned theoretical analysis. The problem of crossing the resonance frequency is undertaken. In this case, the magnetic forces are weakly damped. It means that they are unable to withstand the occurrence of high orbits close to the resonance frequency. The pinned bearing is introduced and the pins are made of POM (polymer), whose contact characteristics are investigated. The different behaviors of the center of the shaft for the two types of backup bearings are analyzed. One concludes that the pinned bearing reduces the interval of impact by advancing the jump towards a safer contactless orbit while crossing the critical speed. The polymeric pins are softer than the rotor's surface, so they wear from the impacts,

saving the rotor. This is confirmed by a Finite-Element model of the contact case. For both types of bearings, the backward whirl could not be detected for the mentioned tests. Moreover, the H&C compliance model reproduced satisfactorily the changes in amplitude performed by the rotor and it is considered appropriate to represent both types of bearings for further investigation.

Also, a full failure of the control and a rotor drop on the ball bearing as backup bearing is investigated by removing the magnetic forces. The nonlinear features of the dynamics of the rotor are assessed for different levels of unbalance. It has been shown that the proposed mechanical model for the rotor drop matches with the conducted experiments, as illustrated by the bifurcation diagrams, where three distinct behaviors are observed. The double-sided spectra demonstrate that higher unbalance values cause the rotor to perform a forward whirl trajectory.

Resumé (Dansk)

Gribelejer er en mekanisk komponent designet til at forbedre sikkerheden og pålideligheden af aktive magnetiske lejer (AMB'er). Realtidsregulering er nødvendig for stabil levitation med AMB'er. Der er derfor risiko for at AMB'erne taber rotoren hvis et strømsvigt indtræder. I dette tilfælde vil rotor og stator komme i kontakt med store friktionskræfter til følge som i sidste ende vil forårsage en annulær baglænshvirvling af rotoren. I denne situation vil rotoren hvirvle langs overfladen af lejet med en dominerende superharmonisk frekvens og med store radielle kræfter. Denne tilstand kan føre til permanent skade eller total fejl i maskinen. Dette er grunden til, at gribelejedesignet skal gennemføres omhyggeligt, og det skal undersøges om designet hjælper til beskyttelse af maskinens integritet.

Denne ph.d.-afhandling giver en omfattende undersøgelse af to typer gribelejer, som undersøges eksperimentelt og teoretisk. Den første type er et konventionelt kugleleje, der almindeligvis anvendes i industrielle applikationer. Den anden er et ukonventionelt leje, som indeholder stifter i klaringen som skal ramme rotoren for at påvirke dens bane. Hovedformålet med dette arbejde er at undersøge rotor-til-stator kontaktdynamikken under visse forhold og at udforske dynamiske fænomener, der opstår, så fordele og ulemper kan fremstilles på baggrund af en velfunderet teoretisk model, der er valideret eksperimentelt.

Den matematiske model er diskontinuerlig, da kontaktkræfterne kun eksisterer, når rotor og stator er i kontakt. Her er grænsen for kontakt/ingen kontakt defineret ud fra type af gribeleje. Modellerne for en elastisk repræsentation af lejeskallen udarbejdet af Lankarani, Hunt og Crossley (H&C) er implementeret til at repræsentere interaktionen mellem rotoren og gribelejet. Den teoretiske og eksperimentelle opførsel af rotorens bane, kontaktkraftværdier i tid og dobbeltsidede frekvensspektre er præsenteret.

Teststanden består af en vandret rotor samt gribelejer der kan udskiftes. Vha. kraftmålerne, forskydningssensorerne og en encoder er man i stand til at karakterisere rotorens laterale vibration, kontaktkræfterne og man kan sikre, at de samme betingelser er opfyldt for hver testkørsel. Parametrene for teststanden er bestemt, så testene stemmer overens med den nævnte teoretiske analyse. Problemet med at krydse resonansfrekvensen er udført. I dette tilfælde er de magnetiske kræfter svagt dæmpet. Det betyder, at de ikke er i stand til at modstå forekomsten af store rotorvibrationer tæt på resonansfrekvensen. Kontaktegenskaber for gribelejet med stifter lavet af POM (polymer) er undersøgt. De forskellige opførsler af akslens centrum for de to typer gribelejer er blevet analyseret. Det kan konkluderes, at gribelejet med stifter reducerer varigheden hvor rotor og stator har kontakt ved at muliggøre at rotoren kan hoppe fra tilstanden med kontakt til den kontaktløse tilstand, mens man krydser den kritiske hastighed.

Polymerstifterne er blødere end rotorens overflade, så de slides fra stødene og skåner rotoren. Dette bekræftes af en Finite-Element model. Det var ikke muligt med nogen af gribelejerne at fremprovokere den annulære baglænse hvirveltilstand under de nævnte tests. H&C-modellen for en elastisk lejeskal var tilfredsstillende overensstemmelse med eksperimenter, og de udarbejdede modeller anses for passende repræsentationer af begge typer lejer til yderligere undersøgelser.

Ydermere undersøges situationen hvor AMB'erne sættes fuldstændig ud af drift og et rotordrop på gribelejet (i dette tilfælde kun et kugleleje) opstår. De ikke-lineære egenskaber ved rotorens dynamik vurderes for forskellige niveauer af ubalance. Det har vist sig, at den foreslåede mekaniske model for rotordroppet passer med de eksperimentelle resultater, som illustreret af bifurkationsdiagrammerne, hvor tre forskellige opførsler er observeret. De dobbeltsidede frekvensspektre viser, at større ubalanceværdier forårsager rotoren til at udføre en forlæns hvirvelbane.

Preface

This thesis is submitted as a partial fulfillment of the requirement for obtaining the Danish Ph.D. degree in the section of Solid Mechanics (FAM), Department of Mechanical Engineering (MEK) at the Technical University of Denmark (DTU). The work was partially funded by the Brazilian National Research Council (CNPq) under the international program Science Without Borders (SwF) with the process number: 249728/2013-3. The conducted research took place from the 1^{st} of August 2014 to 31^{st} of July 2017 under the supervision of Prof. Ilmar Ferreira Santos (DTU) and co-supervised by Prof. Hans Ingo Weber from the Pontifical Catholic University of Rio de Janeiro, Brazil. This work concerns a theoretical-experimental study of a rotating shaft impacting on its own backup bearing. A mechanical model is presented and simulated by a time-variant-solver program, which is validated by an existing test rig at the university.

I would like to express my wishes of gratitude to my supervisors, to whom I'll always be indebted for the trust they have put in me and to have opened the doors of my career. They are truly examples of professionalism, guidance, and mentoring. My deepest thanks specially to Geraldo Rebouças and Alejandro de Miguel for the good time spent together in Denmark. My thanks to my friends and colleagues at DTU, who helped me during my studies: Said Lahriri, Bo Nielsen, André Sekunda, Jorge Salazar, Fabian Pierart, Sebastian von Osmanski, Martin Sanders, Vladislav Sorokin, Niels Jensen, Jonas Lauridsen, Nikolaj Dagnæs-Hansen, Andreas Voigt, and Alejandro Cerda. My friends from Brazil Ian, João, and Guilherme for their companionship. Not forgotten are my thanks to the undergraduate student Svend Andersen, who worked with me in the laboratory. This project could not have been completed without the assistance and the valuable insights from the technical support at DTU of Klaus, Per, and Benny.

My most beloved wishes go to my parents and relatives and, especially, to my finacée, Ana Luisa, who believed in my dream to fulfill my doctorate abroad. Yet, despite the distance, their love, patience, endurance, and support meant everything for me to be here in those long years. I also dedicate this work to you.

To my beloved grandparents

Contents

Chapter 1

Introduction

1.1 Motivation

Among mechanical machines, it is almost impossible to imagine a mechanism without a rotating element inside. It has been an important tool capable of storing or converting energy as simple as the wheels of a car, gears, turbines and the big cranks of diesel engines on ships. Although being always present in the history of civilization, scientific studies regarding rotors only appeared in the late 19^{th} century from the works of scientists and engineers such as DeLaval, Jeffcott, and Föppl. Since then it has been a prolific topic of research in mechanical engineering, known as rotordynamics.

In the 21^{st} century, one of the most cutting edge technologies in this field are the levitated rotors by active magnetic bearings (AMBs) in use in turbines, pumps, and compressors. These rotors work in a vacuum or ambient pressure environment and rely on an active control to change the magnetic field of the AMB in order to maintain the rotor within a reasonable distance from the structure inside the clearance. The dynamics of the rotor is quite predictable and stable if one solves the governing equations of motion and the rotor stays in the vicinity of the equilibrium point. If the rotating machine is affected by an unaccounted phenomenon that generates high orbits, it can make the behavior of the rotor unstable. In the case of an AMB, the main concern is the consequences of the impact when the rotor overcomes the clearance and hits the wall.

During the impact, normal contact forces and friction forces appear, thus leading the rotor into dry-whip trajectories or rolling on the surface of the stator in a full annular backward whirl behavior. These effects are considered highly nonlinear and can eventually cause permanent damage and a sudden stop to the machine. Usually, a full annular whirl is rare, due to the control and its robustness, which create an overdamped response. But a complete power failure while running, even for a brief time, is plausible. Certainly, it will make the rotor fall and hit the structure. Therefore, an additional mechanical element called a "backup bearing"[1] is employed, which leaves a gap between the rotor's shaft, but small enough to be hit first instead. Also, it has to be designed to withstand impacts and to protect the structure.

Understanding the interaction between the rotor and the backup bearing is relevant in order to improve the reliability of magnetic bearing rotors and to help grow the

[1] This nomenclature varies among authors: "catcher bearing", "safety bearing", ' 'auxiliary bearing" and "retainer bearing" are also found in published papers.

number of machines using this kind of technology in the industry. The present thesis aims to approach this with a theoretical and experimental investigation of a test rig assembled specifically for this purpose at the Technical University of Denmark. Two kinds of bearings, an ordinary ball bearing and a pinned one, will be presented and their performance under different scenarios will be assessed. Results concerning unbalance response, orbit patterns, comparison of the magnitudes of the forces and the efficiency to cross the resonance frequency are given and commented on.

1.2 Literature review

As mentioned at the beginning of this section, there is an extensive collection of books and research papers about rotordynamics available in the literature. Among the book authors in this field, the most important ones are [1], [2], [3] and [4]. Also, most of the rub-related works are addressed by Muszynska in her literature survey in [5]. She mentions that backward whirl is the most important problem related to the friction.

On the rotor-to-stator contact

One of the first to deal with the clearance problem in rotors was Johnson [6], in 1962. When he published his work he mentioned that there was some suspicion that a clearance was affecting the overall behavior of the rotor. He introduced two models: a non-damped and a damped model of a rotor; both without friction force, though. Later Billet [7] showed, that close to the resonance, friction induces the rotor to perform a backward whirl. Ehrich and O'Connor [8] published in 1967 a study where they classified the types of vibration depending on the relationship between the stiffnesses of rotor and bearing. In 1968, Black [9] built upon Johnson's work and became one of the most cited references in the field. He added friction to the model and presented the limits for the whirl and whip to happen. His work was later confirmed experimentally by Lingener [10] and Crandall [11], who reported to have found stable coupled eigenfrequencies of the system, but slightly lower.

Beatty [12] compared experimental data on a controlled rubbing test with analytical prediction. The response was calculated in terms of a Fourier series expansion and theoretical-experimental investigation using Fourier expansion terms. One of the conclusions was that the monitoring of only the synchronous vibration is misleading, due to the instabilities created by the full annular rub. In his doctoral thesis, Szcygielski [13] investigated the dynamics of a high-speed rotor touching a rigid boundary. The contact was modeled with a piecewise-linear but strongly nonlinear globally. A high sensitivity to initial conditions was detected dependent on the control parameter. Furthermore, he established the relationship of the motion developing into chaos. The analysis of the transient of the rub interaction was undertaken by Choy and Padovan [14]. They developed a numerical simulation of the rotor-stator rub and showed the variation of the magnitude of the rub forces in time and depending on the imbalance and on the friction coefficient. Zhang [15] presented some analytical results the using perturbation method and verified them experimentally. The contact on the seals problem has also been conducted by Pennachi et al. [16], in which the authors identify the contact dynamics on a test rig and which were reproduced by a finite-element model.

Nonlinear analysis

In parallel to the advances in rub-related phenomena, major advances occurred in the second half of the 20^{th} century regarding techniques for analyzing nonlinear dynamical systems, which became popular worldwide. These techniques can be found in many applied cases. Strogatz's book on chaos [17] covers these nonlinear analyzing tools and presents them using a variety of practical examples in different scientific areas and in nature. It would not be different in rotordynamics. In his paper, Erich [18] showed the appearance of chaotic behavior on a simple rotor model with bilinear spring models. Chaos in rotordynamics was also reported by Goldman and Muszynska [19, 20]. In his PhD. thesis, Isaksson [21] showed several simulated cases of rotor-to-stator contact multivalue solutions and hysteresis jumps. Also, stable solutions existed even for an offset stator and full annular rub contact. Experimental tests were conducted by Piccoli and Weber [22] in 1998, detecting the chaotic motion of a rubbing rotor. The authors concluded that the possibility of a chaotic motion was determined by the observation of Poincaré diagrams and the computation of the Lyapunov exponents. Pavloskaia et al. [23] in 2004 (later confirmed by Karpenko [24] in 2006) demonstrated that preloading changed significantly the bifurcation structure for a two-degree-of-freedom model of the Jeffcott rotor with the preloaded snubber ring and unbalance. In industrial applications rubbing-related problems are in fact rare but, according to Rosenblum [25], damage to a damp turbine has been mentioned to be caused by rubbing. Popprath and Ecker [26] conducted a nonlinear dynamics study of an intermittent-impact rotor. The authors investigated the effect of the visco-elastically suspended stator on the rotor motion and they show that by decreasing damping, periodic solutions with few contacts become less likely and non-periodic behavior of the system dominates. Likewise, a theoretical-experimental work from Chavéz et al. [27] analyzed the onset of impacts between the rotor and the ring for different speeds and validated the proposed model.

Bachshmid [28] presented an useful method for the industry to determine the occurrence of rubbing. Thus he applied his technique to a balanced 320 MW turbogenerator with an identical one, but the latter was showing rub compared with the former. Later he added thermal effects to the theoretical model caused by the rubbing forces in [29] and in [30]. It was validated by experimental results with a 50 MW generator. For a rotor rubbing on non-moving parts van Barten [31] presented in his PhD thesis several impact force models and simulated them for different parameters and compared the results, stating the advantages and disadvantages of each one. In order to have an adequate fast simulation program, the impact was modeled as purely elastic, whose damping contribution was considered as resisting torque on the shaft.

Whip and whirl motion

Bartha's works in [32] and [33] diverged with respect to the findings from Black [9], Lingener [10] and Crandall [11]. The mechanical model used by Bartha was expanded so that the bearing was modelled as a ring capable of moving in the horizontal and vertical directions. He used Floquet multipliers to determine the stability of the system as a whole instead of through static force equilibrium. This seems to be in accordance with the work of Yu et al. [34], in which the onset of dry friction whirl was pointed out to be generated spontaneously outside the region mentioned by Black. Jiang and Ulbrich [35] conducted experiments to explain the onset of dry whips in rotor-stator systems

and discovered that negative (natural) frequencies were the physical reason for it. Using the multiple scale method, the analytical onset condition had good agreement with the numerically simulated one. Yet the forward and backward whirl nonlinear normal modes were investigated by Chen and Jiang [36] with respect to the stability depending on the friction and the cross-coupled stiffness. They show the importance of them to avoid the appearance of stable backward whirl motions. Since friction force is one of the major issues in rotordynamics, one can deal with it via high-frequency analysis to create a smoother function. The work of Thomsen [37] describes how high-frequency excitation effectively turns dry friction into a viscous-like form of damping.

Following the statements of Bartha and Yu et al., Childs and Hattacharya [38] found that accurate whirl-range predictions required an adequate rotor-stator model and predicted multiple whirl regions, but only the first whirl region and its whipping frequency could be reproduced in simulations. Wilkes et al. [39] resumed the investigation of Childs and Hattacharya with experimental and numerical methods of the nature of dry-friction whip and whirl for a variety of materials and clearances. They reported that the whip/whirl regions changed depending on whether the angular velocity was being increased or decreased. In 2011, Inoue et al. [40] showed that the forward rub could be curbed by a directional difference in the support stiffness of the guide or the backup bearing. Their findings were demonstrated theoretically and experimentally that at 600 rpm the forward rub was avoided when the velocity was increased up to 750 rpm. Yu [41] discussed the reverse full annular rub based on a two degrees-of-freedom rotor/seal model in which rubbing occurred. The analytical model together with the experimental setup proposed by the author embraced a variety of whirl/whip motions. The case of a rotor impacting on two points has been addressed by Wilkes and Allison [42]. The authors compared the experimental results with a general model presented in the same paper of a multi-contact dry-friction whip and whirl.

More recently in 2012 Cole and Wongratanaphisan [43] extended the current theory by considering systems for which the rotor–stator contact interaction may occur in multiple transverse planes. They found a good correlation between their theoretical predictions on the whirl modes for a flexible rotor. Subsynchronous whirl induced by friction was investigated by Cole and Hawkins in [44] and [45]. Their case study was undertaken for a 140 kW energy storage flywheel. Model-based predictions were compared with measured data from spindown tests and showed a good level of agreement. The study confirmed the role of friction related forces in driving forward-whirl response behaviors.

Magnetic levitated rotors

The research on rotors with a clearance had not attracted much attention from the industry and remained as an interesting academic topic until the appearance of magnetically levitated rotors, especially those with active magnetic bearings. They rely on the power supply and on the active control techniques to handle the rotor with relatively small orbits. The book of Schweitzer and Maslen [46] is a major reference regarding magnetic bearings. Schweitzer [47] and Ulbrich et al. [48] presented the first theories to approach a rotor suspended by magnets and applications. Also, the advantages of low damping proved that the importance of backup bearings is to restrain high orbits from becoming even greater.

There are essentially two types of backup bearings: axial and radial. Both have to

be designed to hold the rotor in the case of a full power failure and to protect the rest of the machine and everything around. Therefore most of the published works are related to rotor drop and the subsequential interaction with the backup bearings. One of the most cited works is Pradetto and Schmied [49] from 1992 when a one-ton compressor was allowed to fall onto its auxiliary bearings. Followed by Bently [50], he expressed concerns over the reliability of auxiliary bearings in the design of an AMB system due to its finite load capacity. Later, in 1996, Ishii and Kirk [51] studied the transient response of a flexible-rotor drop test theoretically. The simulation began from the time prior to the AMB shutdown and resumed with the rotor drop onto the backup bearing. The fowolling year, Fumagalli [52] presented his PhD thesis, in which he analyzed several rotor drops and investigated impact models such as the ones proposed by Hertz [53] and Hunt and Crossley [54]. The impact parameters were estimated by the signal data of acceleration. Later in 1999, Kirk [55] reviewed the analytical techniques to predict the rotor transient response. Results of transient response evaluation of a full-size compressor rotor were presented to illustrate some of the important parameters in the design for rotor drop. AMBs have also been applied in the diagnosis of turbomachinery by Aenis et al. [56].

Keogh and Cole [57] developed numerical models of a two-dimensional and flexible rotor interacting with a bushing-type auxiliary bearing, where the rotor started with different initial conditions. The manner in which the rotor progressed through these contact modes depends on the initial conditions of the first contact. It also changed the possibility of recovering control of a rotor in a contact mode and is demonstrated in Part 2 of the paper in reference [58]. Hawkins [59] tested the backup system for an expander/generator completing full drops up to 30,000 rpm. Position orbit data and time–history data were presented from one of the full speed drops and a nonlinear simulation analysis helped to interpret the results and to estimate the loads received by the backup bearings. Thermal effects caused by the contact that affect the dynamics were approached by Zhao [60] and published more recently in 2016. Other relevant drop tests were published by Kärkkäinen et al. [61] and later by Halminen et al. [62]. A literature review of rotor-to-stator is offered by Richardet et al. [63].

Backup bearing designs

Different strategies have emerged in the last twenty years to try to bring back the control of the rotor after it started contacting with the backup bearing. After the rotor performs a full backward whirl behavior, the standard procedure would be to shutdown the machine in order to regain a contact free orbit. It has to be done because the rotor stays in a dangerous stable trajectory too difficult to remove. This behavior would be called in nonlinear dynamics a strong attractor. The backup bearing of a flywheel levitated by an AMB was tested by McMullen et al. [64] and the authors showed the damage the inner ring suffered.

Since a round bushing bearing favors the appearance of the backward whirl, Simon [65], in his PhD thesis, proposed that the inner geometry of the backup bearing had a polygonal form. The idea was evaluated theoretically and experimentally for many shapes and the rotor did not develop the backward whirl for the triangle one. Although its trajectory assumed a contacting quasi-periodic motion. Ginzinger et al. [66] presented an active auxiliary bearing with linear actuators, which showed a significant reduction of the contact forces. They used a three-phase control strategy, which

stabilized the rotor system in the case of an impact load. As the load ceases, the auxiliary bearing separates from the rotor again and the normal operation mode resumes. Then Zülow and Liebich [67] designed a flexible pin with a roller on the tip, it was patented later [68]. The roller's purpose was meant to reduce the friction forces during contact. In this way more degrees of freedom were added to the mechanical system. Additionally, in the purely theoretical work of Keogh [69], the author also outlined and discussed the benefits of making the auxiliary bearing as an active element similar to a conventional backup bearing. A ball bearing with an irregular surface of the inner ring was theoretically investigated by Halminen et al. [70] by introducing a waviness function to it. They observed the influence of the frictional losses for different waviness functions and the results were compared with values given in the literature.

Lahriri et al. [71] presented the idea of an unconventional backup bearing: pins were screwed inside the clearance of the backup bearing of a vertical rotor. These authors tested whether the pins helped to maintain the spin of the rotor despite being in a contact orbit. Later, Lahriri and Santos conducted several tests regarding the onset of the backward whirl on a sleeve backup bearing and the friction properties and the magnitude of the contact force between the shaft and the backup bearing. Their findings were published in [72, 73, 74]. In the same test rig assembled vertically by Lahriri et al. [71], Fonseca et al. [75] turned the pins active, thus, whenever the rotor achieved a backward whirl orbit or was spinning close to the known resonance the pins screwed themselves inside. Doing so, the rotor was able to surpass its critical speeds at any speed rate, which otherwise it could not. Also Fonseca et al. [76] presented a nonlinear study of the different shapes of orbits that emerge from the interaction between the rotor and the pins as a function of the applied driven torque.

1.3 Outline and originality of the work

The main objective of this thesis is to develop a consistent theoretical-experimental analysis of a horizontal rotor, which will eventually impact the radial backup bearing. Figure 1.1 presents the actual test rig completely mounted at the facilities of the Technical University of Denmark. The project design of this test rig is available in Petersen [77].

The two types of backup bearings are shown in Figure 1.2. The use of each of them constitutes the scope of the present research. The Ph.D. thesis at DTU can be presented either by a thoroughly documented thesis or by a compendium of the articles developed by the Ph.D. student through his studies. The present work follows the latter.

Thus, the work is divided into three articles, which are presented in chapter 2 [P1], chapter 3 [P2], and chapter 4 [P3]. These articles have been respectively published, accepted for publication and submitted for review. They are followed by a conference paper included in appendix C1 after a comprehensive chapter of conclusions and bibliography.

- The main contribution of the first paper [P1], is to show the influence of unbalance into the orbits pattern. The ball bearing is chosen as the suitable backup bearing. The unbalance was increased up to extreme levels, in order to observe the nonlinear nature of its influence and to detect any appearance of a backward whirl. It is analyzed both theoretically and experimentally. Here the rotor does not levitate, as the magnetic bearing has been removed. So it is in contact with

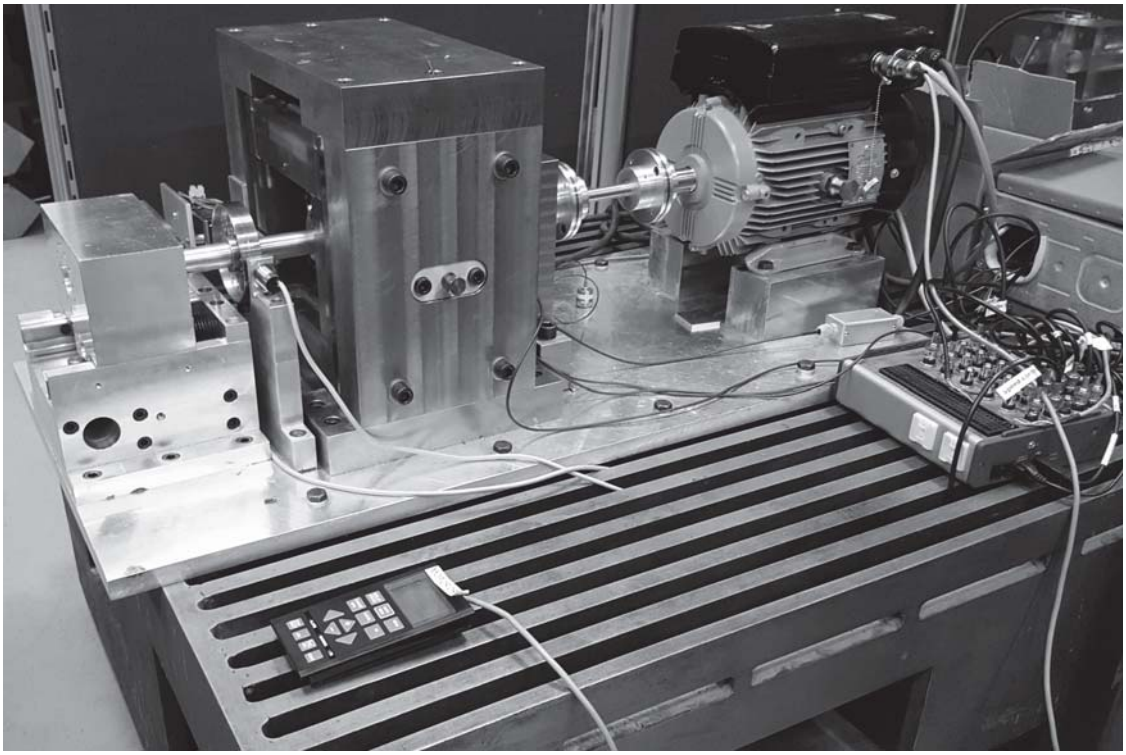

Figure 1.1: The rotor and assembled test rig components.

the surface of the inner ring of the backup bearing. As the unbalance increases, the rotor gains enough kinetic energy to detach from the contact state but falls again immediately after and repeats the process. This cycle creates nonlinear orbit patterns and causes high valued forces at every return of the bearing's inner surface. Higher unbalances completely change the overall behavior of the rotor, as the rotor permanently stays in contact. However, it performs a forward whirl, so one concludes that the rotor is always sliding in this situation on the surface of the inner ring of the bearing. The changes in the orbit pattern are seen in Poincaré maps, where the points are collected every time the rotor crosses the vertical axis positioned at the center backup bearing and the different behaviors are shown in separated regions. The results of this theoretical/experiment work were presented at the conference ISMB15 in Kitakyushu, Japan, which is annexed in C1.

- In [P2], the work takes a different approach. It is completely experimental and starts analyzing how the different bearings affect the rotor. This time the magnetic bearing is present and supports the weight of the rotor, so it levitates. Initially, there is no interaction with the backup bearing and the shaft. Nevertheless, the rotor is driven from a stand-still state to 20 Hz incrementally. As a consequence, it crosses its own natural resonance frequency around 10 Hz. The magnetic forces are weakly damped. It means that they are unable to withstand the occurrence of high orbits close to the resonance frequency. Also, the pinned bearing will be compared with the conventional ball bearing. Its material was defined as polymer known as POM and the friction properties of the interaction with the aluminum shaft were checked on a pin-on-disk test rig. The orbits are plotted

Figure 1.2: The ball and pinned bearings used for experimental test rig as the backup bearings.

and double-sided spectra charts track the governing frequencies of the dynamics and of any appearance of a backward whirl. Besides, the data of the impact force magnitudes are collected to give an overview of the performance between the two types of backup bearings. It is concluded in this article that the pinned bearing had shown a better response to the crossing of the resonance frequency because it removed from the impacting orbits earlier than the ball bearing as a backup bearing. A scenario, in which an unbalanced rotor is tested proved to be catastrophic because the rotor could not remove itself from the contact state till twice the speed of the known resonance speed.

- The main original contribution of the third paper [P3] is the proposal and validation of a theoretical model for the rotor and the backup bearing, which it is used together with an appropriate contact model, developed by Hunt and Crossley [54]. The theoretical model is based on the one studied by Lahriri et al. [74], but the ball bearing and the new type of pinned bearing were included for the present study. In order to do so, all conducted experimental results are necessary to provide a sound model to extract the parameters of the test rig and represent its dynamics. In the first place, the natural frequency and the damping coefficients of the test rig are defined, then experimental drop tests allied to the Hertzian hypothesis of contact provide acceptable interval values for the elastic coefficient of impact and the restitution coefficients. Finally, with all the values determined, the model is integrated in time with zero the initial conditions, so that it generates the same performance as shown by the experimental tests published in [P2]. All of this is done for the ball bearing as well as for the pinned bearing. The benefits and the disadvantages of each are interpreted from the overall results and given in the conclusion.

Chapter 2

Influence of unbalance levels on nonlinear dynamics of a rotor-backup rolling bearing system

Paper published in the Journal of Sound and Vibration and available online since 1st of February 2017. DOI: http://dx.doi.org/10.1016/j.jsv.2017.01.020

Journal of Sound and Vibration 394 (2017) 482–496

Contents lists available at ScienceDirect

Journal of Sound and Vibration

journal homepage: www.elsevier.com/locate/jsvi

Influence of unbalance levels on nonlinear dynamics of a rotor-backup rolling bearing system

Cesar A. Fonseca [a,*], Ilmar F. Santos [a,**], Hans I. Weber [b]

[a] Department of Mechanical Engineering, DTU, Niels Koeppel Allé, 404, 2800 Lyngby, Denmark
[b] Mech. Engineering Department, PUC-Rio, Rua Marquês de São Vicente, 225, Rio de Janeiro, RJ, Brazil

ARTICLE INFO

Article history:
Received 8 September 2016
Received in revised form
15 December 2016
Accepted 10 January 2017
Handling Editor: A.V. Metrikine
Available online 1 February 2017

Keywords:
Safety bearings
Impact
Friction
Contact mechanics
Nonlinear dynamics
Magnetic bearing

ABSTRACT

Rotor drops in magnetic bearing and unbalance in rotors have been objective of study for many years. The combination of these two well-known phenomena led to an interesting chaotic response, when the rotor touches the inner race of the back-up bearing. The present work explores the nonlinear rotor backup bearing dynamics both theoretically and experimentally using a fully instrumented test rig, where the position of shaft, its angular velocity and the contact forces between the shaft and the backup bearing are sampled at 25 kHz. The test rig is built by a removable passive magnetic bearing, which allows for simulation of magnetic bearing failure (loss of carrying capacity and rotor fall). The rotor is studied numerically as well as experimentally. A theoretical approach is given beforehand and supplies the basis of the study. Finally the presented results are commented on the point of view of nonlinear dynamics applied to the practical use. The theoretical and numerical analyses are shown through orbit plots, phase plans, Poincaré maps, force response in time and double sided spectrum. The latter is important to characterize the condition at different levels of unbalance between forward and backward whirl. Our preliminary results indicate that for smaller amount of unbalance the rotor swings at the bottom of the bearing, the more the unbalance increases, other dynamical behavior occur and some can be extremely harmful, since the rotor can be lifted from the contact state and return, starting to impact innumerable times without reaching a steady state.

1. Introduction

The possibility of using magnetic bearing rotors in industrial applications cannot be considered correctly without the use of proper backup bearings. Applications are various, such as in reaction wheels, in centrifuges, in energy efficiency machines, as cited for instance by Gasch [1] and Schweitzer and Maslen [2]. For all these machines, a safety element has to be installed to prevent failures such as power loss, which would cause the shaft to fall. The safety element consists normally of a rolling bearing with inner race diameter greater than the shaft diameter, but smaller than the one of the magnetic bearing. It is designed to withstand the loads and impacts of a rotor. It also protects the whole system and prevents even more disastrous situations.

* Principal corresponding author.
** Corresponding author.
E-mail addresses: cefonse@mek.dtu.dk (C.A. Fonseca), ilsa@mek.dtu.dk (I.F. Santos), hans@puc-rio.com (H.I. Weber).

http://dx.doi.org/10.1016/j.jsv.2017.01.020
0022-460X/

Throughout the years, several works have been published on this subject. A good overview of the state of rotordynamics research of rub-related phenomena is given in Muszynska [3]. In the work of Johnson [4], a vertical shaft was studied analytically and he investigated the changes in the radial peaks when a bearing with clearance is introduced. Black [5] also considered a rotor with a clearance stator but added friction on the contact. He conducted an analytical study, whose results about synchronous and counter whirl were verified experimentally. Also in reference [6], a gyro pendulum with a piecewise linear model was investigated in good agreement with experimental results. Choy and Padovan [7] presented a numerical investigation of the interaction between the rotor and the casing of the bearing wall, in which different parameters were tested, such as imbalance and friction coefficients.

By employing a proper impact model, the occurrence of chaotic behavior was reported by Goldman [8]. Moreover Piccoli and Weber [9] successfully investigated the identification of chaotic motion with Lyapunov exponents and Poincaré diagrams experimentally. In Jiang and Ulbrich [10], the onset of dry friction whip was investigated with an unbalanced rotor to stator contact explaining the recurrence using the multiple scales method. Regarding rotor drops, the work from Pradetto [11] describes the resulting phenomena of the drop of a one-ton rotor as its backup bearing. Fumagalli [12] tested the performance of the ball bearing instead of a plain circular one as a backup bearing when the rotor drops, slides and tumbles on its inner race. His results led to the information about the rotor's whirl and motion as well as the contact forces at each impact. More recently, [13] presented a simulation with experimental validation of a 9-ton-active-magnetic-bearings-rotor drop then compared and validated the proprietary code to several drop test as a tool for future reliability tests. Jacquet-Richardet et al. [14] analyze the rotor-to-stator impact of a turbo-machinery with a thermocoupled model with dynamical system. Their findings explore the nonlinear nature of the impact response and the interaction with the blades of the rotor with the casing.

In combination with Active Magnetic Bearings (AMB) technology as mentioned by Schweitzer [2] and in [15], it is clear that safety bearings are an important subject of study. Chapter 27 in the book of Gasch et al. [16] also treats the cases, in which the rotor starts impacting on the stator including resonance passage and sudden unbalance. Ishii and Kirk [17] analyzed numerically the transient response of a rotor drop. There it is cited that low damping causes backward whirl that leads to high-magnitude forces. The work of [18] presents a very detailed mechanical model of a flywheel with two safety bearings with power loss. The authors conducted a series of simulations, whose response changed according to the parameters such as friction and the preload applied. Ginzinger [19] developed an active actuator to avoid rubbing and thus reduce the severity of the contact. He applies a feedback control with a powerful magnetic actuator to smoothen the transition from an impact-free to full contact eliminating impacts. Moreover, in Keogh [20], a comprehensive study of different performances of auxiliary bearings was presented. Non-conventional geometries of the backup bearing were considered by Simon [21], and later by Zülow [22] and then the new kind of bearing with pins is presented by Lahriri [23] and analyzes the forces that the structure receives on a sleeve backup bearing. The rotor is externally impacted and the dynamics of the first impacts and the high radial forces in that generated by the backward whirl are assessed. In Fonseca et al. [24] it is shown that the same pins help to surpass the critical speed avoiding the backward whirl. However, in most industrial operating machines, the usual safety bearing is a rolling bearing element, and the rotor will lay down at the bottom allowing it to rotate without much damage to the system. An analysis of the rigid rotor on a safety bearing showing chaotic behavior is presented in reference [25]. Later the contact between the shaft and the inner race was modeled using a nonlinear matrix equation and presented by Cole et al. [26], whose authors analyzed different configurations of rolling bearings in order to identify the dynamics conditions of the rotor during impacts events and to try to specify a proper backup bearing. More recently, Inayat-Hussain [27] gives an insight about the response of a two dimensional rotor to different imbalance levels with bifurcation diagrams, which show chaotic behavior when impacting on the wall of the backup bearing. In his thesis, van Rensburg [28] applied to his rotor model and AMB test rig several rotational speeds and showed different dynamical behaviors and harmful cases. In Hakwings et al. [29] the result of a series of drop tests of 140 kW flywheel on a backup bearing is presented and illustrates the dynamical behavior of the rotor in the case of total failure and unassisted spin down.

In the present work, a theoretical and an experimental study of a passive magnetic bearing rotor colliding on the ball bearing inner race is presented. The failure of the rotor will be induced by the rapid removal of the passive magnetic bearing, letting the rotor fall on the backup bearing. The tests will be compared with simulated results coming from a model of the rotor as a rigid body impacting on an compliant surface of a compliant housing support. The main contribution of this work is to show that different levels of unbalance change the dynamical behavior of the system at least into three separate regions, and some of them may lead to harmful situations. In order to create these different levels of unbalance, small masses are added to the disk of the rotor, but the velocity was kept constant. The findings are best portrayed in bifurcation diagrams that describe the changes. Also, these features appear on orbit plots, doubled-sided spectra and time-varying force plots.

In Section 2, the dynamical model for the rotor-backup-bearing interaction is developed. In Section 3, the simulation and experimental results are shown and discussed. Finally, in Section 4, we present our conclusions.

2. Modeling the rotor-housing kinematics

2.1. The shaft

In Figs. 1a and b, a schematic description of the rotor is made to reproduce the assembled test rig. The rotor is supported by one spherical ball bearing at point *O* and one movable passive magnetic bearing at point C. The backup bearing is

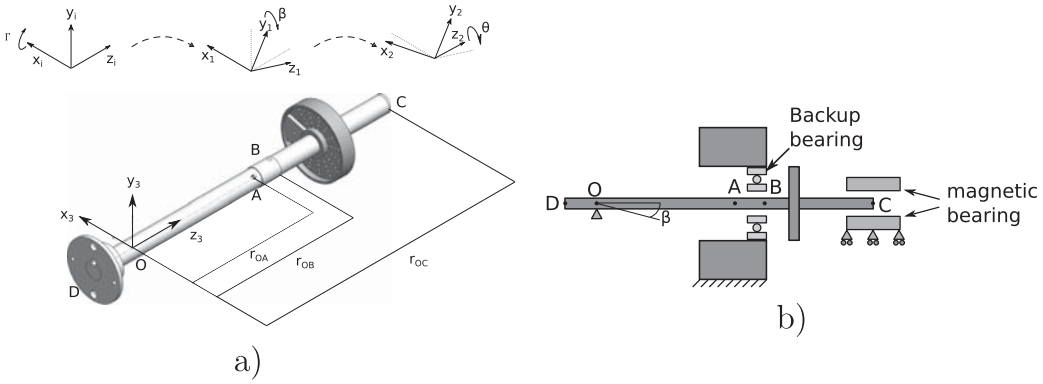

Fig. 1. The moving frame references and the points of interests, *A*, *B* and *C*, where forces are present.

mounted between them at point B. The rotor is modeled as a rigid body and external forces from the magnets, imbalance and coupling are applied at points C, A and D respectively. In these figures the reference frames used are shown and the moving reference frame *B*3 fixed to the rotating shaft and positioned at the supporting point of the rotor. Fig. 2a is a photograph of the complete test rig and Fig. 2b is another one taken above the magnetic bearing and pointed to the backup bearing.

The rotor is only allowed to rotate according to the following three angular degrees of freedom: $\Gamma(t)$, $\beta(t)$, $\theta(t)$, around the respective coordinate axes x_i, y_1, z_2, for which we define the angular velocities

$$ {}_I\dot{\boldsymbol{\Gamma}} = \left[\dot{\Gamma}(t)\ 0\ 0\right]^T, \quad {}_{B1}\dot{\boldsymbol{\beta}} = \left[0\ \dot{\beta}(t)\ 0\right]^T \quad \text{and} \quad {}_{B2}\dot{\boldsymbol{\theta}} = \left[0\ 0\ \dot{\theta}(t)\right]^T. \tag{1} $$

Then the rotational matrices ${}_I T_\Gamma$, ${}_{B1}T_\beta$ and ${}_{B2}T_\theta$ are defined as

$$ {}_I\mathbf{T}_\Gamma = \begin{bmatrix} 1 & 0 & 0 \\ 0 & \cos\Gamma(t) & \sin\Gamma(t) \\ 0 & -\sin\Gamma(t) & \cos\Gamma(t) \end{bmatrix}, \quad {}_{B1}\mathbf{T}_\beta = \begin{bmatrix} \cos\beta(t) & 0 & -\sin\beta(t) \\ 0 & 1 & 0 \\ \sin\beta(t) & 0 & \cos\beta(t) \end{bmatrix}, $$
$$ {}_{B2}\mathbf{T}_\theta = \begin{bmatrix} \cos\theta(t) & \sin\theta(t) & 0 \\ -\sin\theta(t) & \cos\theta(t) & 0 \\ 0 & 0 & 1 \end{bmatrix}. \tag{2} $$

Each external force will generate a moment with respect to *O* and the relevant position vectors are given by

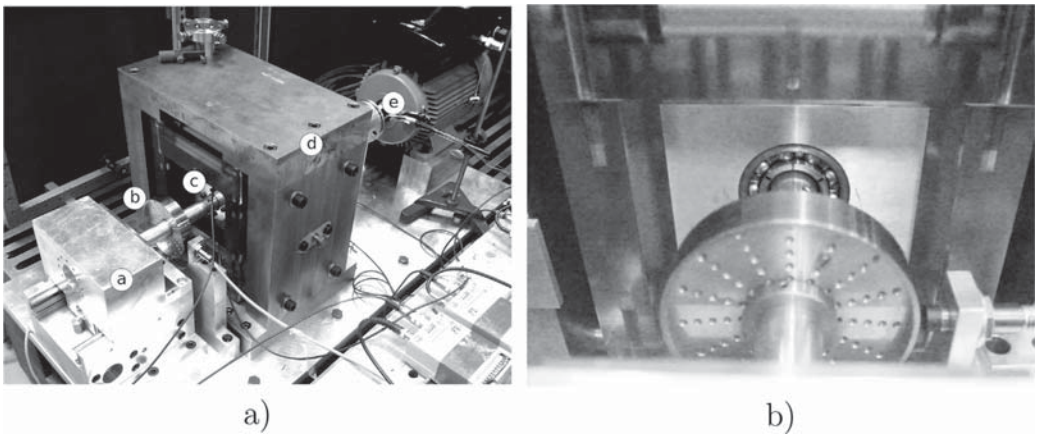

Fig. 2. (a) Photograph from the test rig assembled for tests with different backup bearings. A – Passive magnetic bearing; b – Rotor with disk; c – Backup bearing. Here the backup bearing is a plain wall bearing; d – Backup bearing housing; e – AC Motor. (b) Details from the shaft and the rolling bearing backup bearing.

$$ {}_{B3}\mathbf{r}_{OA} = \left[r_{OA,x} \;\; 0 \;\; r_{OA,z} \right]^T, \quad {}_{B3}\mathbf{r}_{OB} = \left[r_{OB,x} \;\; r_{OB,y} \;\; r_{OB,z} \right]^T \quad \text{and} $$
$$ {}_{B3}\mathbf{r}_{OC} = \left[0 \;\; 0 \;\; r_{OC,z} \right]^T. \tag{3} $$

The inertia tensor referring to the supporting point is

$$ {}_{B3}\mathbf{I}_O = \begin{bmatrix} I_{xx} & 0 & -I_{xz} \\ 0 & I_{yy} & 0 \\ -I_{zx} & 0 & I_{zz} \end{bmatrix}, \tag{4} $$

where $I_{xz} = m_u r_u l_{OD}$. The absolute angular velocity represented in the coordinates of the moving reference frame B3 (where the inertia tensor is constant) is given by

$$ \boldsymbol{\omega}_{B3} = {}_{B3}\dot{\boldsymbol{\Gamma}} + {}_{B3}\boldsymbol{\beta}\,\dot{\boldsymbol{\beta}} + {}_{B3}\boldsymbol{\theta}\,\dot{\boldsymbol{\theta}} = \begin{bmatrix} \cos(\theta)\cos(\beta)\dot{\Gamma} + \sin(\theta)\dot{\beta} \\ -\sin(\theta)\cos(\beta)\dot{\Gamma} + \cos(\theta)\dot{\beta} \\ \sin(\beta)\dot{\Gamma} + \dot{\theta} \end{bmatrix}. \tag{5} $$

The absolute acceleration written in B3 is written as:

$$ \dot{\boldsymbol{\omega}}_{B3} = \begin{bmatrix} -\dot{\theta}\sin(\theta)\cos(\beta)\dot{\Gamma} - \cos(\theta)\dot{\beta}\sin(\beta)\dot{\Gamma} + \cos(\theta)\cos(\beta)\ddot{\Gamma} + \dot{\theta}\cos(\theta)\dot{\beta} + \sin(\theta)\ddot{\beta} \\ -\dot{\theta}\cos(\theta)\cos(\beta)\dot{\Gamma} + \sin(\theta)\dot{\beta}\sin(\beta)\dot{\Gamma} - \sin(\theta)\cos(\beta)\ddot{\Gamma} - \dot{\theta}\sin(\theta)\dot{\beta} + \cos(\theta)\ddot{\beta} \\ \dot{\beta}\cos(\beta)\dot{\Gamma} + \sin(\beta)\ddot{\Gamma} + \ddot{\theta} \end{bmatrix}. \tag{6} $$

2.2. The inner and outer housing

In order to determine and measure the force between the rotor shaft and the inner race, the backup bearing is mounted on a special casing, where there are four force transducers. It is inside a block that is mounted inside a frame, called an outer house. Then, the inner house is only allowed to move vertically inside it. Subsequently, the outer house moves only horizontally. Figs. 3a and b show a scheme of the complete assembly.

The elastic elements k_{ft} represent the force transducers positioned between the bodies; the damping elements c_h and c_v represent the structural damping. These damping terms are present due to the four beams that make the inner house slide vertically and the outer house horizontally, two terms for each direction.

The dynamics of both housings is included in the mechanical model. The dynamical coupling between the inner house and the rotor is introduced by the impact forces, the normal force N and the friction force F_{fric}. The beams that support the housings have the stiffness calculated as clamped–clamped beam $K_{\text{beam}} = \frac{48EI}{Fa^2(3l-4a)}$, and the damping coefficients are approximated by:

$$ c_h = 2\zeta\sqrt{K_{\text{beam}}(m_{ih} + m_{oh})} \quad \text{and} \quad c_v = 2\zeta\sqrt{K_{\text{beam}}(m_{ih})}. \tag{7} $$

Thus the equations of motion for both housings are written as follows:

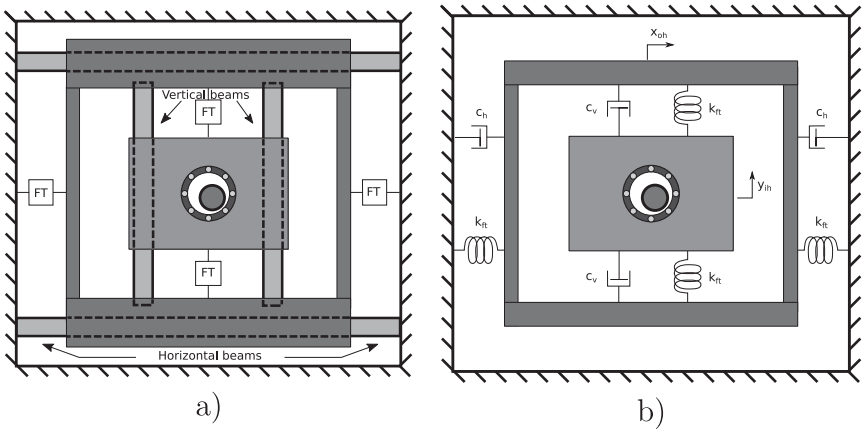

Fig. 3. Assembly of the inner housing and the outer housing.

$$m_{ih}\ddot{y}_{ih} = -2k_{ft}y_{ih} - 2c_v\dot{y}_{ih} - m_{ih}g + N\sin\alpha + F_{\text{fric}}\cos\alpha. \tag{8}$$

$$(M_{oh} + m_{ih})\ddot{x}_{oh} = -2k_{ft}x_{oh} - 2c_h\dot{x}_{oh} + N\cos\alpha - F_{\text{fric}}\sin\alpha. \tag{9}$$

Consequently, the radial term r_r can be calculated and allows one to know whether the system is impacting or not, and it is equal to

$$r_r = \sqrt{(\beta l_{OB} - x_{oh})^2 + (-\Gamma l_{OB}) - y_{ih})^2}. \tag{10}$$

The impact is analyzed at each time step if the rotor displacement at the position of the backup bearing is greater than or equal to the radial gap, $\delta \geq r_0 = r_1 - r_r$. The impact is modeled following a stepwise elastic model proposed by [30], that is:

$$F_{\text{imp}} = N = k_{\text{imp}}\delta^{3/2}\left(1 + \frac{3(1-e^2)}{4}\frac{\dot{\delta}}{\dot{\delta}^-}\right), \quad \text{if } \delta \geq 0, \tag{11}$$

in which the stiffness coefficient is given as:

$$k_{imp} = \frac{4}{3\left(\frac{1-\nu_s^2}{E_s} + \frac{1-\nu_i^2}{E_i}\right)}\left(\frac{r_s r_1}{r_1 - r_s}\right)^{1/2}. \tag{12}$$

and e is the coefficient of restitution. The model of impact has the advantage of avoiding the determination of a damping factor and relies only on the value of the coefficient of restitution, which can be determined easier through experiments. On other side, it is a piece-wise model that can lead to numerical instabilities in the numerical integration in time. Therefore it is recommended to employ techniques like Filipov or manipulate the tolerances into the computational code.

Therefore, the forces acting on the mechanical model are the rotor's own weight, the magnetic force and the damping force plus the impact forces

$$ {}_I\mathbf{F}_g = \begin{bmatrix} 0 \\ -mg \\ 0 \end{bmatrix}, \quad {}_I\mathbf{F}_{mag} = \begin{bmatrix} -K\cos\alpha \\ -K\sin\alpha \\ 0 \end{bmatrix}, \quad {}_I\mathbf{F}_{\text{damp}} = \begin{bmatrix} -c\cos\rho \\ -c\sin\rho \\ 0 \end{bmatrix},$$

$$ {}_I\mathbf{F}_{\text{imp}} = \begin{bmatrix} N\cos\alpha \\ N\sin\alpha \\ 0 \end{bmatrix} \quad \text{and} \quad {}_I\mathbf{F}_{\text{fric}} = \begin{bmatrix} F_{\text{fric}}\sin\alpha \\ F_{\text{imp}}\cos\alpha \\ 0 \end{bmatrix}. \tag{13}$$

Finally, one writes Euler's equation with respect to the supporting point O

$$\sum {}_{B3}\text{Force Moments}_O = {}_{B3}\mathbf{I}_O\left(\frac{\mathrm{d}}{\mathrm{d}t}\boldsymbol{\omega}_{B3}\right) + {}_{B3}\boldsymbol{\omega} \times ({}_{B3}I_O \cdot {}_{B3}\boldsymbol{\omega}) \tag{14}$$

and one solves the set of equations considering the angles Γ and β small. The motor has an independent control and is capable of delivering the necessary torque to keep the angular velocity $\dot{\theta}$ fixed. The differential equations are highly non-linear, with many coupled terms, and the terms of the differential equations may be determined using the symbolic program Maple®. However, we are more interested in the position of the center of shaft at the backup bearing plane and, using the transformation matrices, the coordinates are written as:

$$\begin{bmatrix} X \\ Y \\ Z \end{bmatrix} = \left({}_I\mathbf{T}_\Gamma^T(t) \cdot {}_{B1}\mathbf{T}_\beta^T(t) - {}_I\mathbf{T}_\Gamma^T(0) \cdot {}_{B1}T_\beta^T(0)\right) \cdot {}_{B2}\mathbf{r}_{OC}, \tag{15}$$

where the following initial conditions are taken into consideration: $t=0$, $\Gamma(0) = 0$ and $\beta(0) = 0$.

The complete expressions for $\ddot{\Gamma}$ and $\ddot{\beta}$ are available in Appendix A.

2.3. The backup bearing

When the rotor drops and hits the rolling backup bearing, as seen in Fig. 4, the friction force accelerates the inner race and the spheres. The angular position of the inner race, θ_{Ir}, is also a degree of freedom. Fig. 4a illustrates a schematic view of balls and inner race and their velocities. Since the outer race is not moving and the spheres are not sliding on the touching point with it, point O_{sph}, the tangential velocity is half of the one on the edge between the sphere and the inner race, point E. The force acting on one rolling bearing ball is shown in Fig. 4b and the following equations for one isolated ball are written:

$$\sum \text{Moment}_{O_{sph}} = I_{sph}\ddot{\theta}_{sph} \tag{16}$$

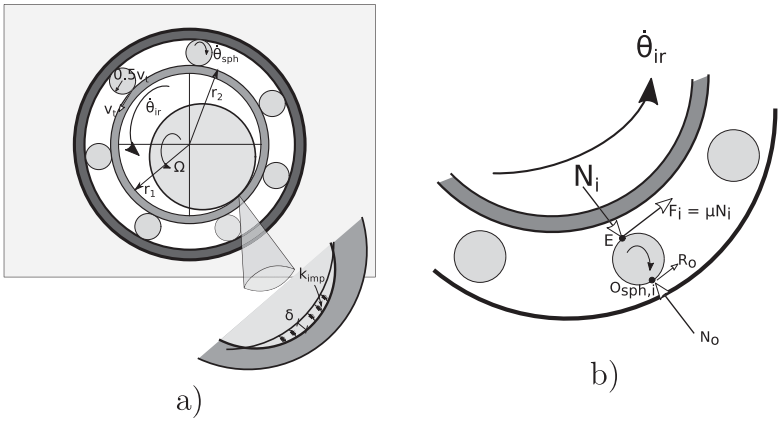

Fig. 4. (a) The shaft inside the inner housing in contact with the inner race. (b) The forces acting at each ball of the backup bearing.

$$2r_{sph}F_i = I_{sph}\ddot{\theta}_{sph}, \quad \text{since } v_t = \dot{\theta}_{ir}r_2 = \dot{\theta}_{sph}r_{sph}, \tag{17}$$

$$2r_{sph}F_i = I_{sph}\ddot{\theta}_{ir}\frac{r_2}{r_{sph}}, \tag{18}$$

where $I_{sph} = 2/5\left(\pi r_{sph}^2\right) + m_{sph}r_{sph}^2$. The Newton equation for the tangential direction leads to

$$F_i + R_o = m_{sph}a_t. \tag{19}$$

From (17) and (18),

$$R_o + I_{sph}\ddot{\theta}_{ir}\frac{r_2}{2\left(r_{sph}\right)^2} = m_{sph}\ddot{\theta}_{ir}r_2. \tag{20}$$

Therefore, the angular acceleration of the inner race $\ddot{\theta}_{ir}$ can be obtained by taking into account the influence of all rolling spheres j:

$$\ddot{\theta}_{ir}I_{ir} = fr_1 - r_2\sum_{j=1}^{N_{sph}}\left(F_{i,j}\right), \tag{21}$$

$$\ddot{\theta}_{ir}I_{ir} = fr_1 - r_2N_{sph}\left(\ddot{\theta}_{ir}\frac{I_{sph}r_2}{2\left(r_{sph}\right)^2}\right) \tag{22}$$

$$\ddot{\theta}_{ir}\left(I_{ir} + N_{sph}\frac{I_{sph}}{2}\left(\frac{r_2}{r_{sph}}\right)^2\right) = fr_1. \tag{23}$$

3. Simulation and nonlinear analysis

3.1. Integration in time

The equations of motion (14), (21), (8) and (9) are integrated in time using a combined Matlab differential equation solver *ode45* and a dedicated Runge–Kutta algorithm. The former is employed together with an *Event* function in order to find the exact moment of the impact. The latter is applied during the short period of impact. This is because it is a highly stiff problem and demands an enormous amount of time with very tight integration tolerances of the algorithm. Therefore, a test of convergence was performed and the adequate step time was set to 10^{-6} s. During the impact, the relative velocity between the shaft and the inner race, v_{rel}, plays an important role. The friction force depends on it, and if the velocities match, there is no friction. Otherwise, the friction force is modeled as $F = \mu N\ \text{sign}(v_{rel})$. The model parameters are shown in Table 1.

Table 1
Parameters set applied to the simulation.

Parameter of the shaft	
Mass without unbalance	$m = 1.28$ kg
Length to magnetic bearing	$r_{OC} = [0,\ 0,\ 0.384\ \text{m}]$
Length to rolling bearing	$r_{OB} = [r_r\cos(\alpha),\ r_r\sin(\alpha),\ 0.211\ \text{m}]$
Shaft diameter	$d_r = 25$ mm
Parameter of the rolling bearing	
Inner diameter	$d_1 = 2r_1 = 28$ mm
Inner race outer diameter	$d_2 = 2r_2 = 37$ mm
Sphere radius	$r_{sph} = 5.0$ mm
Impact stiffness	$k_{imp} = 2.5 \times 10^{10}$ N/m$^{3/2}$
Friction coefficient	$\mu = 0.20$
Restitution coefficient	$e = 0.90$
Parameter of the inner and outer house	
Mass from inner house	$m_{ih} = 1.70$ kg
Damping 1	$c_h = 7.04 \times 10^2$ N s/m
Mass from outer housing	$M_{oh} = 8.87$ kg
Damping	$c_v = 2.28 \times 10^2$ N s/m
Force sensor	
Force transducer stiffness	$k_{ft} = 8.3 \times 10^7$ N/m

3.2. Simulated results and experimental comparison

As mentioned before, in Section 2.1 the test rig is a rotor suspended at one end by a removable passive bearing. From the moment that the magnetic force is removed, there are three distinct stages: (a) the rotor free fall inside the bearing; (b) the recurrence of contact between rotor and the inner race surface leading to the deformation of both of them and the appearance of an angular acceleration of the inner race; and finally (c) the almost vanishing of the relative velocities between the inner race and shaft surfaces with the rotor finding a steady state condition at the bottom of the backup bearing. In fact, since the rotor keeps executing small translational movements around the equilibrium state, rarely will the tangential velocities of the shaft and the inner race coincide. This occurs in spite of the fact that the steady-state general dynamical behavior of the rotor changes significantly according to the unbalance level. After removing the magnetic force, the rotor falls down and impacts several times on the surface of the inner race. The energy will be dissipated by the damping from the coupling between the inner and outer housing and due to the impact with the compliant surface.

The changes in the steady-state behavior can be evaluated more explicitly with a Poincaré map, as seen in Fig. 5. The variables Y, $\dot{X}$ and $\dot{Y}$ are sampled every time the center of the shaft crosses the vertical line; in other words, when $X = 0$. The first plot on the top of Fig. 5 shows the vertical position, Y, through which the rotor crosses the vertical line as a function of the control variable, i.e., the unbalance U.

Overall, the phenomena are captured by both experiment and simulation. We can divide the bifurcation diagram into three specific regions. First, the rotor center is always crossing at the bottom of the shaft at $Y = -1.5$ mm in region I. Suddenly, there is a change and more crossings at the vertical line occur. This can be seen in region II of Fig. 5. The more unbalance, the more evident the fact that the center of the shaft performs chaotic trajectories. In the simulation it is expected that the rotor will cross from the bottom to the top of the bearing, but the mechanical setup shows a gradual increase in the vertical crossing as the unbalance gets bigger until the rotor is able to perform a full whirl. At the right end of the plot, region III, the rotor is only executing a full whirl so the rotor is crossing the vertical line in the extremes, $Y = -1.5$ to $Y = 1.5$ mm. In the following plots, the horizontal and the vertical crossing velocity, $\dot{X}$ and $\dot{Y}$, are plotted against the unbalance and, once again, the experimental and the simulation measurement tend to agree with each other.

It can be seen that the unbalance plays a considerable role in the dynamics of the shaft and its size can strongly influence the dynamical pattern. The initial conditions were kept the same in experiments and simulations but in the experiments the rotor starts in contact with the bearing and the magnetic bearing is removed, while in the simulations, we start with the rotor at the center and the magnetic bearing is turned off later. From the start until the magnets are removed the orbit is painted in black, later, the color is red for one second of simulation, which then changes to blue.

The first case is presented in Fig. 6, where there is no additional mass. The shaft is constantly in contact with the bearing inner race just oscillating. The numerical result shows the shaft falling and impacting the inner race and after some hits it stays on the bottom of the bearing. The difference between them exists because there is a misalignment at the coupling between the shaft and the motor.

Next, in Fig. 7 we see a discrepancy between the experiment and the numerical result. While numerically it is shown that the rotor is whirling, falling and hitting a great number of times, the test rig developed a less complex orbit, in which the

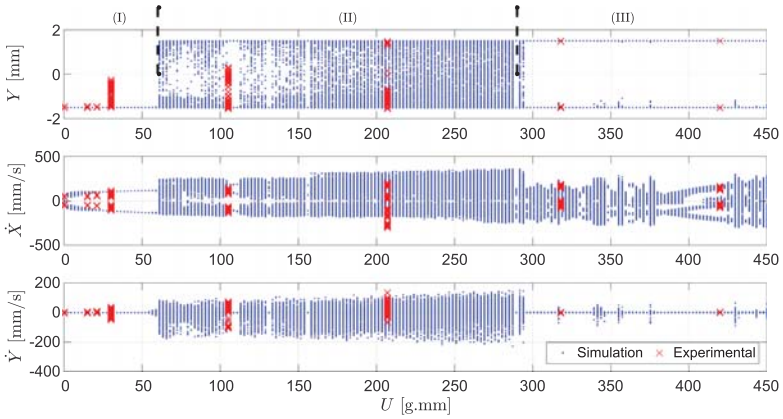

Fig. 5. 10 Hz simulated bifurcation for different unbalance levels together with 8 different experimental tests with unbalance levels of U_1=0.0 g mm, U_2=15 g mm, U_3=21 g mm, U_4=30 g mm, U_5=105 g mm, U_6=207 g mm, U_7=318 g mm and U_8=420 g mm.

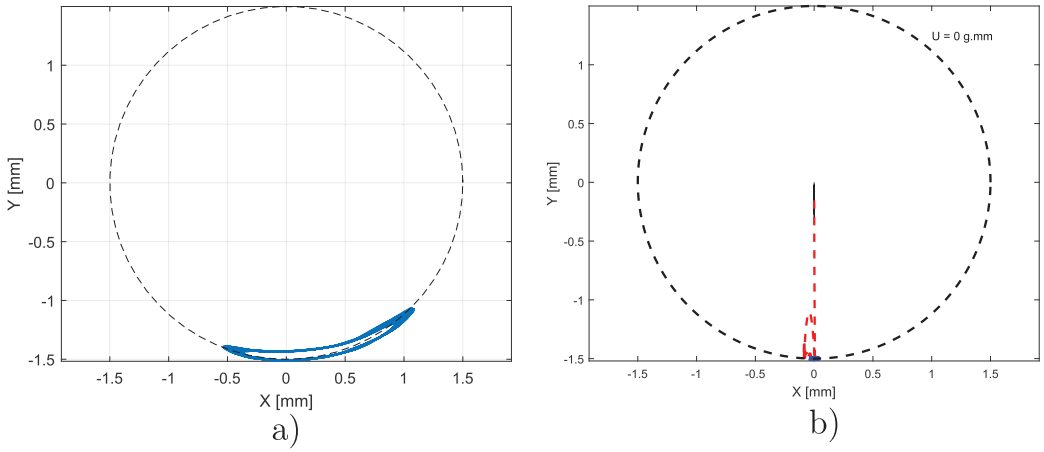

Fig. 6. Angular velocity 10 Hz. Experimental (a) and simulated (b) orbit with no unbalance weight. (U=0.0 g mm). (For interpretation of the references to color in this figure, the reader is referred to the web version of this paper.)

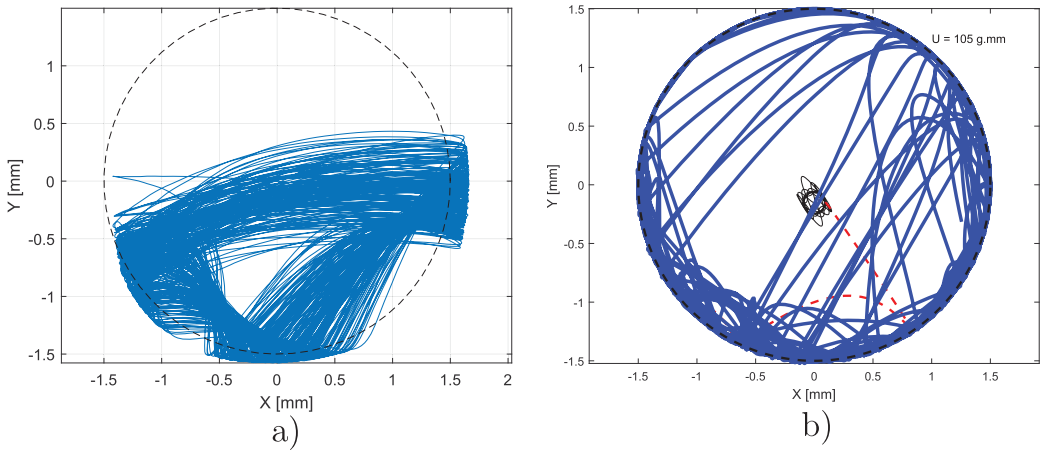

Fig. 7. Angular velocity 10 Hz. Experimental (a) and simulated (b) orbit with unbalance magnitude of U=105.0 g mm. (For interpretation of the references to color in this figure, the reader is referred to the web version of this paper.)

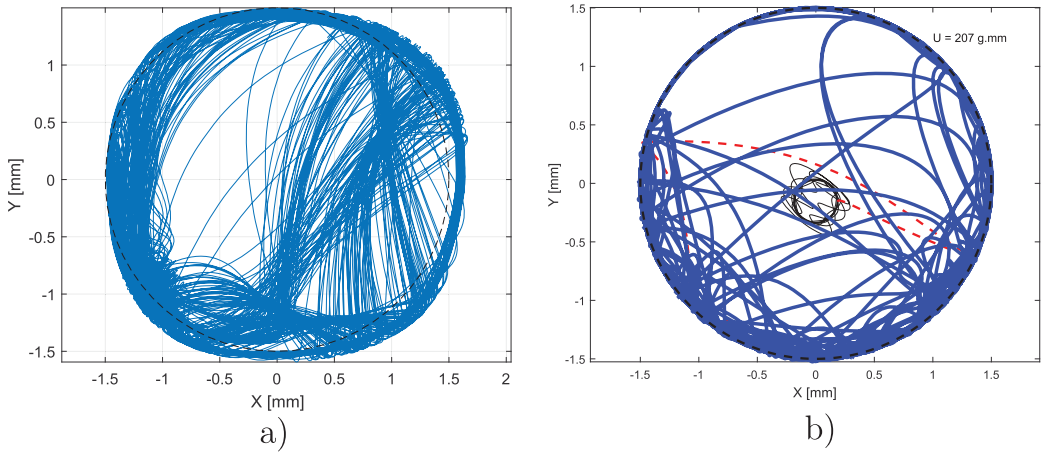

Fig. 8. Angular velocity 10 Hz. Experimental (a) and simulated (b) orbit with unbalance magnitude of $U=207.0$ g mm. (For interpretation of the references to color in this figure, the reader is referred to the web version of this paper.)

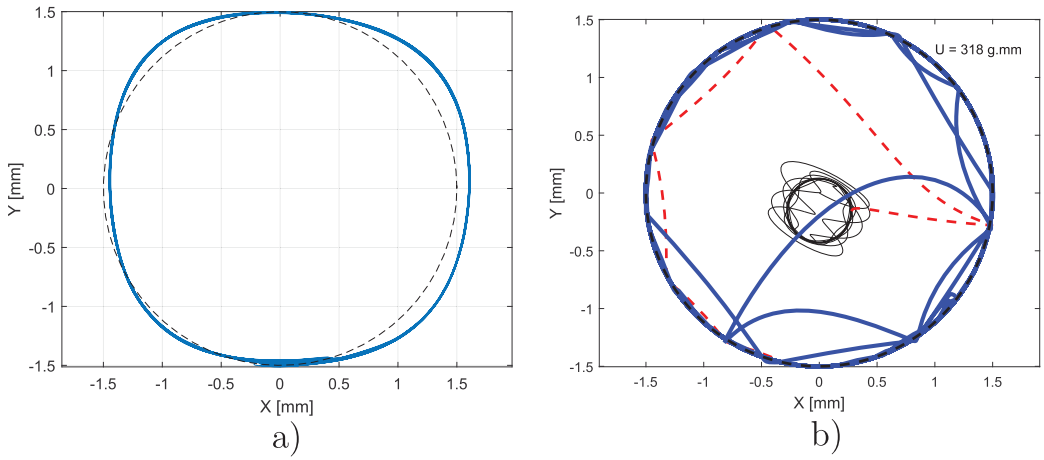

Fig. 9. Angular velocity 10 Hz. Experimental (a) and simulated (b) orbit with unbalance magnitude of $U=318.0$ g mm. (For interpretation of the references to color in this figure, the reader is referred to the web version of this paper.)

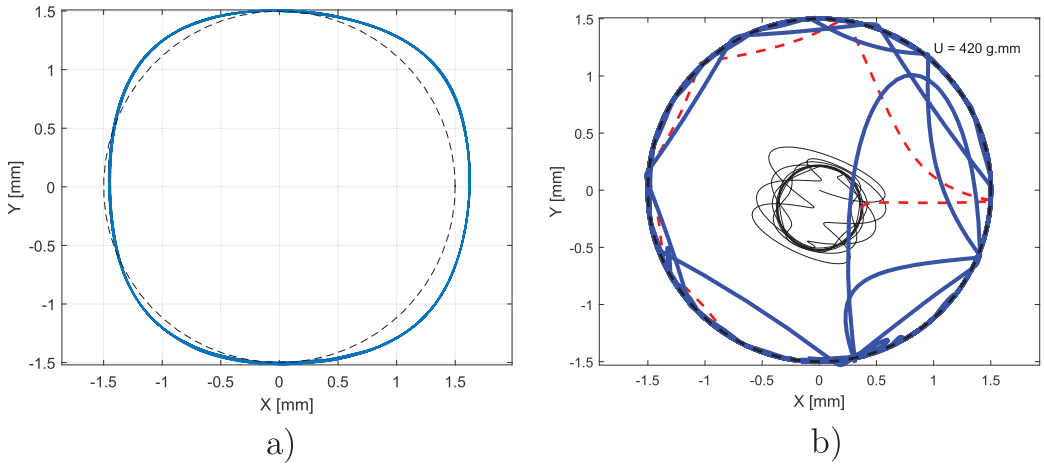

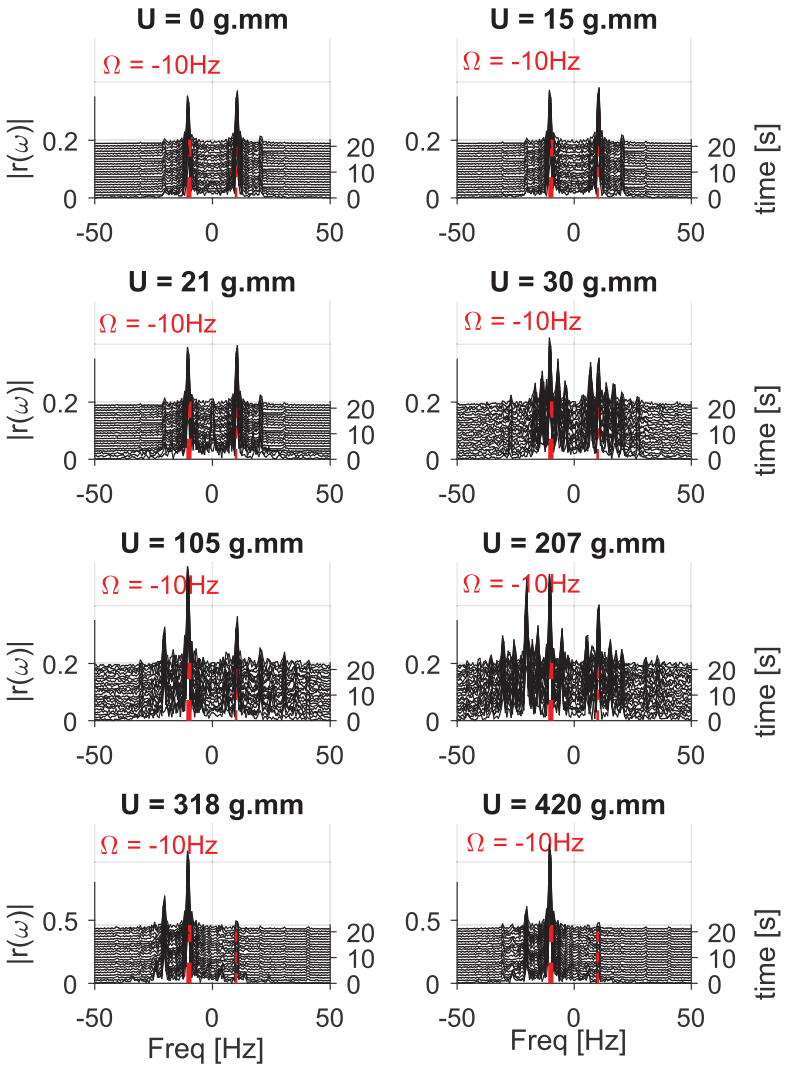

Fig. 11. 10 Hz double sided spectrum. Effect of the unbalance in the general behavior of the rotor; from oscillatory movement, to chaos and full whirl.

center of the shaft makes a quasi-periodic motion. One can see that the hits are concentrated around three regions. An additional increase in unbalance changes the orbit generated by the test rig and matches with the expected behavior as demonstrated by the simulation in Fig. 8. The chaotic behavior shows some similarity when comparing numerical and experimental results.

Finally, Figs. 9 and 10 reveal the last observed change in the rotor trajectories. The unbalance is high enough to maintain the rotor always in contact with the inner race, after the initial hits. Both the experiment and the numerical results are in clear accordance. Besides, there is a predominance of the forward whirl in both of them. The reason for the recurrence of the forward whirl is that the friction force is at a "stick" phase and therefore its magnitude is small and the wall is moving.

To visualize the existence of chaotic trajectories performed by the rotor center, a double-sided spectrum is displayed in Fig. 11. Each graph corresponds to one red unbalance level in Fig. 5. At low levels the heights of the peaks are approximately the same. Several levels of unbalance are chosen; the cases $U=0.0$ g mm, $U=15.0$ g mm, $U=21.0$ g mm, and $U=30.0$ g mm represent region I. The noise clearly rises when the unbalance is $U=105.0$ g mm and $U=207.0$ g mm from region II, which is a clear indication that chaos is happening. In region III higher unbalance levels, $U=210.0$ g mm and $U=420.0$ g mm, show clearly higher peaks at $\Omega = -10.0$ Hz than the opposite pair, confirming the predominance of a full whirl in the same direction as the rotor spinning. Negative values of ω mean the same spinning direction of the rotor.

As mentioned in Section 2.2, the test rig has four force transducers positioned between the inner and outer housing.

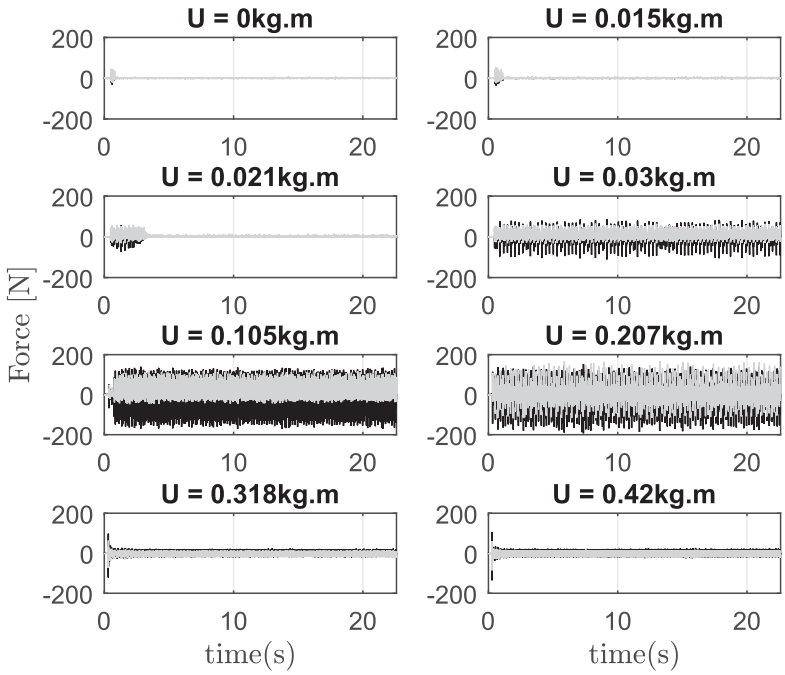

Fig. 12. Force analysis for 10.0 Hz as angular velocity. Light gray is the resultant vertical force and black the horizontal force. The transient time takes longer to cease at every increase in the unbalance. Chaotic cases show high impact magnitude forces, but high unbalance lowered them, when the rotor is permanently in contact.

Their signals are converted to Newtons and are sampled simultaneously with the other signals. For the same unbalance levels from Figs. 6–10, the horizontal (blue) and the vertical force (red) present on the bearing's inner race are plotted in Fig. 12. Every addition in the unbalance increases the transient time until the steady state disappears for a level of unbalance belonging to region II of the bifurcation diagram. At a low level of unbalance there is a predominance of the vertical force, since the rotor is only moving on the bottom of the backup bearing.

Fig. 12 demonstrates the effect of chaotic cases, in which the inner race receives multiple high magnitude impacts. The magnitude of the force reaches up to 200 N in each direction, which is considerably high for a rotor whose weight is only 12.74 N. This situation changes for the regions III cases, since the shaft is always in contact with the surface of the inner race and is no longer impacting. The level of the forces oscillates between -20 and 20 N for both horizontal and vertical forces. The bearing has to be able to only withstand the centrifugal force in order to not break.

4. Conclusion

From the theoretical and experimental nonlinear analysis carried out in this paper, one can conclude that the rotor-backup bearing system has three distinguished dynamical behaviors depending on the level of rotor unbalance. For region I, characterized by low unbalance level from (0, 60] g mm, simple oscillatory movements of the rotor center at the bottom of the backup bearing are seen. For region II with unbalance levels from (60 to 280] g mm, chaotic motions are followed by impacts between the rotor and backup inner race surface. Finally, for region III characterized by high unbalance levels, full forward whirl of the rotor center takes place.

The magnitude of the forces at the three different regions changes and supports the idea that it may damage the backup bearing. At low levels of unbalance, the magnitude of the forces varies slightly in time and just enough to support the fallen rotor. Chaotic cases cause multiple impacts, which means that the contact forces are always high with a short duration. Although a rotor with big unbalance remains in contact with the inner race, the strength of the force drops significantly.

Acknowledgments

The authors express their acknowledgement to CNPq through the Science Without Borders Program with the process number: 249728/2013-3, which sponsored the elaboration of this paper.

Appendix A. Equations for $\ddot{\Gamma}$ and $\ddot{\beta}$

$$
\begin{aligned}
\ddot{\Gamma} = -\frac{1}{I_{yy}\left(I_{xx} - I_{xz}\beta\cos(\theta)\right)}\Big[& -I_{xx}^2\dot{\beta}\beta\dot{\Gamma} + I_{xz}\dot{\beta}^2\left(\cos(\theta)\right)^2 I_{xx}\sin(\theta) \\
& - I_{xz}I_{yy}\dot{\beta}^2\left(\cos(\theta)\right)^2\sin(\theta) + I_{yy}Izz\left(\dot{\beta}\right)\dot{\theta}\left(\cos(\theta)\right)^2 + N\sin(\delta)l_s I_{xx} - \cos(\delta)F_{fric}l_s I_{xx} \\
& + I_{xx}I_{yy}\dot{\beta}\dot{\theta} + Izz\dot{\beta}\dot{\theta}I_{xx} + I_{xx}^2\dot{\beta}\dot{\theta}\left(\cos(\theta)\right)^2 - I_{xx}^2\dot{\beta}\dot{\theta} \\
& - \sin(\rho)cl_Q I_{xx} - K\sin(\alpha)l_Q I_{xx} - I_{xz}\dot{\beta}^2 I_{xx}\sin(\theta) + I_{xz}\dot{\theta}^2 I_{xx}\sin(\theta) \\
& - I_{yy}^2\dot{\beta}\dot{\theta}\left(\cos(\theta)\right)^2 + Izz\beta\cos(\theta)\dot{\Gamma}^2 I_{xx}\sin(\theta) \\
& - I_{yy}Izz\dot{\Gamma}^2\beta\cos(\theta)\sin(\theta) - I_{yy}N\cos(\delta)\beta\left(\cos(\theta)\right)^2 y_B \\
& + I_{yy}N\sin(\delta)\beta\left(\cos(\theta)\right)^2 x_B - I_{yy}\cos(\delta)\beta\left(\cos(\theta)\right)^2 f x_B - I_{yy}\sin(\delta)\beta\left(\cos(\theta)\right)^2 F_{fric}y_B \\
& + 2I_{xz}\beta\dot{\Gamma}\dot{\theta}I_{xx}\sin(\theta) + I_{yy}Izz\dot{\beta}\dot{\Gamma}\beta\left(\cos(\theta)\right)^2 - I_{yy}N\Gamma\cos(\delta)\beta\left(\cos(\theta)\right)^2 l_s - I_{yy}\Gamma\sin(\delta)\beta\left(\cos(\theta)\right)^2 f l_s \\
& - N\Gamma\cos(\delta)\cos(\theta)y_B I_{xx}\sin(\theta) + N\Gamma\sin(\delta)\cos(\theta)x_B I_{xx}\sin(\theta) \\
& - \Gamma\cos(\delta)\cos(\theta)F_{fric}x_B I_{xx}\sin(\theta) - \Gamma\sin(\delta)\cos(\theta)F_{fric}y_B I_{xx}\sin(\theta) \\
& + I_{yy}N\Gamma\cos(\delta)\cos(\theta)\sin(\theta)y_B - I_{yy}N\Gamma\sin(\delta)\cos(\theta)\sin(\theta)x_B + I_{yy}\Gamma\cos(\delta)\cos(\theta)\sin(\theta)F_{fric}x_B \\
& + I_{yy}\Gamma\sin(\delta)\cos(\theta)\sin(\theta)F_{fric}y_B + Izz\cos(\theta)\dot{\Gamma}\dot{\theta}I_{xx}\sin(\theta) \\
& - I_{yy}Izz\dot{\Gamma}\dot{\theta}\cos(\theta)\sin(\theta) + I_{yy}K\cos(\alpha)\cos(\theta)\sin(\theta)l_Q + I_{yy}\cos(\rho)\cos(\theta)\sin(\theta)cl_Q \\
& - K\cos(\alpha)\cos(\theta)l_Q I_{xx}\sin(\theta) - \cos(\rho)\cos(\theta)cl_Q I_{xx}\sin(\theta) - K\Gamma\sin(\alpha)\beta\cos(\theta)l_Q I_{xx}\sin(\theta) \\
& - \Gamma\sin(\rho)\beta\cos(\theta)cl_Q I_{xx}\sin(\theta) - \Gamma\beta\cos(\theta)gmr_{OA,z}I_{xx}\sin(\theta) \\
& + I_{yy}K\Gamma\sin(\alpha)\beta\cos(\theta)\sin(\theta)l_Q + I_{yy}\Gamma\sin(\rho)\beta\cos(\theta)\sin(\theta)cl_Q \\
& + I_{yy}\Gamma\beta\cos(\theta)\sin(\theta)gmr_{OA,z} + Izz\dot{\beta}\beta\dot{\Gamma}I_{xx} + N\sin(\delta)\beta x_B I_{xx} - \cos(\delta)\beta F_{fric}x_B I_{xx} \\
& - \sin(\delta)\beta F_{fric}y_B I_{xx} - I_{yy}\dot{\beta}\beta\dot{\Gamma}I_{xx} - N\cos(\delta)\beta y_B I_{xx} - I_{yy}^2\dot{\beta}\dot{\Gamma}\beta\left(\cos(\theta)\right)^2 \\
& - I_{xx}^2\beta\cos(\theta)\dot{\Gamma}^2\sin(\theta) + I_{yy}^2\dot{\Gamma}^2\beta\cos(\theta)\sin(\theta) \\
& + N\cos(\delta)\cos(\theta)l_s I_{xx}\sin(\theta) + \sin(\delta)\cos(\theta)F_{fric}l_s I_{xx}\sin(\theta) \\
& - I_{yy}N\cos(\delta)\cos(\theta)\sin(\theta)l_s - I_{yy}\sin(\delta)\cos(\theta)\sin(\theta)F_{fric}l_s \\
& - I_{xx}^2\cos(\theta)\dot{\Gamma}\dot{\theta}\sin(\theta) - I_{xz}\left(\cos(\theta)\right)^2\dot{\Gamma}^2 I_{xx}\sin(\theta) \\
& + I_{xz}I_{yy}\dot{\Gamma}^2\left(\cos(\theta)\right)^2\sin(\theta) - 2I_{xz}I_{yy}\dot{\beta}\dot{\Gamma}\left(\cos(\theta)\right)^3 + I_{yy}^2\left(\dot{\Gamma}\right)\dot{\theta}\cos(\theta)\sin(\theta) \\
& + I_{yy}N\sin(\delta)\left(\cos(\theta)\right)^2 l_s - I_{yy}\cos(\delta)\left(\cos(\theta)\right)^2 f l_s - r_{OA,x}\Gamma mgI_{xx}\sin(\theta)
\end{aligned}
$$

$$
\begin{aligned}
&-I_{yy}K\sin(\alpha)\left(\cos(\theta)\right)^2 l_Q - I_{yy}\sin(\rho)\left(\cos(\theta)\right)^2 cl_Q - I_{yy}\left(\cos(\theta)\right)^2 gmr_{OA,z}\\
&- I_{xx}Izz\beta\dot{\beta}\dot{\Gamma}\left(\cos(\theta)\right)^2 + I_{xx}N\beta\cos(\delta)\left(\cos(\theta)\right)^2 y_B - I_{xx}N\beta\sin(\delta)\left(\cos(\theta)\right)^2 x_B\\
&+ I_{xx}\beta\cos(\delta)\left(\cos(\theta)\right)^2 fx_B + I_{xx}\beta\sin(\delta)\left(\cos(\theta)\right)^2 fy_B - I_{xx}Izz\dot{\beta}\dot{\theta}\left(\cos(\theta)\right)^2 + I_{xx}K\sin(\alpha)\left(\cos(\theta)\right)^2 l_Q\\
&- I_{xx}N\sin(\delta)\left(\cos(\theta)\right)^2 l_s + I_{xx}\cos(\delta)\left(\cos(\theta)\right)^2 fl_s\\
&+ I_{xx}\sin(\rho)\left(\cos(\theta)\right)^2 cl_Q + I_{xx}\left(\cos(\theta)\right)^2 gmr_{OA,z}\\
&+ I_{xx}^2\beta\dot{\beta}\dot{\Gamma}\left(\cos(\theta)\right)^2 + 2I_{xx}I_{xz}\dot{\beta}\dot{\Gamma}\left(\cos(\theta)\right)^3\\
&+ I_{xx}N\beta\Gamma\cos(\delta)\left(\cos(\theta)\right)^2 l_s + I_{xx}\beta\Gamma\sin(\delta)\left(\cos(\theta)\right)^2 fl_s - gmr_{OA,z}I_{xx}\\
&-2I_{xz}\dot{\beta}\cos(\theta)\dot{\Gamma}I_{xx} - N\Gamma\cos(\delta)\beta l_s I_{xx} - \Gamma\sin(\delta)\beta F_{fric}l_s I_{xx}\Big]
\end{aligned}
\tag{A.1}
$$

$$
\begin{aligned}
\ddot{\beta} = -\frac{1}{I_{yy}\left(I_{xx} - I_{xz}\cos(\theta)\beta\right)}\Big[&I_{xz}^2\left(\cos(\theta)\right)^2\dot{\beta}^2\beta + 2I_{xz}^2\dot{\theta}\dot{\Gamma}(\beta)^2 - I_{xz}^2\left(\cos(\theta)\right)^2\dot{\Gamma}^2\beta\\
&+ I_{xx}^2\left(\cos(\theta)\right)^2\dot{\Gamma}^2\beta - I_{yy}I_{xx}\dot{\theta}\dot{\Gamma} - I_{xz}\beta\Gamma gmr_{OA,x} - I_{xx}I_{xz}\dot{\theta}\sin(\theta)\dot{\beta}\beta\\
&- I_{xx}I_{xz}\dot{\Gamma}\sin(\theta)\dot{\beta}\beta^2 + I_{xz}I_{yy}\dot{\theta}\sin(\theta)\dot{\beta}\beta + I_{xz}I_{zz}\dot{\theta}\sin(\theta)\dot{\beta}\beta - I_{xz}I_{yy}\dot{\Gamma}\sin(\theta)\dot{\beta}\beta^2\\
&+ I_{xz}I_{zz}\dot{\Gamma}\sin(\theta)\dot{\beta}\beta^2 - I_{xz}K\sin(\alpha)\sin(\theta)\beta l_Q - I_{xz}\sin(\rho)\sin(\theta)\beta cl_Q - I_{xz}\sin(\theta)\beta gmr_{OA,z}\\
&- I_{xz}N\sin(\theta)(\beta)^2\cos(\delta)y_B - I_{xz}\sin(\theta)\beta^2\cos(\delta)F_{fric}x_B - I_{xz}\sin(\theta)\beta^2\sin(\delta)F_{fric}y_B\\
&+ I_{xz}N\sin(\theta)\beta^2\sin(\delta)x_B + I_{xz}N\cos(\theta)\beta\cos(\delta)l_s + I_{xz}\cos(\theta)\beta\sin(\delta)F_{fric}l_s - I_{xz}\sin(\theta)\beta\cos(\delta)F_{fric}l_s\\
&- 3I_{xx}I_{xz}\dot{\theta}\cos(\theta)\dot{\Gamma}\beta + I_{xz}N\sin(\theta)\beta\sin(\delta)l_s - 2I_{xz}^2\cos\theta\dot{\Gamma}\sin(\theta)\dot{\beta}\beta - I_{yy}^2\cos(\theta)\dot{\Gamma}\sin(\theta)\dot{\beta}\beta\\
&+ I_{xz}I_{zz}\dot{\theta}\cos(\theta)\dot{\Gamma}\beta - I_{xz}K\cos(\alpha)\cos(\theta)\beta l_Q + I_{xx}^2\dot{\theta}\cos(\theta)\sin(\theta)\dot{\beta} + I_{xx}K\cos(\alpha)\left(\cos(\theta)\right)^2 l_Q\\
&+ I_{xx}\cos(\rho)\left(\cos(\theta)\right)^2 cl_Q - I_{xx}I_{zz}\dot{\theta}\left(\cos(\theta)\right)^2\dot{\Gamma} - I_{yy}^2\dot{\theta}\cos(\theta)\sin(\theta)\dot{\beta} - I_{xx}N\left(\cos(\theta)\right)^2\cos(\delta)l_s\\
&- I_{xx}\left(\cos(\theta)\right)^2\sin(\delta)F_{fric}l_s + I_{xx}N\left(\cos(\theta)\right)^2\Gamma\cos(\delta)y_B + I_{xx}\left(\cos(\theta)\right)^2\Gamma\cos(\delta)F_{fric}x_B\\
&+ I_{xx}\left(\cos(\theta)\right)^2\Gamma\sin(\delta)F_{fric}y_B + I_{xx}\cos(\theta)\Gamma gmr_{OA,x} - I_{xx}N\left(\cos(\theta)\right)^2\Gamma\sin(\delta)x_B - I_{xz}\cos(\rho)\cos(\theta)\beta cl_Q\\
&+ I_{yy}I_{xz}\dot{\theta}\cos(\theta)\dot{\Gamma}\beta + I_{xx}^2\cos(\theta)\dot{\Gamma}\sin(\theta)\dot{\beta}\beta - I_{yy}N\cos(\theta)\sin(\theta)\beta\Gamma\cos(\delta)l_s + I_{xx}N\cos(\theta)\sin(\theta)\beta\Gamma\cos(\delta)l_s
\end{aligned}
$$

$$
\begin{aligned}
&+I_{xx}\cos(\theta)\sin(\theta)\beta\dot{\Gamma}\sin(\delta)F_{fric}l_s - I_{yy}\cos(\theta)\sin(\theta)\beta\dot{\Gamma}\sin(\delta)F_{fric}l_s + I_{xz}^2\dot{\theta}^2\beta + I_{xx}I_{xz}\cos(\theta)\dot{\beta}^2\\
&- I_{xx}I_{xz}\dot{\theta}^2\cos(\theta) - I_{xx}I_{xz}\left(\cos(\theta)\right)^3\dot{\beta}^2 + I_{xx}I_{xz}\left(\cos(\theta)\right)^3\dot{\Gamma}^2 - I_{xz}^2\dot{\beta}^2\beta - 2I_{yy}I_{xz}\left(\cos(\theta)\right)^2\dot{\Gamma}\sin(\theta)\dot{\beta}\\
&+ I_{yy}N\cos(\theta)\sin(\theta)\sin(\delta)l_s - I_{yy}\cos(\theta)\sin(\theta)\cos(\delta)F_{fric}l_s + I_{yy}I_{zz}\dot{\theta}\cos(\theta)\sin(\theta)\dot{\beta}\\
&- I_{xx}I_{zz}\dot{\theta}\cos(\theta)\sin(\theta)\dot{\beta} + I_{xx}\cos(\theta)\sin(\theta)\cos(\delta)F_{fric}l_s - I_{xx}N\cos(\theta)\sin(\theta)\sin(\delta)l_s\\
&+ 2I_{xx}I_{xz}\left(\cos(\theta)\right)^2\dot{\Gamma}\sin(\theta)\dot{\beta} + I_{xx}K\sin(\alpha)\cos(\theta)\sin(\theta)l_Q + I_{xx}\sin(\rho)\cos(\theta)\sin(\theta)cl_Q\\
&+ I_{xx}\cos(\theta)\sin(\theta)gmr_{OA,z} - I_{yy}K\sin(\alpha)\cos(\theta)\sin(\theta)l_Q - I_{yy}\sin(\rho)\cos(\theta)\sin(\theta)cl_Q\\
&- I_{yy}\cos(\theta)\sin(\theta)gmr_{OA,z} + I_{yy}N\cos(\theta)\sin(\theta)\beta\sin(\delta)x_B + I_{xx}N\cos(\theta)\sin(\theta)\beta\cos(\delta)y_B\\
&+ I_{xx}\cos(\theta)\sin(\theta)\beta\cos(\delta)F_{fric}x_B + I_{xx}\cos(\theta)\sin(\theta)\beta\sin(\delta)F_{fric}y_B\\
&- I_{xx}N\cos(\theta)\sin(\theta)\beta\sin(\delta)x_B - I_{yy}\cos(\theta)\sin(\theta)\beta\cos(\delta)F_{fric}x_B - I_{yy}\cos(\theta)\sin(\theta)\beta\sin(\delta)F_{fric}y_B\\
&- I_{yy}N\cos(\theta)\sin(\theta)\beta\cos(\delta)y_B - I_{xx}I_{zz}\cos(\theta)\dot{\Gamma}\sin\theta\dot{\beta}\beta + I_{yy}I_{zz}\cos(\theta)\dot{\Gamma}\sin(\theta)\dot{\beta}\beta\\
&- I_{xz}N\sin(\theta)\beta^2\Gamma\cos(\delta)l_s - I_{xz}\sin(\theta)\beta^2\Gamma\sin(\delta)F_{fric}l_s - I_{xz}\cos(\theta)\beta^2\Gamma gmr_{OA,z}\\
&+ I_{xz}N\cos(\theta)\beta\Gamma\sin(\delta)x_B - I_{xz}K\sin(\alpha)\cos(\theta)\beta^2\Gamma l_Q - I_{xz}N\cos(\theta)\beta\Gamma\cos(\delta)y_B\\
&- I_{xz}\cos(\theta)\beta\Gamma\cos(\delta)F_{fric}x_B - I_{xz}\cos(\theta)\beta\Gamma\sin(\delta)F_{fric}y_B - I_{xz}\sin(\rho)\cos(\theta)\beta^2\Gamma cl_Q\\
&+ I_{xx}\left(\cos(\theta)\right)^2\beta\Gamma gmr_{OA,z} + I_{xx}K\sin(\alpha)\left(\cos(\theta)\right)^2\beta\Gamma l_Q + I_{xx}\sin(\rho)\left(\cos(\theta)\right)^2\beta\Gamma cl_Q + I_{xx}^2\dot{\theta}\left(\cos(\theta)\right)^2\dot{\Gamma}\\
&+ I_{xz}I_{zz}\cos(\theta)\dot{\Gamma}^2\beta^2 - I_{xx}I_{xz}\cos(\theta)\dot{\Gamma}^2\beta^2 - I_{xx}I_{zz}\left(\cos(\theta)\right)^2\dot{\Gamma}^2\beta + I_{yy}^2\dot{\theta}\dot{\Gamma}\\
&+ I_{yy}^2\dot{\Gamma}^2\beta - I_{yy}\left(\cos(\theta)\right)^2\cos(\delta)\Gamma F_{fric}x_B - I_{yy}\left(\cos(\theta)\right)^2\sin(\delta)\Gamma F_{fric}y_B\\
&- I_{yy}N\left(\cos(\theta)\right)^2\cos(\delta)\Gamma y_B + I_{yy}N\left(\cos(\theta)\right)^2\sin(\delta)\Gamma x_B - I_{yy}K\sin(\alpha)\left(\cos(\theta)\right)^2\beta\Gamma l_Q\\
&- I_{yy}\sin(\rho)\left(\cos(\theta)\right)^2\beta\Gamma cl_Q - I_{yy}\left(\cos(\theta)\right)^2\beta\Gamma gmr_{OA,z} + I_{yy}I_{zz}\left(\cos(\theta)\right)^2\dot{\Gamma}^2\beta + I_{yy}I_{zz}\dot{\theta}\left(\cos(\theta)\right)^2\dot{\Gamma}\\
&- I_{yy}K\cos(\alpha)\left(\cos(\theta)\right)^2l_Q + I_{yy}N\left(\cos(\theta)\right)^2\cos(\delta)l_s - I_{yy}\cos(\rho)\left(\cos(\theta)\right)^2cl_Q + I_{yy}\left(\cos(\theta)\right)^2\sin(\delta)F_{fric}l_s\\
&- I_{yy}^2\dot{\theta}\left(\cos(\theta)\right)^2\dot{\Gamma} - I_{xz}I_{yy}\left(\cos(\theta)\right)^3\dot{\Gamma}^2 + I_{xz}I_{yy}\left(\cos(\theta)\right)^3\dot{\beta}^2 - I_{yy}^2\left(\cos(\theta)\right)^2\dot{\Gamma}^2\beta\\
&+ I_{yy}\sin(\rho)\beta\Gamma cl_Q + I_{yy}\beta\Gamma gmr_{OA,z} + I_{yy}K\sin(\alpha)\beta\Gamma l_Q - I_{yy}I_{zz}\dot{\Gamma}^2\beta - I_{yy}N\cos(\delta)l_s - I_{yy}\sin(\delta)F_{fric}l_s\\
&+ I_{yy}\cos(\rho)cl_Q + I_{yy}I_{xz}\cos(\theta)\dot{\Gamma}^2 - I_{yy}I_{xz}\cos(\theta)\dot{\beta}^2 - I_{yy}I_{zz}\dot{\theta}\dot{\Gamma} + I_{yy}K\cos(\alpha)l_Q + I_{yy}\Gamma\cos(\delta)F_{fric}x_B\\
&+I_{yy}\Gamma\sin(\delta)F_{fric}y_B + I_{yy}N\Gamma\cos(\delta)y_B - I_{yy}N\Gamma\sin(\delta)x_B\Big]
\end{aligned}
\tag{A.2}
$$

References

[1] R. Gasch, R. Nordmann, H. Pfützner, *Rotordynamik*, 2nd ed. Springer Verlag, Berlin, 2002.
[2] G. Schweitzer, E.H. Maslen, *Magnetic Bearings*, 1st ed. Springer-Verlag, Berlin, Heidelberg, 2009.
[3] A. Muszynska, Rotor-to-stationary element rub-related vibration phenomena in rotating machinery - literature survey, *Shock Vib. Dig.* 21 (3) (1989) 3–11.
[4] D.C. Johnson, Synchronous whirl of a vertical shaft having clearance in one bearing, *Arch. J. Mech. Eng. Sci. 1959–1982 (vols. 1–23)* 4 (1) (1962) 85–93.
[5] H.F. Black, Interaction of a whirling rotor with a vibrating stator across a clearance annulus, *Arch. J. Mech. Eng. Sci. 1959–1982 (vols. 1–23)* 10 (1) (1968) 1–12.
[6] M.S. Wojciech, Dynamisches Verhalten eines schnell drehenden Rotors bei Anstreifvorgangen (Ph.D. thesis), TU Karlsruhe, 1986.
[7] F.K. Choy, J. Padovan, Non-linear transient analysis of rotor-casing rub events, *J. Sound Vib.* 113 (1987) 529–545.
[8] P. Goldman, A. Muszynska, Chaotic behavior of rotor/stator systems with rubs, *J. Eng. Gas Turbines Power* 116 (3) (1994) 692.
[9] H.C. Piccoli, H.I. Weber, Experimental observation of chaotic motion in a rotor with rubbing, *Nonlinear Dyn.* 16 (1) (1998) 55–70.
[10] J. Jiang, H. Ulbrich, The physical reason and the analytical condition for the onset of dry whip in rotor-to-stator contact systems, *J. Vib. Acoust.* 127 (6) (2005) 594.
[11] J.C. Pradetto, J. Schmied, Behaviour of a one ton rotor being dropped into auxiliary bearings, in: Proceedings of 3rd International Symposium on Magnetic Bearings, 1992, pp. 145–156.
[12] M.A. Fumagalli, Modelling and measurement analysis of the contact interaction between a high speed rotor and its stator (Ph.D. thesis), ETH – Swiss Institute of Technology Zurich, 1997.
[13] G. Siegl, T. Tzianetopoulou, J. Denk, Simulation and experimental validation of a 9 ton AMB rotor landing in rolling element back-up bearings, *Mech. Eng. J.* 3 (1) . 15-00136.
[14] G. Jacquet-Richardet, M. Torkhani, P. Cartraud, F. Thouverez, T. Nouri-Baranger, et al., Rotor to stator contacts in turbomachines. Review and application, *Mech. Syst. Signal Process.* 40 (2) (2013) 401–420.
[15] G. Schweitzer, Applications and research topics for active magnetic bearings, in: Proceedings of IUTAM-Symposium on Emerging Trends in Rotor Dynamics, March 2009.
[16] R. Gasch, R. Nordmann, H. Pfützner, Die harte Statorberührung – Fanglager [The Strong Stator-Contact – Catcher Bearing], Springer, Berlin, Heidelberg, 1975, pp. 555–573.
[17] T. Ishii, R.G. Kirk, Transient response technique applied to active magnetic bearing machinery during rotor drop, *Trans. ASME* 118 (April) .
[18] G. Sun, A. Palazzolo, A. Provenza, G. Montague, Detailed ball bearing model for magnetic suspension auxiliary service, *J. Sound Vib.* 269 (3–5) (2004) 933–963.
[19] L. Ginzinger, H. Ulbrich, Control of a rubbing rotor using an active auxiliary bearing, *J. Mech. Sci. Technol.* 21 (6) (2007) 851–854.
[20] P.S. Keogh, Contact dynamic phenomena in rotating machines: *active/passive considerations*, *Mech. Syst. Signal Process.* 29 (May) (2012) 19–33.
[21] U. Simon, Rotor - Stator - Kontakt in polygonförmigen Fanglagern [Rotor–stator-contact in polygonal catcher bearings] (Ph.D. thesis), Technischen Universität Carolo-Wilhelmina zu Braunschweig, 2001.
[22] D. Zülow and R. Liebich, Ein aussenrollenlager als fanglagerkonzept für magnetgelagerte rotoren [An external ball bearing as catcher bearing concept], in: SIRM 8. Internationale Tagung Schwingungen in rotierenden Maschinen, Wien, Austria, paper-ID 11, 2009.
[23] S. Lahriri, I.F. Santos, Experimental quantification of dynamic forces and shaft motion in two different types of backup bearings under several contact conditions, J. Mech. Syst. Signal Process. 40 (1) (2013) 301-321.
[24] C.A. Fonseca, H. Weber, P. Fleischer, I. Santos, Analyzing the use of pins in safety bearings, *J. Braz. Soc. Mech. Sci. Eng.* 37 (2015) 1425–1434.
[25] X.X. Wang, S.S. Noah, Nonlinear dynamics of a magnetically supported rotor on safety auxiliary bearings, *ASME J. Vib. Acoust.* 2 (120) (1998) 596–606.
[26] M.T. Cole, P.S. Keogh, C.R. Burrows, The dynamic behavior of a rolling element auxiliary bearing following rotor impact, *ASME J. Tribol.* 2 (124) (2001) 406–413.
[27] J.I. Inayat-Hussain, Nonlinear dynamics of a magnetically supported rigid rotor in auxiliary bearings, *Mech. Mach. Theory* 45 (11) (2010) 1651–1667.
[28] J.J.J. van Rensburg, Delevitation modelling of an active magnetic bearing supported rotor (Ph.D. thesis), North-West University, 2014.
[29] L. Hawkins, P. McMullen, V. Vuong, Development and testing of the backup bearing system for an AMB energy storage flywheel, in: Proceedings of GT2007, ASME ed., May 2007.
[30] H.M. Lankarani, P.E. Nikravesh, A contact force model with hysteresis damping for impact analysis of multibody systems, *J. Mech. Des.* 112 (3) (1990) 369.

Chapter 3

Experimental comparison of the nonlinear dynamic behavior of a rigid rotor interacting with two types of different radial backup bearings: Ball & Pinned

Paper accepted for publication in the journal Tribology International on 18^{th} of July 2017. Available online on 6^{th} of November 2017. DOI: https://doi.org/10.1016/j.triboint.2017.07.018

Tribology International 119 (2018) 250–261

Contents lists available at ScienceDirect

Tribology International

journal homepage: www.elsevier.com/locate/triboint

Experimental comparison of the nonlinear dynamic behavior of a rigid rotor interacting with two types of different radial backup bearings: Ball & pinned

Cesar A.L.L. Fonseca [a], Ilmar F. Santos [a,*], Hans I. Weber [b]

[a] Mechanical Department, Denmark Technical University, Nils Koppel Allé, 404, Kongens Lyngby, 2800 Denmark
[b] Department of Mechanical Engineering, Pontifícia Universidade Católica, R. Marquès de São Vicente, 225 Gávea, Rio de Janeiro - RJ, 22430-060, Brazil

ARTICLE INFO

Keywords:
Rotordynamics
Backup bearings
Experimental nonlinear dynamics
Dry friction whirl

ABSTRACT

Rotors on magnetic bearings rely on external controls to guarantee stability and are designed in case of partial or total failures, when impacts happen and potentially lead to a breakdown. Therefore backup bearings are indispensable. In such rotor-stator interactions the main undesired phenomenon is the backward whirl. The current work investigates the experimental behavior of a horizontal rigid rotor interacting laterally with two types of backup bearings during run up testing. The experimental data is analyzed by orbit analysis, spectrum analyzers, and force magnitudes collected by sensors installed. It is shown experimentally the nonlinear behavior of the rotor-bearing system and the elimination of backward whirl. The advantages and drawbacks of each type of backup bearing are given.

1. Introduction

Developments in the field of rotordynamics have increased the important role of mechanical devices required by safety measures to protect the rotating machines, thanks mainly to the recent advances in magnetic bearings. These machines have still not been used in many industrial applications due to safety concerns among others. Therefore a lot of effort and research has been done to understand the consequences of the interaction between the rotor and the backup bearing for improving the quality and thus the safety properties of such elements. The safety bearing consists usually of a bearing with a slightly smaller clearance than that of the magnetic bearing, thus avoiding contact on the final one.

Johnson [1] was one of the first to publish a study on rotors with clearance. His model describes two cases, one undamped and another damped, with the rotor impacting on a circular surface, but he did not include the friction force itself. His investigation was more related to equilibria stability and whether the solutions of the synchronous whirl are positive. The friction force was added in the work of Black [2], whose 2D model presented a whirling and whipping effect caused by the friction coefficient when the rotor is in contact with the surface. Szcygielski [3] performed an analytical and experimental comparison of a gyro pendulum. His results showed good agreement with his piecewise linear model for impacts on the mechanical model. Lingener [4] and Crandall [5] published their findings confirming Black's theoretical results that the rotor may whirl with a slightly lower coupled eigenfrequency. However in 2000, Bartha [6] contested their results using an extended model. He proposed that the system should be modeled as a rotor inside nested rings.

Since the rotor with clearance is subjected to non-smooth impact and friction forces, other nonlinear phenomena may appear such as chaotic motion. Ehrich [7] indicated that when the rotor is performing a rubbing it can develop into chaotic behavior. This was confirmed by Goldman and Muszynska [8] as long as a proper impact model is employed. Muszynska [9], and Jacquet-Richardet [10], have also published an extensive review on the contact of a rotor and stator mentioning some of its most common problems in the academia and industries and how to deal with it.

The backup bearing is an essential element for the feasibility of magnetic rotors according to Schweitzer [11]. These machines are designed to be levitated rotors in vacuum and to operate at very high speeds. Therefore the control of the magnetic field has to be reliable. Nevertheless, failures and external factors can lead to malfunctioning and shutdown that eventually will cause the rotor to execute bigger amplitudes. The safety bearings work as the final mechanical threshold, in order to save the rest of the machine from further damages. The several contacts between the shaft and the backup bearing introduce nonlinear features in the dynamics of the system. In the thesis of Isaksson [12] the contact between a disk with a moving wall showed clearly nonlinear

* Corresponding author.
E-mail addresses: cefonse@mek.dtu.dk (C.A.L.L. Fonseca), ilsa@mek.dtu.dk (I.F. Santos), hans@puc-rio.br (H.I. Weber).

https://doi.org/10.1016/j.triboint.2017.07.018
Received 5 April 2017; Received in revised form 17 July 2017; Accepted 18 July 2017
Available online 6 November 2017
0301-679X/

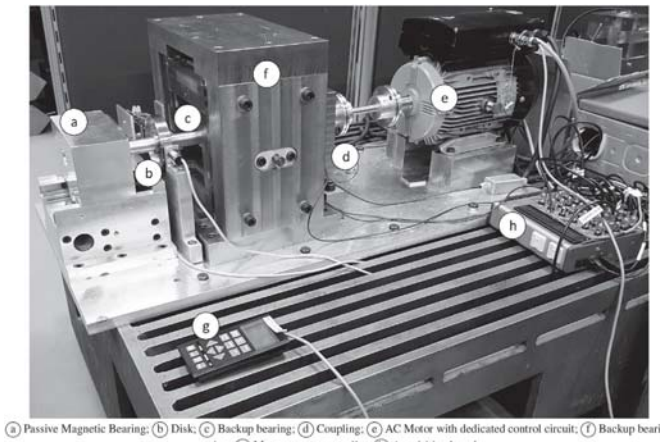

(a) Passive Magnetic Bearing; (b) Disk; (c) Backup bearing; (d) Coupling; (e) AC Motor with dedicated control circuit; (f) Backup bearing casing; (g) Motor remote controller; (h) Acquisition board.

Fig. 1. Test rig setup.

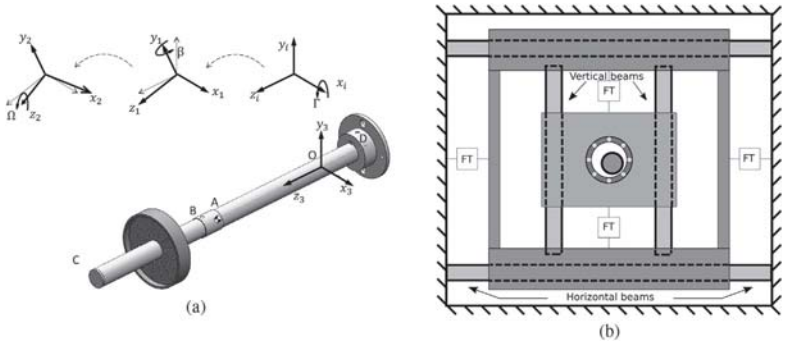

Fig. 2. The drawings illustrate how the shaft is able to move inside the bearing. In a), one sees the angles that describe the movement of the shaft. In b), the force transducers.

Table 1
Specifications of the levitated test rig at DTU's facilities.

Rotor		Inner and outer house	
Mass without unbalance	1.28 kg	Mass from inner house	1.70 kg
Length to magnetic bearing	384 mm	Mass from outer housing	8.87 kg
Length to rolling bearing	211 mm	**Force Sensor**	
Shaft diameter	$d_r = 25$ mm	Force transducer stiffness	83 MPa
Rolling bearing		**Pins**	
Inner diameter	28 mm	Length of the pins	2.0 mm
Inner race outer diameter	32 mm	Radius of the pins	4.0 mm
Sphere radius	5.0 mm	Radius of the circular wall	38 mm

phenomena such as bifurcation diagrams and hysteresis when accelerating and decelerating. Fumagalli [13] developed an investigation of the contact with different impact models previously done by Hertz [14] and Hunt and Crossley [15]. The impact parameters were determined and how they influence the dynamics of the system when the rotor slides and tumbles on the backup bearing. Pradetto and Schmied [16] presented an experimental investigation with a one-ton rotor drop, which provided valuable results on a real rotating machine drop test on its auxiliary bearing. In 1998, Piccoli and Weber [17] observed experimentally chaotic motion in rotors and confirmed it using Lyapunov exponents. Polygonal shapes of backup bearings were tested analytically and experimentally by Simon [18]. The bearing wall was geometrically varied from a simple circular wall, to a triangle and a square and could be extended to any polygon. In any of these cases the numerical simulations showed that the disk described a quasi periodic trajectory while hitting all edges of the bearing, although the circular one induced a backward whirl motion. Ginzinger et al. [19] presented an active auxiliary bearing with linear actuators, which showed a significant reduction of the contact forces. Then Zü low and Liebich [20] designed a flexible pin with roller on the tip, which was meant to reduce the friction forces during contact.

More recent published works by Said et al. [21,22] determined through a pin-on-disk experiment the coefficient of friction of a body probe and later tested it on a horizontal rotor. Later in 2012 the Said and Santos [23] tested the idea of using pins instead of a circular guide as a backup bearing. Both papers give a good overview of the advantages of employing pins instead of circular wall, especially when avoiding the backward whirl scenario. A further study from Fonseca et al. [24] used length varying pins on a vertical rotor bench. The setup helped the rotor to surpass the known resonance while accelerating. Hui Ma et al. [25] also investigated theoretically the dynamical response of a pinned

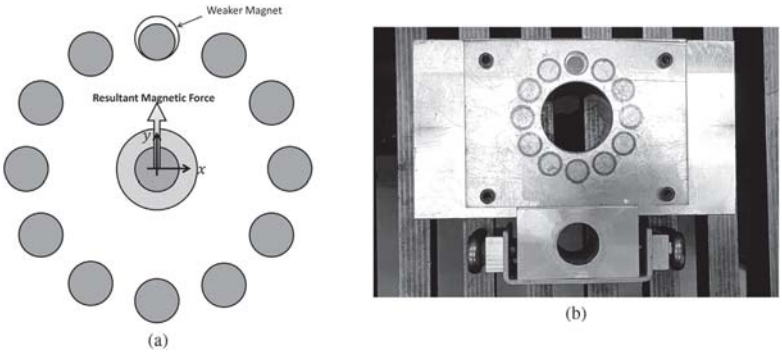

Fig. 3. The passive magnetic bearing.

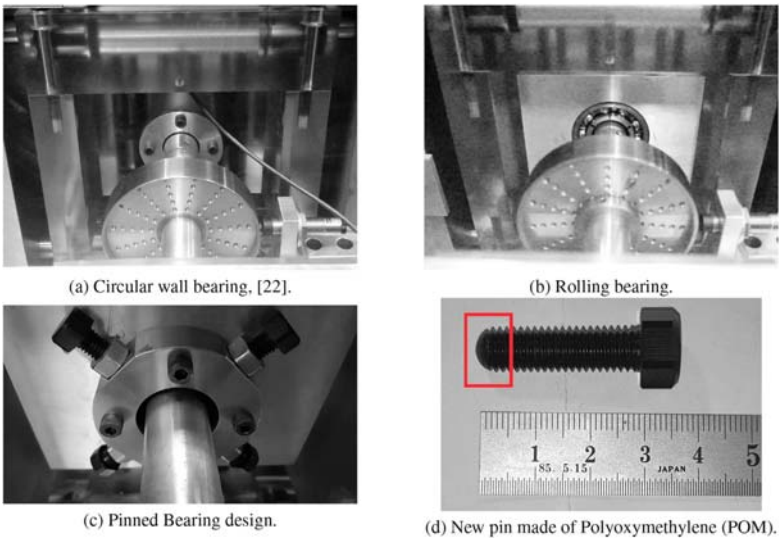

Fig. 4. Different types of backup bearings.

backup bearing using the Finite Elements Method to characterize the impact phenomenon. The authors also showed the difference between three to four pins in the orbit patterns and performed a frequency analysis where multiple frequencies were excited. In his Phd Thesis, van Rensburg [26] let an active magnetic bearing rotor to drop on backup bearings and defined delevitation levels for several angular velocities. Similarly, in Fonseca et al. [27], chaotic orbits were observed depending on the unbalance mass the rotor has. Both works conducted an experimental and theoretical approach to the topic. In Ref. [28] the authors used a Stribeck-model of friction model for a thermal analysis of a drop test on a sleeve backup bearing. Halminen et al. [29] published a rotor drop test model of misaligned backup bearings, where a ball bearing isconsidered as backup bearing. They mentioned that in case of large misalignment, it may lead to significant damage to the rotor and the bearing. In Ref. [30], the authors proposed a technique to acquire experimentally the forces of an active magnetic bearing during contact with backup bearing. Cole and Hawkins [31] developed a model to predict possible subsynchronous whirl behaviors found in rotor drops.

The current work aims mainly to compare two types of backup bearings for magnetic bearings rotors through experiments. The first one will be an ordinary ball bearing, widely used in the industry, and the second one a pinned bearing designed to withstand the impact forces. Meanwhile, this pin is intentionally made of a polymer instead of metal from past tests. Its friction properties will be assessed with a pin-on-disk device in order to present the pinned bearing a solution to the safety issue. The magnets at the magnetic bearing of the test rig are, in fact, not capable of limiting the orbit of the shaft as it crosses through its own natural frequency. Therefore the test rig is ideal for representing the cases of real active magnetic bearings, whose control is faulty or weak. In this work, the shaft is run at different speeds and its position is constantly being tracked and the forces measured by force transducers inside the backup bearing housing. The different ways that the rotor crosses its own resonance will now be presented and dynamical nonlinear features explored for each type of backup bearing.

2. Rotor-bearing-system

Fig. 1 is a photo of the test rig at the facilities at DTU. This test bench

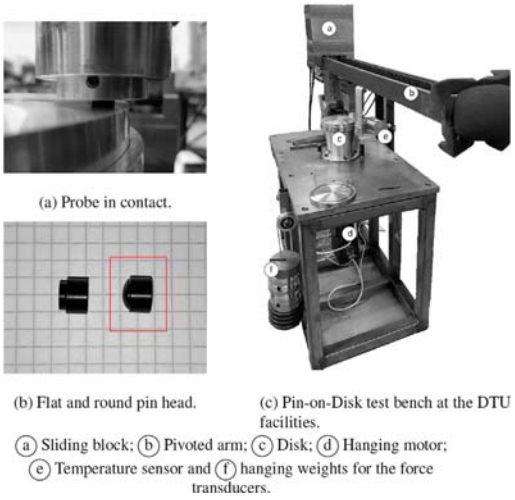

Fig. 5. Photographs of the Pin-on-Disk test rig.

rotor with a passive magnetic bearing in one end of the shaft is simply supported at the other end and also connected through a coupling to an embarked control AC-Motor. The shaft is made of aluminum and contains a disk which can hold an unbalance mass, (see Fig. 2a). This setup has been widely tested in previous works [22]- [23] and the design and construction of the parts in Ref. [32] with the main specifications given in Table 1. The rotor has a backup bearing mounted inside a housing, in which four internal force transducers allow the force vector to be measured. Thus, it is possible to determine the contact forces that eventually occur when the rotor touches the backup bearing. The housing can be separated into three pieces: the external structure, the outer housing and the inner housing. The external structure is considered rigid all the time, while the others are only allowed to move each in one direction. The outer house moves horizontally and the inner house, vertically. Therefore there is no coupling between the movements. Observe Fig. 2b where the locations of the transducers are shown.

The magnetic bearing is built as a set of cylindrical neodymium magnets distributed circularly. Although the shaft is made of aluminum, there are also magnets inside it. Therefore the shaft interacts always repelling with each magnet in the bearing, except the top one, which has its polarity inverted. A schematic of the faulty magnet and the assembled piece is displayed in Fig. 3.

The type of backup bearing varies according to the desired study. In previous works [22],- [23], the backup bearing was a simple circular wall, Fig. 4a. When the rotor impacted on it, the risk of developing a backward whirl was high and consequently high radial forces were detected. For this reason, in industrial applications, the most common safety device is the ball bearing, Fig. 4b.

The backup bearing is inside the inner house and is a common ball bearing, on whose inner ring the shaft impacts, slides and rolls. The inner ring accelerates until its tangential angular velocity matches with the one on the surface of the shaft. The acceleration is only caused by the existing friction force. As long as the tangential velocities are not the same, the friction force is considered as a sliding force proportional to the normal contact force and is acting on both bodies. The design of this test rig has the advantage of being rather easy to change the type of backup bearing by just modifying the inner housing.

Another backup bearing type is the adjustable length pinned bearing, Fig. 4c and d. It is a circular bearing that contains four screwed pins. The

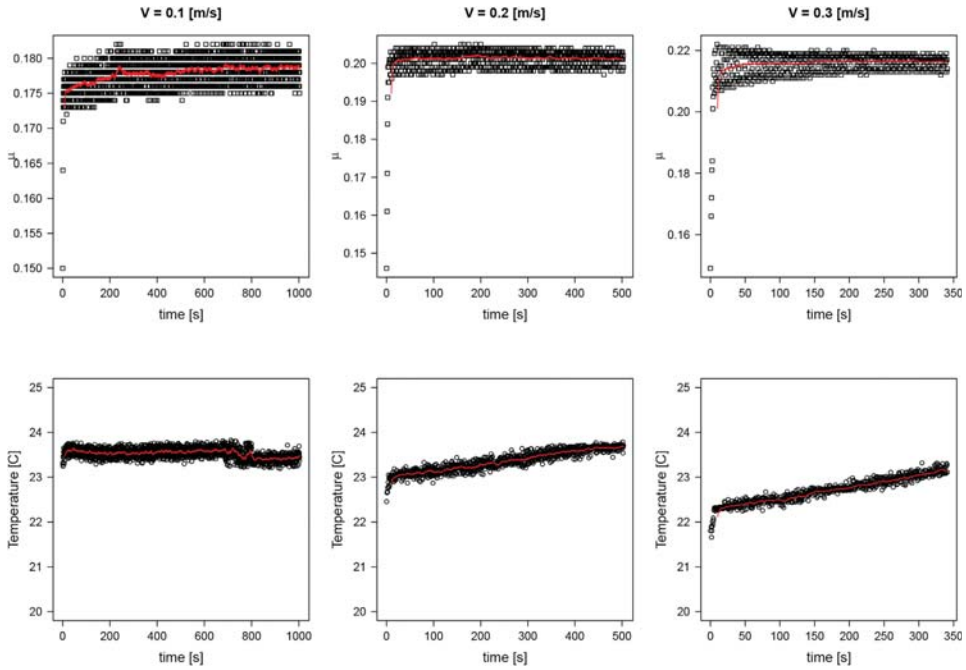

Fig. 6. The change in time of μ due to wear.

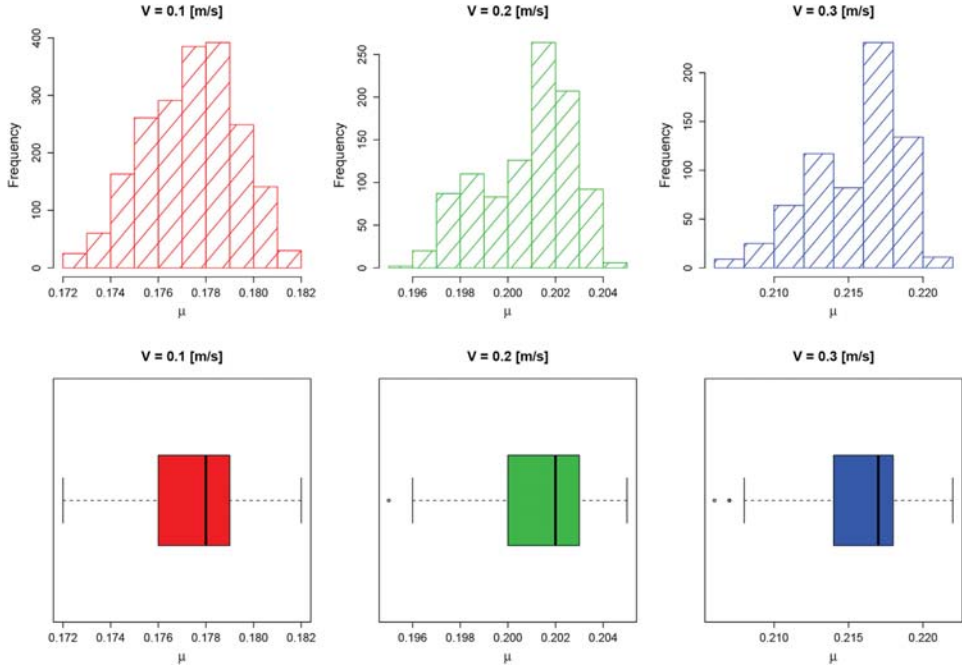

Fig. 7. Histograms of the coefficient μ.

Table 2
μ parameter.

Average pin-on-Disk test results for friction		
$V_{contact} = 0.1$ m/s	$\mu = 0.1778$	$\sigma^2 = 0.00194$
$V_{contact} = 0.2$ m/s	$\mu = 0.2012$	$\sigma^2 = 0.00190$
$V_{contact} = 0.3$ m/s	$\mu = 0.2180$	$\sigma^2 = 0.00299$

length of the pins are equal and set to match the minimum in order to avoid any contact with the metallic structure. Further details will be discussed in sections 3 and 4.

The purpose of the present work is to compare the dynamical behavior of the rotor while it is levitated by a weak magnetic bearing and is in contact with two types of the backup bearing. The impacts will happen, when the rotor slowly reaches and crosses the resonance, or it is hit by an external device.

3. Characterization of the pins

If one is interested in the determination of the efficiency of a new mechanical design, its parameters and physical properties should be analyzed. The pinned bearing will have to support strong impacts and the shaft would certainly not settle down or stay at a permanent contact state if there is any kind of failure. Since the interaction is between polymer (POM) and aluminum, two parameters become the subject of investigation, *i.e.* the friction coefficient and wear rate. The test rig available at DTU, shown in Fig. 5c, is designed to acquire those two parameters. The test rig was developed by Jacobsen and Christiansen [33] and follows the specifications given by the American Society for Testing and Materials (ASTM) standard G99. The test pin is positioned under a pivoted arm and it touches a 134 mm diameter disk that is rotated by a hanging motor under the test rig frame. The structure that supports the rotor has a lever, which is attached to a force transducer. Therefore it is possible to measure the friction force as a relationship between the radial distance from the center of the disk to the point of contact of the pin with the lever length. Finally the normal force applied to the pin can be adjusted by block sliding over the arm. The setup is actuated and run by a Labview acquisition board and it gathers all possible information on time. The tests are performed following the work of Sarkar [34]. The test rig is also able to measure temperature at the point of contact through a laser sensor and the vertical gap from the pin to the disk for wear related problems.

Two types of pins are tested for simulating friction and wear on the backup bearing pin end. One is flat and the other is round, Fig. 5b. The former is required for the determination of the coefficient of friction and the latter is strictly used for wear tests and to verify the dynamics of this coefficient in time when the contact is extended for hours. For the purpose of this work the pin is made of POM and has the same diameter as the pin. Observe also in Fig. 3d the round tip on the pin, that is then reproduced in the pin with a round surface. The disk is made of aluminum, the same as the shaft.

Three different speeds at the point of contact are tested; $V_{contact} = 0.1$ m/s, $V_{contact} = 0.2$ m/s and $V_{contact} = 0.3$ m/s. Since the scenario of a permanent contact between the shaft and the pins is not probable, a steady but slower angular velocity with an applied force of 200 N (≈ 3.9 MPa) is enough for the desired tests. Then one sees the evolution in time of the coefficient of friction in Fig. 6. In every test the distance the pin should slide is 100 m. It is clear that in a few seconds, the values converge and the results show that the sliding friction between the two materials is approximately between 0.18 and 0.22. Fig. 7 illustrates the histograms together with a boxplot for each of the runs as summarized in Table 2.

3.1. Wear test

Subsequently, another test is performed, in which a round tip pin is

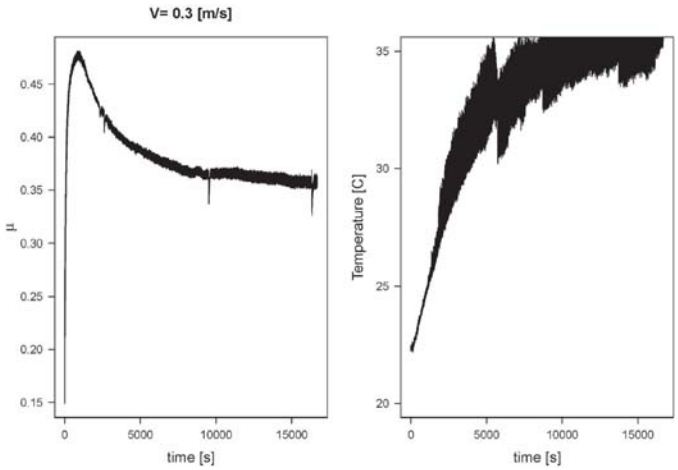

Fig. 8. Dynamics of the coefficient of friction during a long wear test.

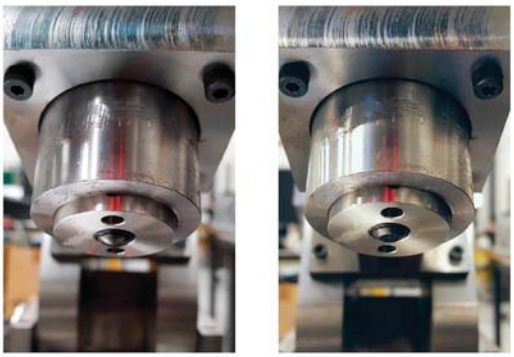

Fig. 9. Wear on the round pin.

installed. The idea behind this test is to observe the wearing process between the two materials. It is not unrealistic to think that a device that withstands a lot of impact will experience some wear effects. Also, as mentioned in the beginning of this section, the round pin serves to imitate the result of a long used pin in the backup bearing, Fig. 4c and d.

The test differs from the previous ones not only with the type of pin, but also with the normal force applied (150 N) and most importantly for the distance, which now is 5000 m until the stop as observed in Fig. 8. The development of the friction coefficient is similar to the previous one, because it shows an earlier saturation around 0.2. Actually its value rose reaching a peak of 0.4 and slowly went back and stayed at 0.35 while the temperature kept steadily rising. The result is seen in Fig. 9b where the punctual contact became a wide area. In the beginning, the area of contact is zero thus the tension on the surface is theoretically infinite. This means it is expected that there will be initially some wear but would slow down later. After the test the pin has lost around 20% of its original volume and the surface flattened.

4. The ball bearing experimental results

The main reason that there is a backup bearing is to limit the orbits of a rotor and to protect the rest of the machine. The gap between the shaft and backup bearing is smaller than the one where the magnets are, and thus the magnetic bearing is spared. Here the rotor is accelerated by a Danfoss 4 HP AC motor that is capable of keeping its angular velocity constant, thanks to an embedded controller. The desired angular velocity is given by a signal from a computer. Also an encoder is connected to the rear end of the motor the angular position and the actual velocity are monitored in real time.

So, the rotor is configured to run an increased stepped response in time from 0.5 Hz until it reaches 20 Hz increasing every 10 s by 0.5 Hz. This result in 40 different levels of angular velocities applied to the rotor. The time interval is enough to eliminate any transient. The velocity pattern is plotted in Fig. 10 Through a Fourier Spectrum graph, the natural frequency of the rotor is close to 11 Hz and high orbits are expected close to this velocity. The weak magnetic bearing force and the shaft's own weight cause the resting position to be already close to the backup bearing inner ring. Consequently, the first impacts are already seen at speeds higher than 8.5 Hz.

The impacts and the shaft's interaction with the magnets change the

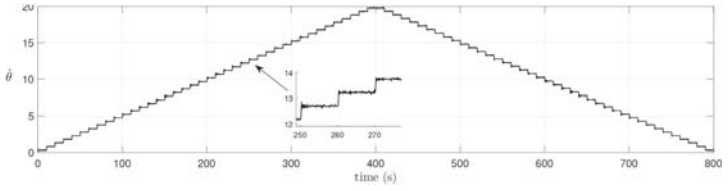

Fig. 10. Velocity pattern applied to the rotor. In the detail, one sees the angular velocity being constant after each increase.

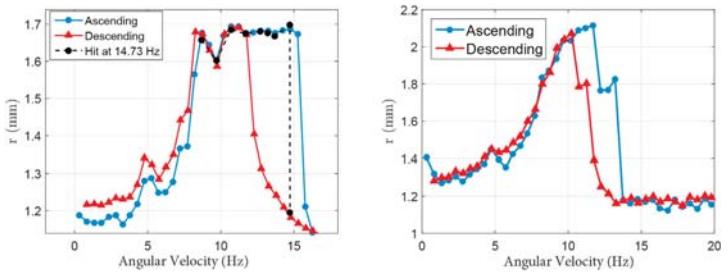

(a) Ball bearing. (b) Pinned bearing.

Fig. 11. Captured hysteresis of different scenarios. a) The given hit at the shaft changes the shaft's behavior. b) The pinned bearing case.

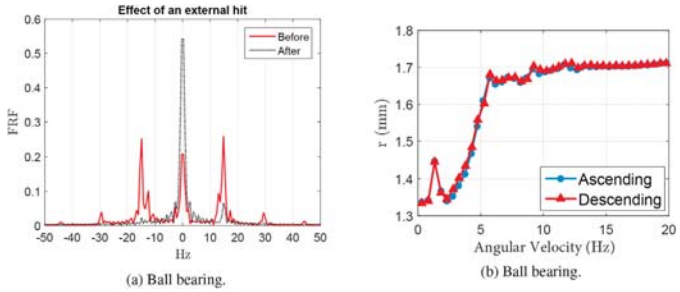

(a) Ball bearing. (b) Ball bearing.

Fig. 12. Captured hysteresis of different scenarios. a) The change at 14.7 Hz in the double sided spectrum before and after an external hit. b) Permanent contact due to high unbalance.

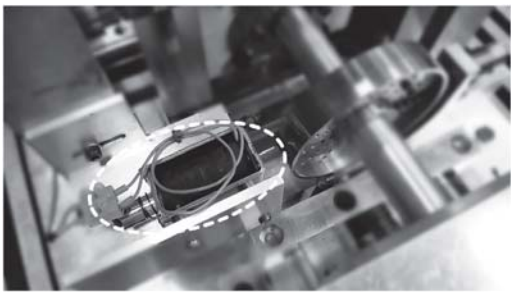

Fig. 13. Solenoid actuator with return spring.

shape of the orbit. Primarily, the impacts happen at one point inside the circular bearing surface, but as the angular velocity increases the shaft impacts on more locations. Besides, the rotor keeps in this whip movement even after the resonance is surpassed. After 15 Hz the orbits get smaller and there is no more contact on the backup bearing. Interestingly, when decelerating from 20.0 Hz to 0.0 Hz the rotor will only return to impact at 12 Hz. This is a common nonlinear hysteresis case in which there is a stiffening effect happening acting on the mechanical system, see Fig. 11a.

Thanks to the position sensors placed on the disk, it is possible to recreate the orbits for each angular velocity. Fig. 14a and b illustrate the run up and down accordingly. These orbit plots give us a good insight into the trajectory of the shaft. It became clear that there is a shift in the trajectory after the resonance. What was once a rather large orbit hitting the backup bearing in two points, now shifts to a "hop" movement almost vertically. With these impact dynamics conditions, an external hit is given to the rotor and it lowers the orbit. On the side of the rotor, a solenoid actuator is mounted to hit the rotor, (see in detail in Fig. 13). The purpose of the actuator is to try to provoke a hysteresis jump, or in other words, to remove from an impactless orbit to a repeatable impacting one and vice-versa. Here a single hit was capable to remove from the impact state at 15 Hz to an ordinary circular orbit. This change is seen in Fig. 11a with a dashed line.

4.1. Effect of the unbalance

When running close to the natural frequency, the expected large amplitudes caused by the unbalance are limited by the backup bearing. Consequently the impacts on the bearing wall may happen earlier at slower angular velocities and the hysteresis is broader. If the unbalance is big enough and if the magnetic bearing is completely deactivated, it is possible that the rotors perform a chaotic trajectory. A sequence of hits done by the solenoid tried to remove the shaft from the contact state when decelerating. For every decrement in angular velocity, a single hit is given, but proved to be unsuccessful.

Problems regarding the unbalance in rotor-machinery are also dealt with in testing. In the present case, where there is an imperfect suspended magnetic rotor with an additional unbalance mass (30.0 g at 33 mm from the center of the shaft), the nonlinear hysteresis phenomenon is not present and it stayed always in contact. The rotor radial displacement is displayed in Fig. 12a and their respective orbits are plotted in Fig. 15. A sequence of hits done by the solenoid tried to remove the shaft from the contact state unsuccessfully when decelerating. For every decrement in angular velocity, a single hit is given.

The contact state is dependent on the relative velocity between the shaft and the inner ring surfaces. When it reaches zero the friction force is minimum, the backward whirl is not excited and the rotor executes a 1X-

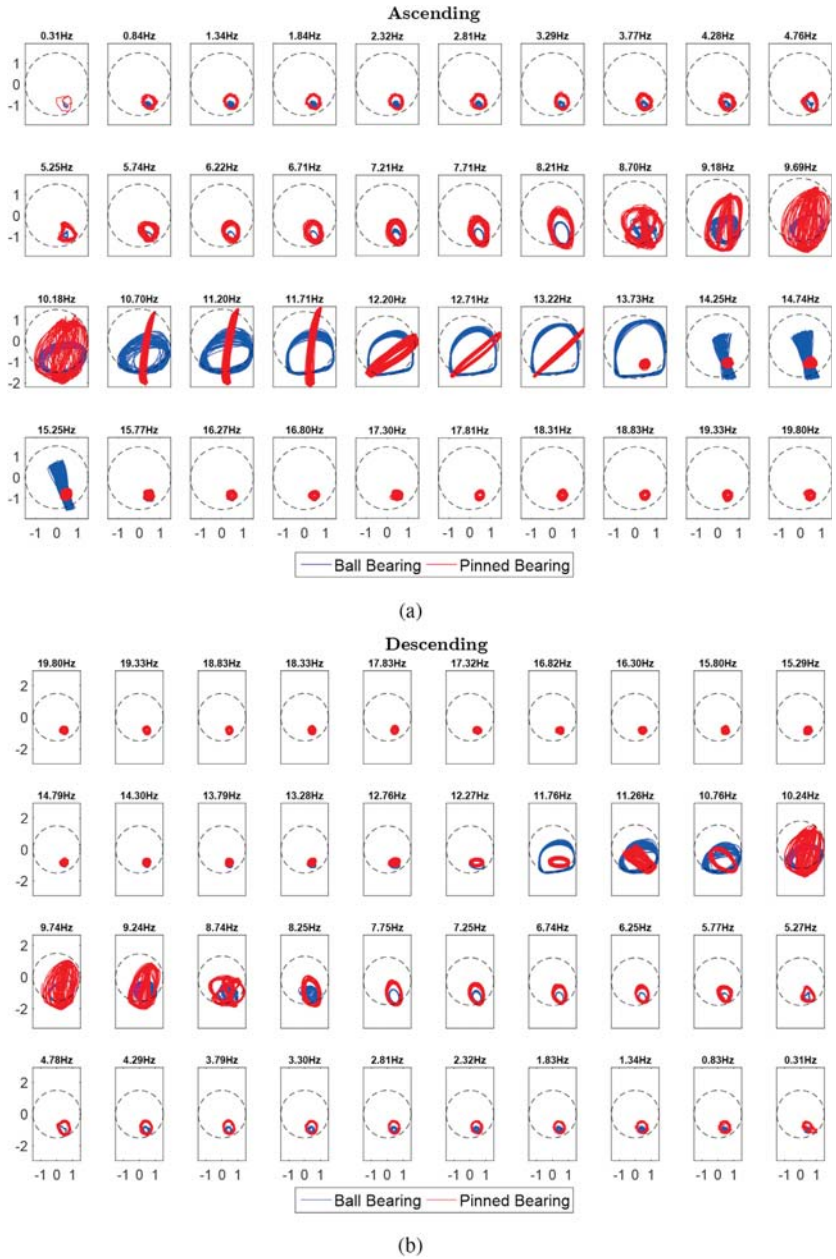

Fig. 14. Comparison of the rotor's orbit between the two types of backup bearings: the ball bearing and pinned bearing. The angular velocity is kept constant at 40 different values from 0 to 20 Hz a) run-up 0–20 Hz b) run-down 20-0 Hz.

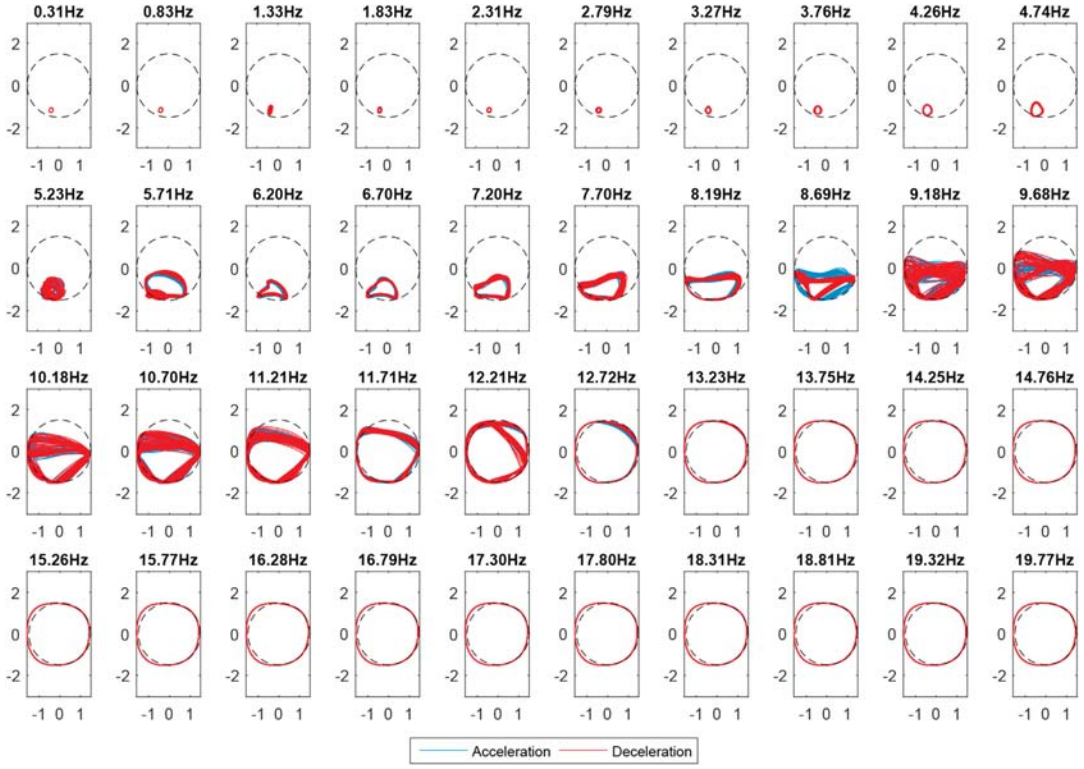

Fig. 15. Unbalance test.

forward whirl, even if the unbalance is high. In Fig. 16a and b one can compare the nature of the trajectory (whether it is forward or backward), through a waterfall diagram. The solid lines represent the 1X and 2X frequencies on the positive and negative sides. The region painted in green in Fig. 16b is the permanent contact state and only the 1X frequency is seen as relevant.

Additional pieces of information that are important can also be extracted from this test rig. First, the rotor can be accelerated/decelerated fast enough so that it does not impact the backup bearing. Then, the maximum allowed unbalance mass is determined that can be mounted at 33 mm radially on the shaft's disk. All of these results are written in Table 3.

5. A pinned bearing solution

The test rig is designed in a way that it is easy to change the type of backup bearing. In past works [22],- [23], a pinned bearing was proposed and its efficiency tested in many cases. The back up bearing has slightly more space for the shaft to move, but this is determined by the length of the pins. The tighter and smaller the inner space is, the more the pinned backup bearing would look like a simple circular wall. The current set up provides the maximum space of the shaft to move around without touching the metallic casing. Hence the shaft needs to touch on two pins at the same time and hypothetically in one point on the metal casing. To avoid any encounter between the shaft and the wall, each pin was given an additional quarter turn. If one has loose or broken pins the shaft will impact the structure and it will cause a metallic sound hit that is easily perceived. Extremely tight pins can provoke the shaft to develop a backward whirl trajectory.

In previous experimental tests, the pins were made of steel [22],- [23], then the angular velocity of the rotor was never higher than 7.0 Hz, because it damaged the shaft significantly, while crossing the resonance around 10.0 Hz due to the high magnitude of the impacts. The solution to this problem was to change the pin to a different and softer material, which is Polyoxymethylene (POM). This polymer has some advantages, for example, a relevant damping effect, and it has been in use in industrial applications to avoid mechanical vibrations such as pump parts and connectors.

The same 0–20.0 Hz velocity pattern shown in Fig. 10 is employed again, which means that the rotor shall cross the resonance and impact on the pins. The radial displacement is displayed in Fig. 11b and shows the rotor does bigger displacements in relation to the previous case, Fig. 11a. In the same manner as before with the ordinary ball bearing, the rotor has a slightly different behavior when decelerating which produces a hysteresis effect.

The expected behavior showed that impacts happened when the angular velocity was close to the resonance hitting from one pin repeatably to three pins in a disordered manner. However, the trajectory changes to a rather simple contact state, in which the rotor impacts on pins in opposition to each other around 10.5 Hz. Later, the trapped trajectory dissolves into an ordinary circular one after being increased to 13.7 Hz, see Fig. 14.

The behavioral change of the rotor when impacting is related to the friction force. It strengthens the backward whirl orbits and stays “hopping” in the vertical direction because it is weaker in this direction.

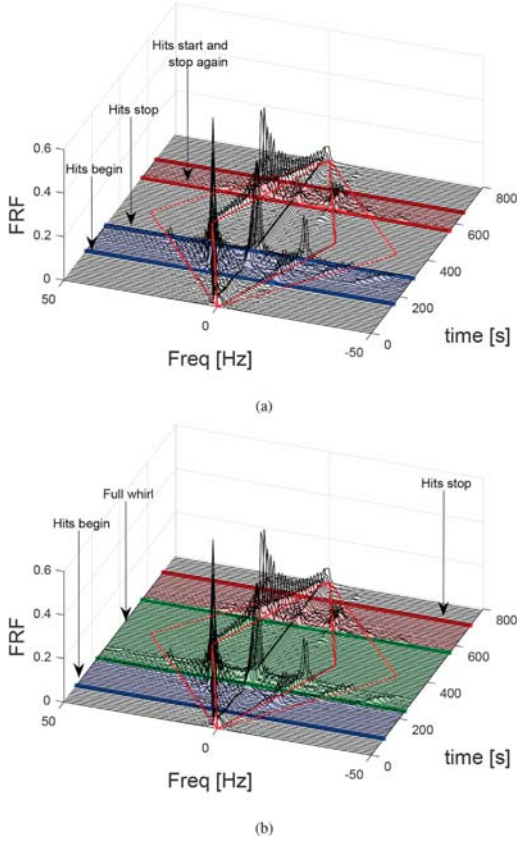

Fig. 16. a) Double sided FRF no unbalance mass. b) Double sided FRF with unbalance mass.

Table 3
Special characteristics for the current test rig.

Time to accelerate without any impacts (no unbalance)	0.75 s
Time to decelerate without any impacts (no unbalance)	0.50 s
Maximum allowed imbalance for permanent contact state	6.20 g

6. Force comparison

As mentioned previously, section 2, the test rig contains four force transducers between two housings. Hence, it is possible to measure the horizontal and vertical impact force components. During acceleration the rotor's impacts are detected when it spins closer to the resonance. The closer it reaches the resonance the bigger the magnitude of the impact is. The changes in magnitude for each angular velocity are shown in Fig. 17, where the black line represents the ball bearing case and the gray line is the pinned bearing case.

The first difference between them is that the pinned bearing allows the rotor to enter a safe circular orbit at a slower angular velocity. Consequently it avoids the highest forces detected by the ball bearing case, which happen after resonance around 15 Hz. This transition is shown above the main plot. Here the gray spikes of each impact vanish after 271.5 s when the black ones continue. But the pinned bearing presents bigger force magnitudes especially at every change in velocity. However, when decelerating not only the shapes of the orbits are different, but also the magnitudes of the force start considerably lower in the pinned bearing case in relation to the ball bearing case.

- Stress analysis on the pin

In light of the impact problems of the test rig and since the pin material was changed, a stress analysis of the pin becomes indispensable. A finite element model (FEM) is generated in the Ansys environment with two bodies representing the pin and half a shaft, whose opposing faces are configured as contact elements with friction. The bottom of the pin is fixed and the half plane of the shaft receives a normal force of 90 N. Also the shaft is set to have an angular velocity of 94 rad/s (15.0 Hz), which corresponds to the last impacting velocity orbit. These values were extracted from the experimental data shown in Fig. 17 in the worst case scenario.

The FEM produced a consistent result, where one sees the tip of the pin showing extremely higher stresses, Fig. 18a. The highest calculated stress is located in the pin and is in the order of magnitude of 130 MPa. This magnitude of the stress is above any measured yield strength of POM ($\sigma_{yield} = 64$ MPa).[1] On the other side, the shaft's surface receives the same magnitude, but it is below the yield strength of the aluminum, see Fig. 18b. Therefore the surface of the rotor is preserved.

7. Conclusions

The test performed helped to understand the different advantages and drawbacks between two types of backup bearings designed for rotors such as magnetic levitated rotors. The rolling bearing and the pinned one as backup bearings showed efficiently that the rotor could surpass its critical speed step-by-step in the test scenarios of a faulty magnetic bearing. The case of the rotor with an unbalance mass was revealed as troublesome, because it remained in the contact state after crossing the resonance for a long period and even the external small hits were ineffective to remove from the contact state. Further tests could not be performed due to high radial force that would lead to damages to the shaft. Also during the tests the onset of backward whirl was not observed, highlighting the efficiency of both types of bearings as the speed accelerates and decelerates.

When comparing the both types of bearings, it is possible to conclude that the pinned bearing can better prevent sustained contact when running through critical speeds due to the fact the pins are made of POM. POM has definitely better properties towards vibration attenuation than a wall made of steel. Nevertheless, comparing the clearances of the pinned bearing with the ball bearing, one can conclude that they are slightly larger in the case of the pinned bearing, allowing the rotor to execute orbits with larger amplitudes. Besides, the friction forces will be discontinuous and their direction will change at each impact. This definitely plays a role. It is important to highlight that too tight clearances with longer pins approximate the borderline to a square gap, as presented in Ref. [21], and causes the rotor to perform backward whirl, which invalidates any advantages of the use of pins.

The material POM has also revealed itself to be a good choice for manufacturing the pins especially after their friction and wear characteristics were assessed. Since POM is a softer material, wear is expected to happen mostly on it, however, wear was only determined for a very long contact case meaning pins have to be checked after a series of many impact events. These results are corroborated by the finite element model showed that pin's tip experiences loads higher than yield stress, whereas the shaft is not.

[1] Online resource in Ref. [35].

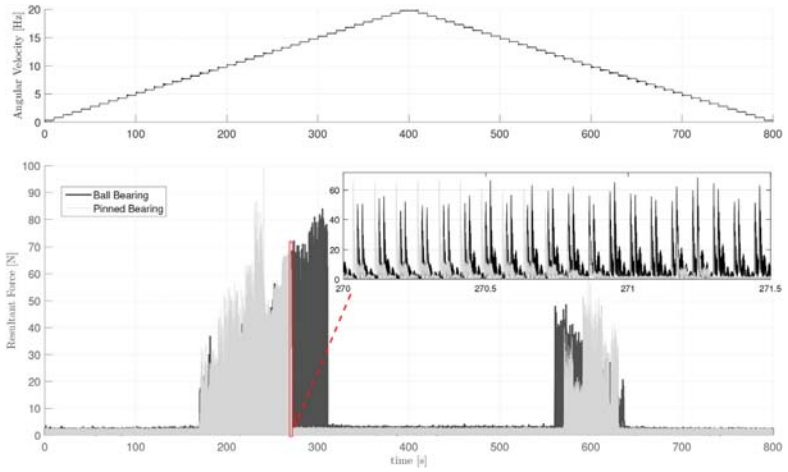

Fig. 17. Overview of the magnitude force measured between both types of backup bearings during run up and down.

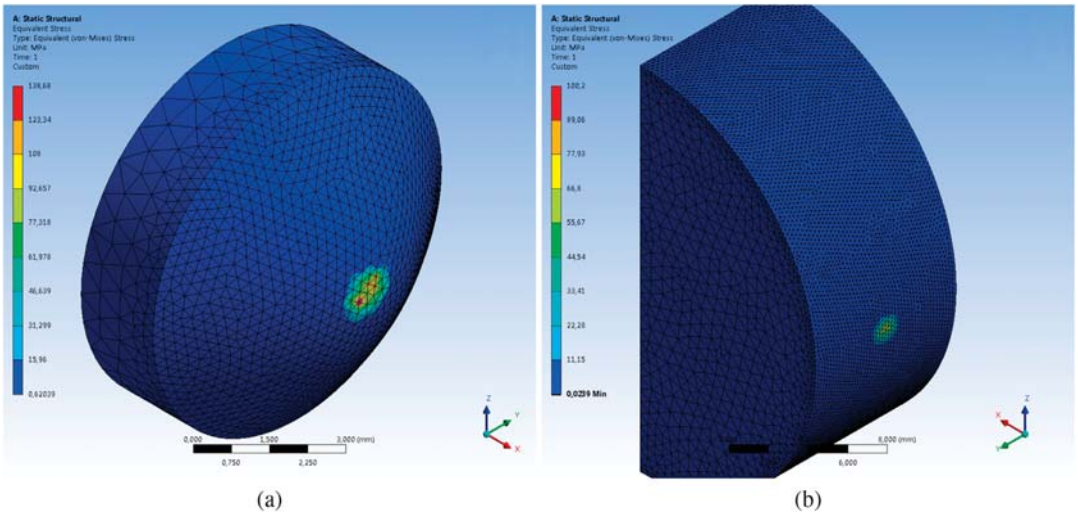

Fig. 18. The stress on the pin above the yield strength on the top, (a), and the opposed shaft face, (b), below its yield stress.

Acknowledgement

The authors express their acknowledgement to CNPq through the Science Without Borders Program with the process number: 249728/2013–3, which partially sponsored the elaboration of this paper.

References

[1] Johnson DC. Synchronous whirl of a vertical shaft having clearance in one bearing. 1959-1982 (vols. 1-23) Arch J Mech Eng Sci 1962;4(1):85–93. https://doi.org/10.1243/JMES_JOUR_1962_004_012_02.
[2] Black HF. Interaction of a whirling rotor with a vibrating stator across a clearance annulus. 1959-1982 (vols. 1-23) Arch J Mech Eng Sci 1968;10(1):1–12. https://doi.org/10.1243/JMES_JOUR_1968_010_003_02.
[3] Wojciech MS. Dynamisches Verhalten eines schnell drehenden Rotors bei Anstreifvorgangen. Phd thesis. TU Karlsruhe; 1986.
[4] Lingener A. Experimental investigation of reverse whirl of a flexible rotor. In: Proceedings of the 3rd IFToMM international conference on rotordynamics; 1990. p. 13–8.
[5] Crandall S. From whirl to whip in rotordynamics. In: Transactions of the 3rd IFToMM international conference on rotordynamics; 1990. p. 19–26.
[6] Bartha AR. Dry friction backward whirl of rotors. Thesis no. 13817. ETH – Swiss Federal Institute of Technology Zurich; 2000.
[7] Ehrich F. Observations of subcritical superharmonic and chaotic response in rotordynamics. J Vib Acoust 1992;114(1):93.
[8] Goldman P, Muszynska A. Chaotic behavior of rotor/stator systems with rubs. J Eng Gas Turbines Power 1994;116(3):692.
[9] Muszynska A. Rotor-to-stationary element rub-related vibration phenomena in rotating machinery - literature survey. Shock Vib Dig 1989;21(3):3–11.
[10] Jacquet-Richardet G, Torkhani M, Cartraud P, et al. Rotor to stator contacts in turbomachines. review and application. Mech Syst Signal Process 2013;40(2):401–20.
[11] Schweitzer G, Maslen EH. Magnetic bearings. first ed. Springer-Verlag Berlin Heidelberg; 2009.

[12] Isaksson JL. On the dynamics of a rotor interacting with non-rotating parts. Phd thesis. Linköping University; 1994.
[13] Fumagalli MA. Modelling and measurement analysis of the contact interaction between a high speed rotor and its stator. Ph.D. thesis. ETH - Swiss Institute Of Technology Zurich; 1997.
[14] Hertz H. On the contact of solids-on the contact of rigid elastic solids and on hardness. 1896.
[15] Hunt KH, Crossley FRE. Coefficient of restitution interpreted as damping in vibroimpact. Ser E J Appl Mech Trans ASME 1975;42(2):440–5.
[16] Pradetto JC, Schmied J. Behaviour of a one ton rotor being dropped into auxiliary bearings. Proceeding 3rd Int Symp Magn Bear 1992:145–56.
[17] Piccoli HC, Weber HI. Experimental observation of chaotic motion in a rotor with rubbing. Nonlinear Dyn 1998;16(1):55–70.
[18] Simon U. Rotor stator kontakt in polygonförmigen fanglagern. Ph.D. thesis. Technischen Universität Carolo Wilhelmina zu Braunschweig; 2001.
[19] Ginzinger L, Heckmann B, Ulbrich H. Feedback control to prevent damage by rotor rubbing after an impact load. Proc Asme Turbo Expo, Proc Asme Turbo Expo 2009; 6:1003–12. https://doi.org/10.1115/GT2009-60195.
[20] Zülow D, Liebich R. Ein aussenrollenlager als fanglagerkonzept für magnetgelagerte rotoren. SIRM 8. Wien, Austria: Internationale Tagung Schwingungen in rotierenden Maschinen; 2009. paper-ID 11.
[21] S. Lahriri, I. F. Santos, H. I. Weber, H. Hartmann, On the nonlinear dynamics of two types of backup bearings theoretical and experimental aspects vol. 134 805–818. doi:10.1115/1.4007166.
[22] Lahriri S, Santos IF. Experimental quantification of contact forces with impact, friction and uncertainty analysis. Tribol Int 2013;66:93–104. https://doi.org/10.1016/j.triboint.2013.04.016.
[23] S. Lahriri, I. F. Santos, Experimental quantification of dynamic forces and shaft motion in two different types of backup bearings under several contact conditions, J Mech Syst Signal Process 40 301–312. doi:10.1016/j.ymssp.2013.05.013.
[24] Fonseca CA, Weber H, Fleischer P, Santos I. Analyzing the use of pins in safety bearings. J Braz Soc Mech Sci Eng 2015;37:1425–34.
[25] Ma H, Wu Z, Tai X, Wen B. Dynamic characteristics analysis of a rotor system with two types of limiters. Int J Mech Sci 2014;88:192–201. https://doi.org/10.1016/j.ijmecsci.2014.08.001.
[26] van Rensburg JJJ. Delevitation modelling of an active magnetic bearing supported rotor. Phd thesis. North-West University; 2014.
[27] Fonseca CA, Santos IF, Weber HI. Influence of unbalance levels on nonlinear dynamics of a rotor-backup rolling bearing system. J Sound Vib 2017;394:482–96. https://doi.org/10.1016/j.jsv.2017.01.020.
[28] Xiao K, Palazzolo A. Dynamic and thermal analysis of rotor drop on sleeve type catcher bearings in magnetic bearing systems. In: Proceedings of ASME turbo expo 2017 turbomachinery technical conference and exposition; 2017. p. 10. Charlotte, NC USA, GT2017-63662.
[29] Halminen O, Kärkkäinen A, Sopanen J, Mikkola A. Active magnetic bearing-supported rotor with misaligned cageless backup bearings: a dropdown event simulation model. Mech Syst Signal Process 2015;5051:692–705. https://doi.org/10.1016/j.ymssp.2014.06.001.
[30] Saket FY, Sahinkaya MN, Keogh PS. Touchdown bearing contact forces in magnetic bearing systems. In: Proceedings of ASME turbo expo 2013 turbomachinery technical conference and exposition; 2013. p. 7. San Antonio, Texas, USA.
[31] Cole MOT, Hawkins L. Model-based analysis of friction-induced subsynchronous whirl for a rotor contacting with clearance bearings under axial load, vol. 138; 2016. p. 072507. https://doi.org/10.1115/1.4032343.
[32] Petersen NPP. Rotor drop rig – design & simulation. Master thesis. Department of Mechanical Engineering, Technical University of Denmark; August 2011.
[33] Jacobsen MD, Christiansen CK. Development of a pin-on-disk test rig, Bachelor project. Technical University of Denmark, Department of Solid Mechanical; 2010.
[34] Sarkar AD. Friction and wear. Academic Press; 1980.
[35] BASF Ultraform product information.

Chapter 4

An experimental and theoretical approach of a pinned bearing and a conventional ball bearing

Paper sent for publication to the Journal Mechanical Systems and Signal Processing on 1st of August 2017. Ref. No.: MSSP17-977

An experimental and theoretical approach of a pinned bearing and a conventional ball bearing

Cesar Augusto Fonseca[a], Ilmar Santos[a,*], Hans I. Weber[b]

[a] *Dept. of Mechanical Engineering, DTU, Niels Koeppel Allé, 404, 2800, Lyngby, Denmark*
[b] *Dept. of Mechanical Eng., PUC-Rio, Rua Marquês de de São Vicente, 225, 22451-900, Rio de Janeiro, Brazil*

Abstract

The magnetic bearing rotors are present nowadays in many industrial applications. However, a damage or a malfunctioning of the magnetic bearing can produce a dangerous high lateral vibration. Backup bearings hold them to protect the machine integrity. The present study investigates the effectiveness of a pinned bearing on a horizontal rotor compared with a conventional rolling bearing. Experimental tests have been conducted; a mathematical model to describe the motion is then developed and validated numerically. It is shown that both the simulation and the test rig are in good agreement with each other and that the pinned bearing is able to reduce the interval of impacting velocities. The experimental set up is able to gather data fast enough to observe the dynamics and the forces acting on the structure. The orbits and the magnitudes of the impact forces are the key elements to assess the validity of the pinned in contrast to the rolling one as a relevant type of backup bearing.

Keywords: Safety bearings, impact, friction, nonlinear dynamics, magnetic bearing

*Corresponding author
Email addresses: cefonse@dtu.mek.dk (Cesar Augusto Fonseca), ifs@dtu.dk (Ilmar Santos), hans@puc-rio.br (Hans I. Weber)

1. Introduction

The use of levitated rotors through magnetic bearings has been in the last few years an interesting topic of research with a broad interdisciplinary coverage in mechanical systems; from the nonlinear dynamics of interacting bodies with impacts to nonlinear control design. It has many advantages such as to be able to rotate at a very high speed in a low friction environment, to provide high efficiency and a low maintenance demand. Therefore these magnetic rotors have been used in industrial application such as pumps, turbines and on energy-storing flywheels, Gash et al. [1]. But the rotor relies on the safety bearings as a fail-proof mechanical design that should hold the spinning shaft and protect the structure in case of a sudden or partial breakdown. Besides, since the rotor is running in a vacuum environment, any unknown disturbance can cause the occurrence of high orbits of the center of the shaft. Also, crossing the resonance or the appearance of sudden unbalance can make the rotor to impact on the bearing wall, thus leading it to a highly destructive behavior well known in rotordynamics, namely, the backward whirl.

The design and study of magnetic bearings can be found in the book of Schweitzer and Maslen [2]. The rotor is levitated either by passive or active magnets and the shaft is set to spin within a gap in vacuum or low-pressurized air. Before active magnetic bearings became a novelty, earlier results in the 1950s already explored the relationship between a rotor and bearing with a clearance. Black [3] was one of the first to deal with the subject of rotors with a clearance. In his modeling the friction force was neglected and it would be treated later in the work of Choy and Padovan [4]. In the work of Jin and Ulbrich [5] the dry friction whip movement of the unbalanced rotor was observed when it collided on the stator and was explained through the multiple-scale method.

The worst-case scenario for a magnetic bearing is a power loss, which makes the rotor to fall completely. Therefore rotor drop tests are of immense value. One of the most cited works is from Pradetto [6] in which a one-ton rotor was left to fall and orbit and forces were sampled. In the work of Ishii and Kirk [7] the transient response of a rotor drop was assessed. Fumagalli [8] replaced the circular clearance wall by a ball bearing and tested for several rotor drops, where the rotor interacts with the inner ring, on which the rotor slides and tumbles. The different levels of unbalance were also tested by Fonseca [9] during a rotor drop. Depending on how high the level of the

unbalance was, the behavior changed from a simple oscillating body resting on the inner ring of a ball bearing to a chaotic dynamics impacting several times.

The compliance interaction between the rotor and the structure is highly nonlinear. Contact dynamics is a complex topic and the literature is wide. The first one to propose a model was Hertz [10], in which the impact force is proportional to the power of the deformation, $F = k\delta^n$, but this model is purely energy conservative although nonlinear. It would later be generalized to include the dissipative effects and it is known as the Kelvin-Voigt model, *i.e.*, $F = k\delta^n + c\dot{\delta}$. Such a model can be observed as a simple spring damping system where the displacement is substituted by the deformation. Nonetheless, the model causes a sudden increase of the force at the moment the impact begins and a negative net force when the system returns. To correct this phenomenon a new updated model was presented by Hunt and Crossley [11], $F = k\delta^n + c\dot{\delta}\delta^n$, see Figure 1. Other models like the one by Lankarani-Nikavesh [12] reinterpreted the Hunt and Crossley model to express the damping term as a direct function of the coefficient of restitution and the initial impact velocity. The approach of contact analysis was condensed in a literature survey by Gilardi [13] and later by Machado et al. [14].

The shape of the impact region plays also an important role in the dynamics of the impact and on the efficiency of the backup bearing. Polygonal shapes have been tested by Simon [15] in his doctoral thesis. He compared the geometries with a theoretical approach and mounted a test rig to observe their dynamical response. Later, a more complex geometry for the backup bearing was considered in that pins are placed inside the bearing, that adds pins inside the circular wall. One of the first to deal with this problem was Said et al. [16]. They described the mathematical model impacting on a housing in order to extract the forces and validated the model with a test rig. The goal was to set the rotor to perform the backward whirl on a common circular wall and compared with the pinned solution. Other examples of backup bearing can be found in the work of Ginzinger and Ulbrich [17] with linear actuators and Zülow and Liebich [18, 19], who added small ball bearings to the stator. Its design can be found in the patent [19]. Hui Ma et al. [20] also investigated theoretically the dynamical response of a pinned backup bearing using the finite-element method to characterize the impact phenomenon. The authors also showed the difference between three to four pins in the orbit patterns and performed a frequency analysis, where multiple

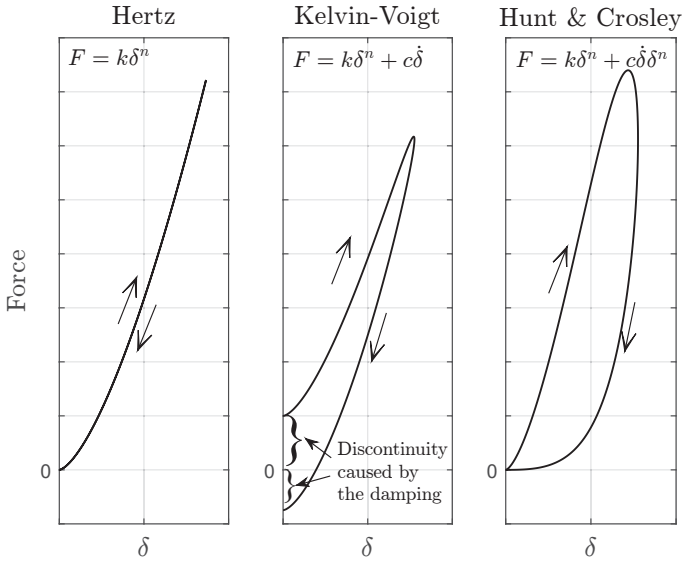

Figure 1: Differences between the impact models.

frequencies were excited.

The main contribution of the present work is to validate the vibro-impact dynamical model with the observed behavior performed by the rotor on the test bench at the Technical University of Denmark (DTU). The tests consist on increasing the angular velocity step-wise until it crosses the rotor's resonance. Two types of backup bearings were tested: one with pins and an ordinary ball bearing. A mathematical model is proposed to describe the dynamics of the rotor and the compliance equations of impact with the backup bearing are presented. The parameters are extracted from the test rig and the equations are integrated in time and compared with the experimental data. Finally, a comment of the effectiveness of the pinned bearing is addressed in the point of view of the orbits, maximum vibration and the contact forces.

2. Modeling the rotor-housing kinematics

The photograph in Figure 2 shows the test rig to be analyzed. It is a horizontal rotor with a steel disc and a passive magnetic bearing at one end. At the other extremity the shaft is connected to the motor by a flexible coupling

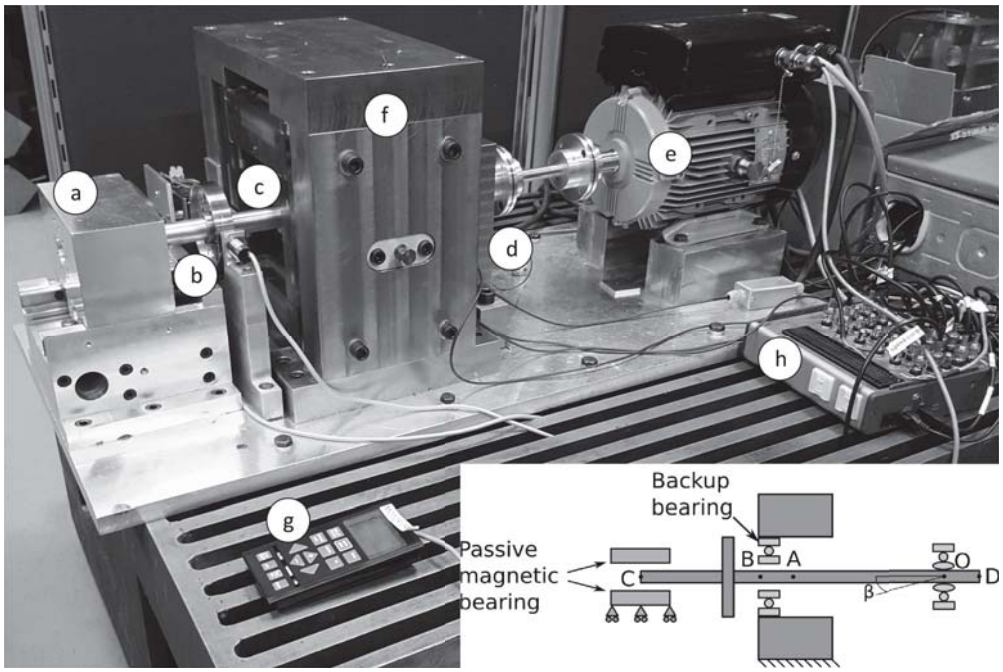

(a) Passive Magnetic Bearing; (b) Disk; (c) Backup bearing; (d) Coupling; (e) AC Motor with dedicated control circuit; (f) Backup bearing casing; (g) Motor remote controller; (h) Acquisition board.

Figure 2: Test rig assembly.

and the motor is controlled externally by an embedded control hardware in order to ensure a constant driven velocity. Next to the coupling there is a spherical bearing that supports the rotor but lets it rotate in this position. Then between the disc and the spherical bearing, one finds the casing where the backup bearing is. Depending on how loose the gap at this backup bearing is, impacts between the surfaces occur at a certain angular velocity as it approaches the resonance frequency. Thanks to the design of the magnetic bearing, it works as a linear spring, creating a single resonance frequency around 10 Hz.

Figures 3a and b show the two types of bearings that are analyzed in the present work. The ball bearing is a SKF 62/28 and the pinned bearing is custom made for the test rig. Each one is tested individually and mounted in the same position.

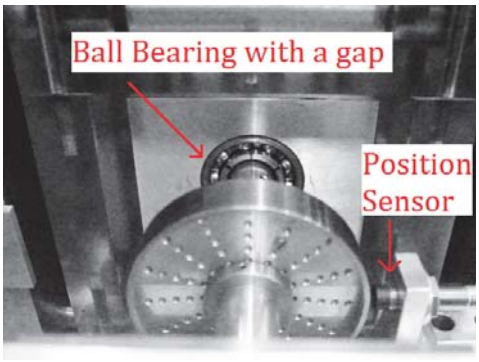

a)

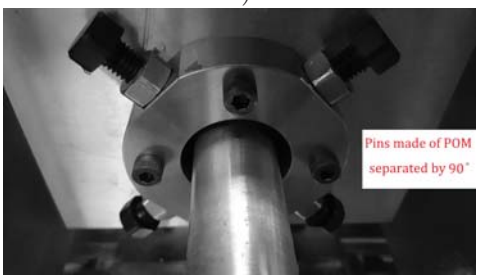

b)

Figure 3: a) Photograph from the test rig assembled for tests with different backup bearings. a) ball bearing; b) Pinned bearing.

2.1. The shaft

In Figure 4, a schematic description of the rotor is presented to reproduce the dynamics of the assembled test rig shown in Figure 2. The fixed reference frame is positioned where the rotor is supported by one spherical bearing at point O. The moving reference frames $B1$ and $B2$ are also positioned at the supporting point of the rotor and correspond to a rotation at the x_I and y_1-axes, respectively. The rotor turns around the z-axis which forms the last reference frame $B3$. However, to develop the dynamics of the rotor, it is enough to describe the system from the reference frame $B2$. Thus, the rotor is only allowed to rotate according to the following three angular degrees of freedom: $\Gamma(t)$, $\beta(t)$, $\theta(t)$, around the coordinate axes x_I, y_1, z_2, respectively, whose angular velocities are defined as

$$ {}_I\dot{\boldsymbol{\Gamma}} = \begin{bmatrix}\dot{\Gamma}(t) & 0 & 0\end{bmatrix}^T, \quad {}_{B1}\dot{\boldsymbol{\beta}} = \begin{bmatrix}0 & \dot{\beta}(t) & 0\end{bmatrix}^T \text{ and } \quad {}_{B2}\dot{\boldsymbol{\theta}} = \begin{bmatrix}0 & 0 & \dot{\theta}(t)\end{bmatrix}^T. \quad (1) $$

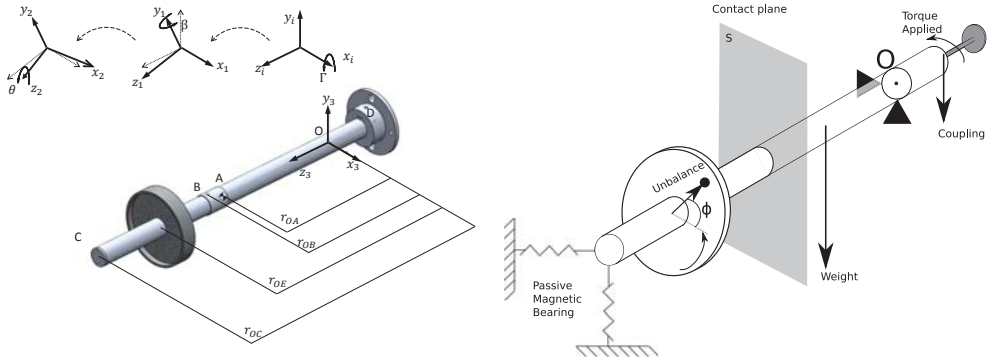

a) b)

Figure 4: The reference systems of the shaft in a) and a schematic of the forces acting on the rotor in b).

The backup bearing is mounted at point B and the passive magnetic bearing is at point C. The rotor is modeled as a rigid body and external forces from the magnets, gravity, imbalance and coupling are applied at points C, A, E and D respectively.

Then the rotational matrices ${}_{I}T_{\Gamma}$, ${}_{B1}T_{\beta}$ and ${}_{B2}T_{\theta}$ are defined as

$$
{}_{I}\mathbf{T}_{\Gamma} = \begin{bmatrix} 1 & 0 & 0 \\ 0 & \cos\Gamma(t) & \sin\Gamma(t) \\ 0 & -\sin\Gamma(t) & \cos\Gamma(t) \end{bmatrix}, \quad {}_{B1}\mathbf{T}_{\beta} = \begin{bmatrix} \cos\beta(t) & 0 & -\sin\beta(t) \\ 0 & 1 & 0 \\ \sin\beta(t) & 0 & \cos\beta(t) \end{bmatrix},
$$
$$
{}_{B2}\mathbf{T}_{\theta} = \begin{bmatrix} \cos\theta(t) & \sin\theta(t) & 0 \\ -\sin\theta(t) & \cos\theta(t) & 0 \\ 0 & 0 & 1 \end{bmatrix}. \tag{2}
$$

The inertia tensor referred to the supporting point is

$$
{}_{B2}\mathbf{I}_{O} = \begin{bmatrix} I_{xx} & 0 & 0 \\ 0 & I_{yy} & 0 \\ 0 & 0 & I_{zz} \end{bmatrix}. \tag{3}
$$

The absolute angular velocity represented in the coordinates of the moving reference frame B2 is given by

$$
{}_{B2}\boldsymbol{\Omega} = {}_{B2}\,\dot{\boldsymbol{\Gamma}} + {}_{B2}\,\dot{\boldsymbol{\beta}} = \begin{bmatrix} \dot{\Gamma}\cos\beta \\ \dot{\beta} \\ \dot{\Gamma}\sin\beta \end{bmatrix}, \tag{4}
$$

whereas the absolute reference frame velocity is

$$ {}_{B2}\boldsymbol{\omega} = {}_{B2}\boldsymbol{\Omega} + {}_{B2}\dot{\boldsymbol{\theta}} = \begin{bmatrix} \dot{\Gamma}\cos\beta \\ \dot{\beta} \\ \dot{\Gamma}\sin\beta + \dot{\theta} \end{bmatrix}. \tag{5} $$

The absolute acceleration in ref. frame B2 is written as:

$$ {}_{B2}\dot{\boldsymbol{\omega}} = \begin{bmatrix} \ddot{\Gamma}\cos\beta - \dot{\Gamma}\dot{\beta}\sin\beta \\ \ddot{\beta} \\ \ddot{\Gamma}\sin\beta + \dot{\Gamma}\dot{\beta}\cos\beta + \ddot{\theta} \end{bmatrix}. \tag{6} $$

In the present case, the angular acceleration with respect to the z-axis, $\ddot{\theta}$ is zero. Any change in velocity is considered instantaneous.

The determination of the equations of motion comes from the Euler formulation.

$$ \sum {}_{B2}\text{Moments}_0 = {}_{B2}\boldsymbol{I}_O \cdot {}_{B2}\dot{\boldsymbol{\omega}} + {}_{B2}\boldsymbol{\Omega} \times \left({}_{B2}\boldsymbol{I}_O \cdot {}_{B2}\,\boldsymbol{\omega} \right). \tag{7} $$

The equations are:

$$ \sum {}_{B2}\mathbf{M}_0 = \begin{bmatrix} I_{xx}\left(\ddot{\Gamma}\cos\beta - \dot{\beta}\dot{\Gamma}\sin\beta\right) + \left(I_{zz} - I_{yy}\right)\dot{\Gamma}\dot{\beta}\sin\beta + I_{zz}\dot{\beta}\dot{\theta} \\ I_{yy}\ddot{\beta} + \left(I_{xx} - I_{zz}\right)\dot{\Gamma}^2\sin\beta\cos\beta - I_{zz}\dot{\Gamma}\dot{\theta}\cos\beta \\ I_{zz}\left(\dot{\beta}\dot{\Gamma}\cos\beta + \ddot{\Gamma}\sin\beta\right) + \left(I_{yy} - I_{xx}\right)\dot{\Gamma}\dot{\beta}\cos\beta \end{bmatrix}. \tag{8} $$

The forces applied to the rotor are the magnetic $\boldsymbol{F_{Mag}}$, the damping force $\boldsymbol{F_D}$, the unbalance force $\boldsymbol{F_u}$ and the contact forces $\boldsymbol{F_N}$, $\boldsymbol{F_{\mathbf{fric}}}$, the shaft's weight $\boldsymbol{P}$, and finally a vertical coupling force,$\boldsymbol{F_{\mathbf{coupl}}}$, which necessary for the equilibrium position and written as:

$$ {}_{B2}\boldsymbol{F_u} = \begin{bmatrix} m_u\varepsilon\dot{\theta}^2\cos\left(\dot{\theta}t + \phi\right) \\ m_u\varepsilon\dot{\theta}^2\sin\left(\dot{\theta}t + \phi\right) \\ 0 \end{bmatrix}, \; {}_{I}\boldsymbol{P} = \begin{bmatrix} 0 \\ -mg \\ 0 \end{bmatrix}, \tag{9} $$

$$ {}_{I}\boldsymbol{F_N} = \begin{bmatrix} N\cos\alpha \\ N\sin\alpha \\ 0 \end{bmatrix}, \; {}_{I}\boldsymbol{F_{\mathbf{fric}}} = \begin{bmatrix} \mu N\sin\alpha \\ -\mu N\cos\alpha \\ 0 \end{bmatrix}, \tag{10} $$

$$ {}_{I}\boldsymbol{F_{\mathbf{Mag}}} = \begin{bmatrix} K\cos\xi \\ K\sin\xi \\ 0 \end{bmatrix}, \; {}_{I}\boldsymbol{F_D} = \begin{bmatrix} c\cos\rho \\ c\sin\rho \\ 0 \end{bmatrix}, \; {}_{I}\boldsymbol{F_{\mathbf{coupl}}} = \begin{bmatrix} 0 \\ -F_{\text{coupl}} \\ 0 \end{bmatrix}, \tag{11} $$

where the two angles ξ and ρ are defined; ξ is the angle of the displacement of the rotor to the origin in the fixed reference frame and ρ is the angle of the velocity of the rotor to the origin in the fixed reference frame. At the contact on the backup bearing the angle of contact is designated as α. Each force is applied at points, whose vectors are as follows:

$$ {}_{B2}\boldsymbol{r_{OA}} = \begin{bmatrix} 0 \\ 0 \\ l_A \end{bmatrix}, \; {}_{B2}\boldsymbol{r_{OB}} = \begin{bmatrix} 0 \\ 0 \\ l_Q \end{bmatrix}, \; {}_{B2}\boldsymbol{r_{OC}} = \begin{bmatrix} x_B \\ y_B \\ l_S \end{bmatrix}, \tag{12} $$

$$ {}_{B2}\boldsymbol{r_{OD}} = \begin{bmatrix} 0 \\ 0 \\ -l_D \end{bmatrix}, \; {}_{B2}\boldsymbol{r_{OE}} = \begin{bmatrix} 0 \\ 0 \\ l_E \end{bmatrix}. \tag{13} $$

Finally, a torque from the motor is given as $\boldsymbol{T} = \begin{bmatrix} 0 & 0 & T \end{bmatrix}^T$. But the value of T is unimportant in the present analysis, because it is supposed that the torque is ideally supplied by the motor to keep the angular velocity $\dot{\theta}$ constant. Therefore the expression of the sum of the moments is

$$ \begin{aligned} \sum {}_{B2}\mathrm{M}_0 = {}_{B2}\Big(& \boldsymbol{r_{OA}} \times \boldsymbol{P} + \boldsymbol{r_{OC}} \times \boldsymbol{F}_{\mathbf{Mag}} + \boldsymbol{r_{OC}} \times \boldsymbol{F_D} + \boldsymbol{r_{OB}} \times \boldsymbol{F_N} + \\ & + \boldsymbol{r_{OB}} \times \boldsymbol{F}_{\mathbf{fric}} + \boldsymbol{r_{OE}} \times F_u + \boldsymbol{r_{OD}} \times \boldsymbol{F_{coupl}} + \boldsymbol{T} \Big). \end{aligned} \tag{14} $$

2.2. Contact criteria and housing dynamics

The contact on the backup bearing is responsible for the appearance of an interaction with the whole dynamics of the rotor in a way that is strong enough to be represented by linear models. Moreover, the impact force influences the dynamics of the structure that holds the backup bearing. This means its dynamics has to be included in the mechanical system. Two housings holding the backup bearing are built in a manner that each one moves in a different direction, *i.e.* the inner house moves vertically and the outer house horizontally and no coupled movement is present. Between them there are force transducers that are modeled as spring elements. A sketch of the inner and outer houses and the four force transducers is shown in Figure 5. Sliding beams provide the damping effect and the restriction of other movements. Their equations of motion are written as:

$$ m_{ih}\ddot{y}_{ih} = -2k_{ft}y_{ih} - 2c_v y_{ih} - m_{ih}g + N\sin\alpha + \mu N\cos\alpha \tag{15} $$

$$ \left(M_{oh} + m_{ih}\right)\ddot{x}_{oh} = -2k_{ft}x_{oh} - 2c_h x_{oh} + N\cos\alpha - \mu N\sin\alpha. \tag{16} $$

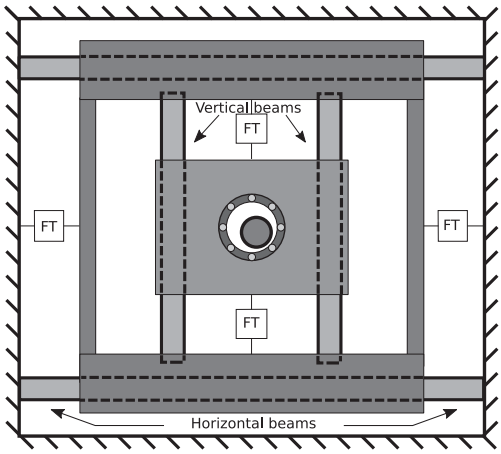

Figure 5: Housing and the four force transducers (FT).

For the impact to happen, the shaft center has to cross a boundary surface, otherwise the normal force is nonexistent, $N = 0$. The two types of backup bearings have different geometries implying two rules for the threshold. The rolling bearing is the easiest to define since it is a round surface too and yet it is a moving wall. So, whenever the shaft center, r, at the plane S of backup bearing is at a distance greater than the nominal gap, r_0, an impact state is in place.

$$r_{ir} - r_s = r_0, \text{ or the gap} \tag{17}$$

$$r > r_0, \rightarrow \text{in contact}, \tag{18}$$

where r_{ir} is the inner radius of the inner ring and r_s the radius of the shaft. The tangential velocity at the contact point is also relevant, because the friction force is exerted against the relative velocity between the edge of the shaft and the inner ring of the ball bearing.

Therefore we should include another degree of freedom to the mechanical system, namely, the acceleration of the bearing's inner ring:

$$I_{\text{ring}}\ddot{\theta}_{ir} = |_{B2}\boldsymbol{r_s} \times_{B2} \boldsymbol{F_{\text{fric}}}| - c_{ir}\dot{\theta}_{ir}, \tag{19}$$

where c_{ir} is a damping coefficient exclusive for the bearing that comes from the friction with the spheres.

The model of the contact is the one proposed by Hunt and Crossley [11]. This expression has been applied to model the impact between rotors and

the inner ring in the works of references [21] and [22]:

$$N = k_{\text{imp}}\delta^n \left(1 + 1.5\eta\dot{\delta}\right). \tag{20}$$

The term in η represents the damping contribution of the impact, which depends not only on the velocity of the deformation but also on the deformation itself, so with it one avoids the hysteresis effects or numerical errors. The value of this parameter was determined experimentally and will be commented later in this work. The term η is correlated to the coefficient of restitution c_e and the initial velocity of contact as follows:

$$c_e = 1 - \eta\dot{\delta}^{-}. \tag{21}$$

The pinned backup bearing simplifies the mechanical system, because the walls are not rotating, yet it makes the the geometry of contact more complicated. If we consider only the tip of the pin as a punctual element, the resulting boundary has the shape of a parametric curve known as an astroid. It is the combination of four circle-like curves equally distant from the origin. The equation of the curve is written as

$$[X(s),\ Y(s)] := [a\cos^3(s),\ a\sin^3(s)], \quad \text{for } 0 \leq s \leq 2\pi, \text{ see Figure 6.} \tag{22}$$

Figure 6 illustrates the difference between the geometries of the contact from the circular gap and the astroid function.

The aperture δ formulae necessary for equation (20) are written as:

$$\delta = \sqrt{(X - x_{oh})^2 + (Y - y_{ih})^2} - r_0, \tag{23}$$

for the ball bearing and

$$\delta \cong |\,(X - x_{oh},\ Y - y_{ih}) - \text{Pin}_i| \tag{24}$$

for the pinned one. Here X and Y are the displacement of the center of the shaft at the contact plane S, given by

$$\begin{bmatrix} X \\ Y \\ Z \end{bmatrix} = {}_I\mathbf{T}_\Gamma^T\ {}_{B1}\mathbf{T}_\beta^T \begin{bmatrix} 0 \\ 0 \\ l_s \end{bmatrix}. \tag{25}$$

Figure 7 demonstrates geometrically the meaning of the penetration for the pinned case, where $\mathbf{r}_{\text{pin}}$ is the position of the tip of a pin in relation to the moving housing.

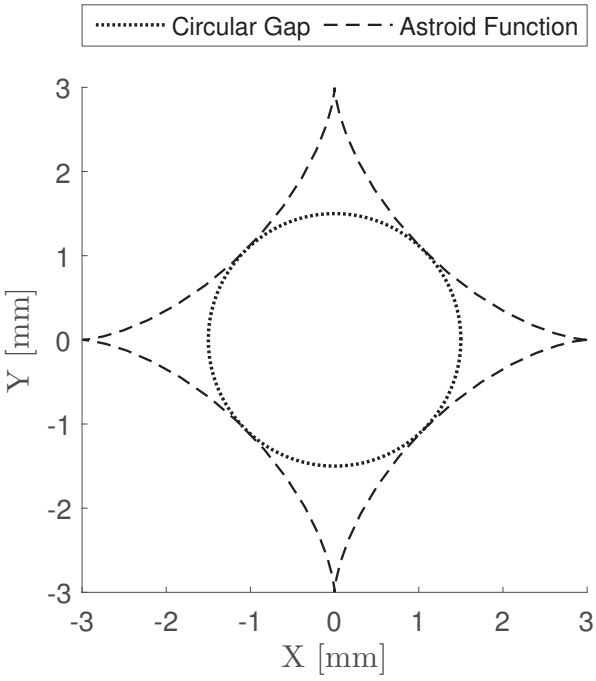

Figure 6: Difference between the types of contact geometries.

3. Simulation of the mechanical system

With all the parameters mentioned before having been defined, one needs to develop a numerical time integration program in order to reproduce the test rig dynamical behavior. Two state variable vectors are introduced, the first for ball bearing case and the second for the pinned one as:

$$\boldsymbol{X} = \begin{bmatrix} \Gamma & \dot{\Gamma} & \beta & \dot{\beta} & y_{oh} & \dot{y}_{oh} & x_{ih} & \dot{x}_{ih} & \theta_{ir} & \dot{\theta}_{ir} \end{bmatrix}^T, \tag{26}$$

or for the pinned bearing case:

$$\boldsymbol{X} = \begin{bmatrix} \Gamma & \dot{\Gamma} & \beta & \dot{\beta} & y_{oh} & \dot{y}_{oh} & x_{ih} & \dot{x}_{ih} \end{bmatrix}^T. \tag{27}$$

The vectors can be split in two because the link between the elements (shaft and the casings) is defined by an expression, given by eq. (20), which only exists when contact happens, $\delta \geq 0$. The shaft can be independently calculated alone so that eq. (8) can be rewritten as:

$$A\ddot{\boldsymbol{Z}} + G(\dot{\theta})\dot{\boldsymbol{Z}} + N_e(\boldsymbol{Z}, \dot{\boldsymbol{Z}}) = \sum {}_{B2}\mathbf{M}_0, \tag{28}$$

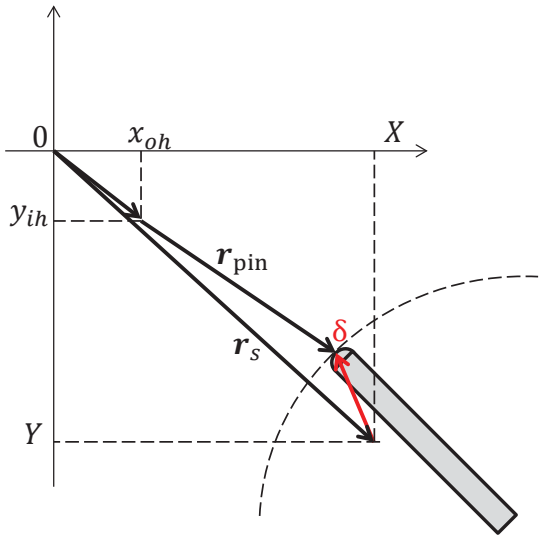

Figure 7: Deformation δ shown for the pinned case.

where

$$A = \begin{bmatrix} I_{xx} & 0 \\ 0 & I_{yy} \end{bmatrix}, \; G(\dot{\theta}) = \begin{bmatrix} 0 & I_{zz}\dot{\theta} \\ -I_{zz}\dot{\theta}\cos\beta & 0 \end{bmatrix},$$
$$N_e(\boldsymbol{Z}, \dot{\boldsymbol{Z}}) = \begin{bmatrix} -I_{xx}\dot{\Gamma}\dot{\beta}\sin(\beta) + (I_{zz} - I_{yy})\dot{\Gamma}\dot{\beta}\sin(\beta) \\ (I_{xx} - I_{zz})\dot{\Gamma}^2\sin(\beta)\cos(\beta) \end{bmatrix} \text{ and}$$
$$\boldsymbol{Z} = \begin{bmatrix} \Gamma & \beta \end{bmatrix}^T.$$

It results:

$$\ddot{\boldsymbol{Z}} = A^{-1}\left[\sum {}_{B2}\mathbf{M}_0 - \left(G(\dot{\theta})\dot{\boldsymbol{Z}} + N_e(\boldsymbol{Z}, \dot{\boldsymbol{Z}})\right)\right]. \tag{29}$$

Thus equations (29), (19), (16) and (19) can be assembled together and integrated in time using a combination of *ode45* from Matlab and a simple 4^{th}-order Runge-Kutta routine for the impact state, when required. The dynamics the during the impact is a stiff numerical problem to be calculated with an adequate precision. When the solver is unable to reach the error tolerances, the fixed-step-4^{th}-order-Runge-Kutta integrator takes over and resumes. The angular velocity of the rotor changes in time stepwise, which means that it is considered constant during a desired time interval. The rotor goes from 0-20 Hz. A fluxogram of the program is illustrated in Figure 8.

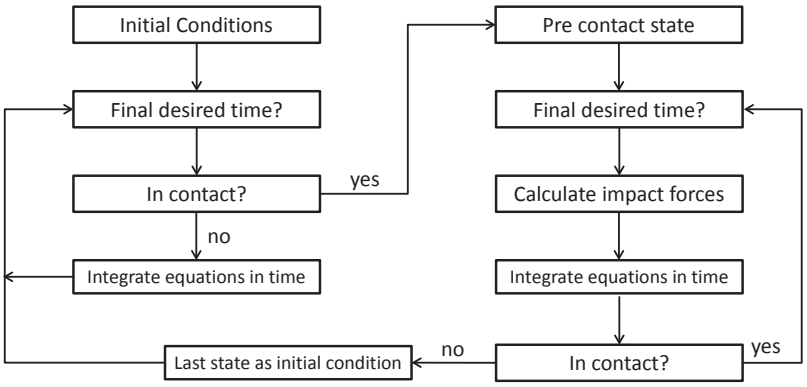

Figure 8: Illustration of the algorithm to calculate the dynamics of the rotor housing interaction.

4. The test rig and its parameter identification

For a theoretical-experimental work it is important that the values of the coefficients and parameters are well defined under a solid theoretical background are experimentally validated. The geometric and physical properties come from project's technical drawings, ref. [23], and the masses and moments of inertia are measured on a scale and calculated by CAD software. The first parameters to be determined are the natural frequency and damping factor. The displacement of the shaft is acquired by two proximity probes located in the same plane where the disk is assembled and the time data are represented in Figure 9. With the rotor at rest, $\dot{\theta} = 0$ rad/s, one observes the validity of the assumption of a linear spring, since there is only one relevant natural frequency at 10.1 Hz. One gets that the elastic coefficient is $K = 2090$ N/m to match the natural frequency of the rotor. The damping c is calculated from the oscillatory decays after an impulsive response. The damping comes from a combination of many sources: the coupling with the motor, from the magnets, the supporting spherical bearing and friction with the air. All effects are considered as a single damping element at the end of the shaft together with the spring element and its value is determined to be as $c = 1.5$ Ns/m.

The damping coefficient of the ball bearing, c_{ir} is also determined by observing that the inner ring stopped after few seconds. We define a proper value that takes the inner ring from 10 Hz to 1.0 Hz in one second. The

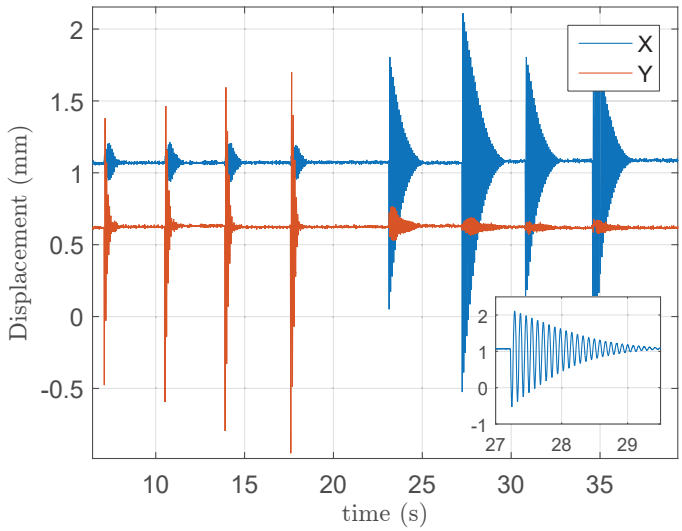

Figure 9: Displacement captured at the disk caused by lateral impacts.

friction coefficient between the shaft and the inner ring μ is set at 0.4 and 0.2 for the ball bearing and pinned bearing respectively. These values come from the nominal aluminum-steel sliding contact and a from pin-on-disk test for the pin case.

Finally, the coupling with the motor applies a vertical force on the rotor. This force can be determined, because the resting position of the shaft at the backup bearing is slightly downwards, and because the shaft is considered as a rigid body. Therefore we include a force $\boldsymbol{F}_{\mathbf{coupl}} = -12\boldsymbol{j}$ N. Besides that, a weak linear torsional spring elements is added. Its value is very low so it does not change significantly the natural frequency mentioned before.

The remaining parameters of the mechanical system are available in Tables 1, 2 and 3.

4.1. Defining the value of the impact parameters

The setup has two different backup bearings to be tested, therefore two different methods to determine the elastic coefficients have been performed. The case of ball bearing is hard to do, mainly because the contact case is not easily found on the lists of hertzian contacts. This is due to the fact that the contact between the shaft and the inner ring is a line contact with an angle.

Rotor	
Mass	m =1.28 kg
Residual unbalance	$m_u.\varepsilon = 7.5 \cdot 10^1$ g.mm
Length to magnetic bearing	l_Q =384 mm
Length to disk	$l_D = 303.5$ mm
Length to rolling bearing	$l_S = 211$ mm
Length to center of mass	$l_A = 195.9$ mm
Length to motor coupling	$l_E = 60.8$ mm
Shaft diameter	$d_r = 25$ mm
Diametral inertia	$I_{xx} = I_{yy} = 0.07714$ kg.m^2
Polar inertia	$I_{zz} = 7.8 \cdot 10^{-4}$ kg.m^2

Table 1: Specifications of the rotor.

Inner and outer house	
Mass of inner house	$m_{ih} = 1.70$ kg
Mass of outer housing	$M_{oh} = 8.87$ kg
Damping coefficient horizontal	$c_h = 704$ Ns/m
Damping coefficient vertical	$c_v = 228$ Ns/m
Force Sensor	
Force transducer stiffness	83 MPa

Table 2: Specifications of the housing.

In fact the shaft makes a contact with the surface of the edge of the ring, which means that the contact type approximates the case of a cylinder on a sphere. Thus we define the value of the exponent in eq. (20) as $n = 1.5$. Besides there are other contacts between the inner ring and the spheres and subsequently to the outer ring and the inner housing, which will not be dealt here. So an equivalent elastic coefficient was determined after making a series of rotor drop tests and observing the aperture δ^n and its velocity $\dot{\delta}$ versus the measured contact force F_n. Figure 10 illustrates the center of the shaft falling from the top of the bearing to the opposite bottom. The elastic coefficient k_{imp} and the damping term η were determined by using a Nonlinear Least Square (NL-LSq) method, using the *trust-region-reflective* algorithm, which minimizes a function using the experimental data set:

$$\min\|g(\delta,\dot{\delta})\|^2 = \min\left(g_1(\delta,\dot{\delta})^2 + g_2(\delta,\dot{\delta})^2 + \ldots g_n(\delta,\dot{\delta})^2\right), \tag{30}$$

Rolling bearing	
Inner diameter	28 mm
Inner race outer diameter	32 mm
Inner ring inertia	$I_{ir} = 3 \cdot 10^{-5}$ kg.m^2
Pinned bearing	
Total length of the pins	2.0 mm
Radius of the pins	4.0 mm
Radius of the circular wall	38 mm

Table 3: Specifications of the backup bearings.

where

$$g(\delta, \dot{\delta}) = k_{\text{imp}} \delta^{1.5} \left(1 + \frac{3}{2}\eta\dot{\delta}\right) - F_n. \tag{31}$$

Each impact force versus the aperture is shown in Figure 12 together with the solution obtained by the NL-LSq in a dashed black line. One sees the agreement between the obtained solution and the experimental data, although another oscillation is seen experimentally due to the housing own dynamics. From η, a value of the coefficient of restitution is obtained for the simulation, namely $c_e = 0.71$ [0.58; 0.84]. Then we get for the elastic term $k_{\text{imp}} = 8.35 \pm 3.38 \cdot 10^7 \text{N/m}^{1.5}$. The velocity of the aperture during the impact is plotted in Figure 12 on the right side, which shows that the impacts had the same initial condition. The impact dynamics is also compared in time and is shown in Figure 11, where the standard deviation is plotted with 0.95% of confidence. It is seen that the model follows the trend during the impact. Points out of the confidence range are caused by the housing oscillation.

On the other hand the contact of the shaft on a pin is a classical case of a cylinder on a sphere contact, *i.e.* $n = 1.5$. But the NL-LSq could not be applied to this case because the penetration δ could not be determined experimentally. So the elastic coefficient is determined by the geometric features of both surfaces and the material properties *i.e.* its Young Modulus and the Poisson number for Aluminum and POM polymer. Thus $k_{\text{imp}}^{\text{pin}} = 5 \cdot 10^7$ N/m$^{1.5}$ and the coefficient of the restitution was obtained by comparing the total velocity before and after the impact by monitoring the measured force. The coefficient was determined as $c_e = 0.68 \pm 0.12$.

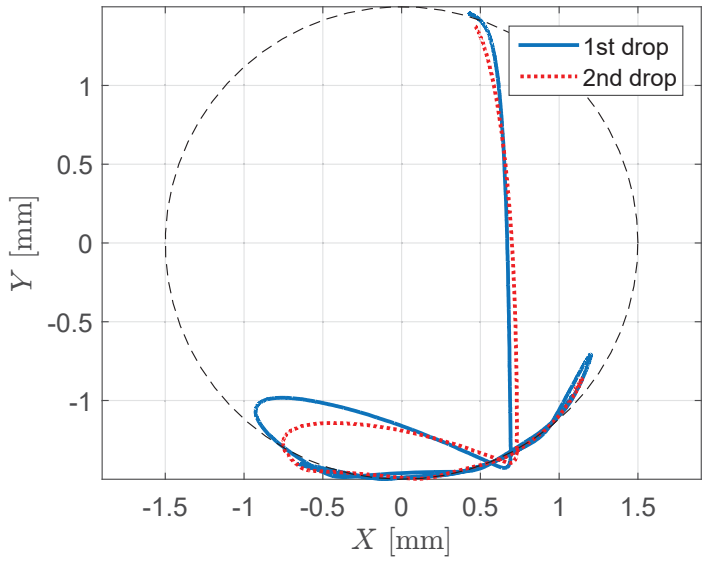

Figure 10: Center of the shaft at a rotor drop test. (Experiments)

5. Crossing the natural the frequency. Experience and theoretical results

In the experiments, we rely on a dedicated control that guarantees the desired angular speed and gives enough power to the motor to keep it spinning at constant speed. Nonetheless, an encoder gives the correct angular velocity and its signal is captured and so the steadiness of the angular velocity on time can be guaranteed. The angular velocity increased step-wise every 10 seconds by 0.5 Hz from 0-20 Hz. The same velocity profile was given as an input to the simulation program.

In Figure 13 it is shown the maximal radial displacement of the center of the shaft inside the backup bearing after the transient phase. In a linear model without impacts, after the resonance is crossed, the shaft should have acquired a low orbit away from the level of impact, but the shaft remains in contact with the backup bearing. The mechanical barrier of the safety bearing creates a stiffening effect and the rotor is able to return to a safer orbit only at a much higher angular velocity than predicted by the simple linear case. This is seen in both cases of backup bearing when the radial position drops sharply after 15.5 Hz for the ball bearing and 14 Hz for the pinned case.

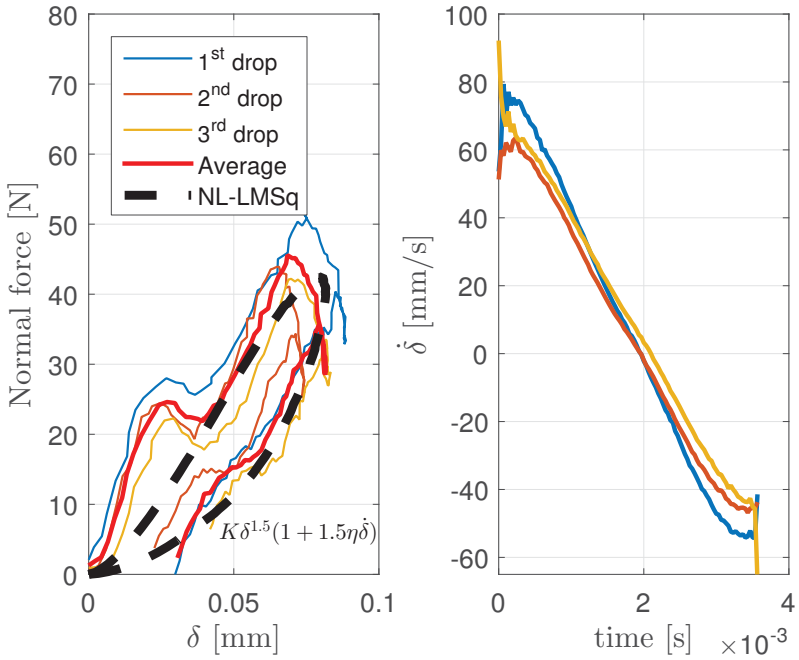

Figure 11: Impact dynamics with experimental data and the NL-LSq solution.

One sees that the theoretical results follow the same experimental pattern. To achieve this goal the values of the elastic term of the impact k_{imp} and the coefficients of restitution were adjusted between the interval defined by the standard deviation.

It is worth mentioning that the influence of the residual unbalance in the model was tested. The initial angle ϕ of the rotor was changed from 0 to $\pi/2$, π and $3\pi/2$. Although the unbalance is small, it was able to remove the shaft from the impact condition at the pinned case 1 Hz before at π while the other two only 0.5 Hz. The rolling bearing is indifferent to the angular initial condition of the rotor.

Figure 14 shows some selected orbits for the rolling bearing case, all of them above the resonance. On the top there are the experimental data for their respective nominal angular velocity. Right below we see the simulated result for the same velocities. The patterns are similar. The rotor hits the lower half of the inner ring of the bearing. Later, at 14.5 Hz, the orbit changes to an almost vertical one and is equally reproduced by the simulation.

In Figure 15, the same analysis is done for the pinned bearing. Instead

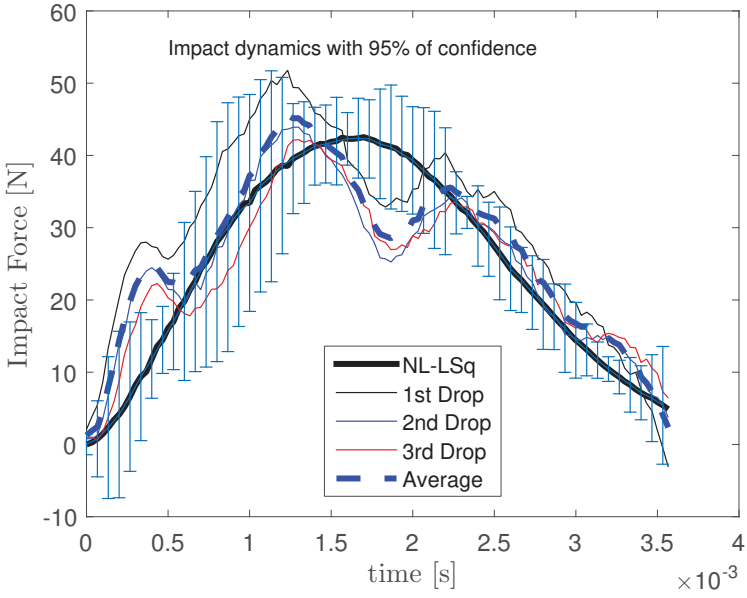

Figure 12: Impact in time with the NL-LSq solution.

of a circular gap, the astroid function is plotted. We see that the center of the shaft follows the barrier created by the pins. Initially the rotor does an erratic trajectory impacting on multiple pins, but later it performs a diagonal movement hitting on a single pin. This change explains the sudden fall in Figure 13 at 12 Hz before the definitive one at 14.5 Hz. The diagonal orbit appears only at one case at 14 Hz. Still, the last value velocity to show impacts remains the same.

6. The feasibility of the backup bearings

One of the goals of representing the rotor with mathematical models and then simulating and comparing with the experimental phenomena is to confirm the efficiency of the safety elements and to design a proper one for a certain rotor machinery. Being so, the machine elements are subject to forces and moments and have to be able to withstand all loads involved in them. Here the forces felt by the whole structure are stipulated by the following expression:

$$F_{\text{contact}} = k_{\text{ft}}\sqrt{x_{oh}^2 + y_{ih}^2}, \tag{32}$$

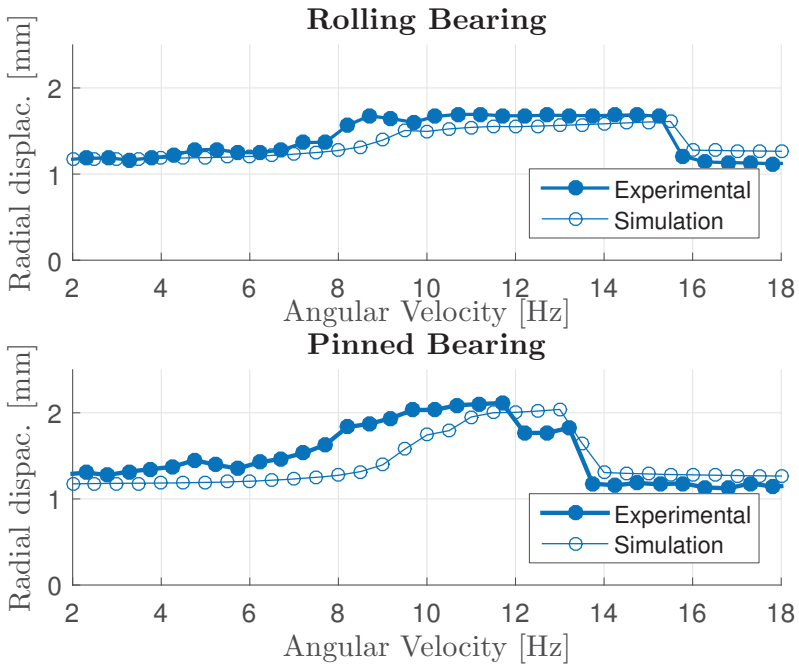

Figure 13: Maximum radial displacement of the rotor for both types of bearings.

where k_{ft} is the elastic coefficient of the force transducers located inside the test rig. Its value is determined from the manufacturer data sheet by dividing the maximum allowed displacement by the corresponding maximum force. So, equation (32) represents the whole magnitude force, that is a normal and friction forces. They come from the vectorial sum of the displacements of the inner and outer housing.

In Figure 16a and b we show the calculated forces of contact and the measured forces respectively. The forces from the simulation at the pinned bearing clearly reaches a higher magnitude than the force from the test rig. The rolling bearing has an agreement between the experiments and the simulated results. Nevertheless, it is clearly seen that the pinned bearing makes the shaft to stop impacting before as the magnitudes of the forces disappear whereas the ones in the rolling bearing case remain.

To illustrate even more the validity of the model of rotor-structure interaction, the transition from the impacting orbit to the safer one is plotted in Figure 17 for the rolling bearing and in Figure 18 for the pinned case. The rotor decreases its orbit after each impact on the backup bearing every

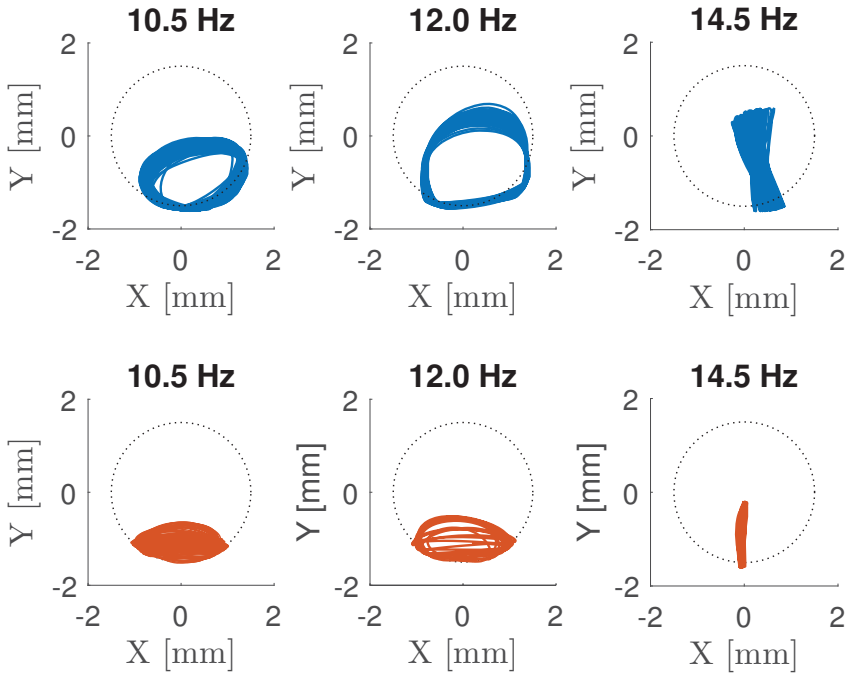

Figure 14: Comparison between experimental in blue and on the top and theoretical orbits in red below for the ball bearing case.

time the angular velocity is increased by 0.5 Hz. Therefore the safe orbit is achieved during the transient of the sudden increase of the angular velocity. The simulation had the expected behavior from the test rig. The value of the last impact forces have the same order of magnitude and the same rate of decay.

7. Conclusion

In this work a set of governing equations with a discontinuous contact interaction is presented in order to reproduce the dynamical behavior of the test rig. These equations are integrated in time with the parameters obtained from the test rig. Within the parameters' standard deviation the numerical results are shown to be in good agreement with the experimental data. We have also found that one compliance model based on the Hunt and Crossley work [11] was adequate to reproduce the interaction between the shaft and both types of backup bearings. The following conclusions are

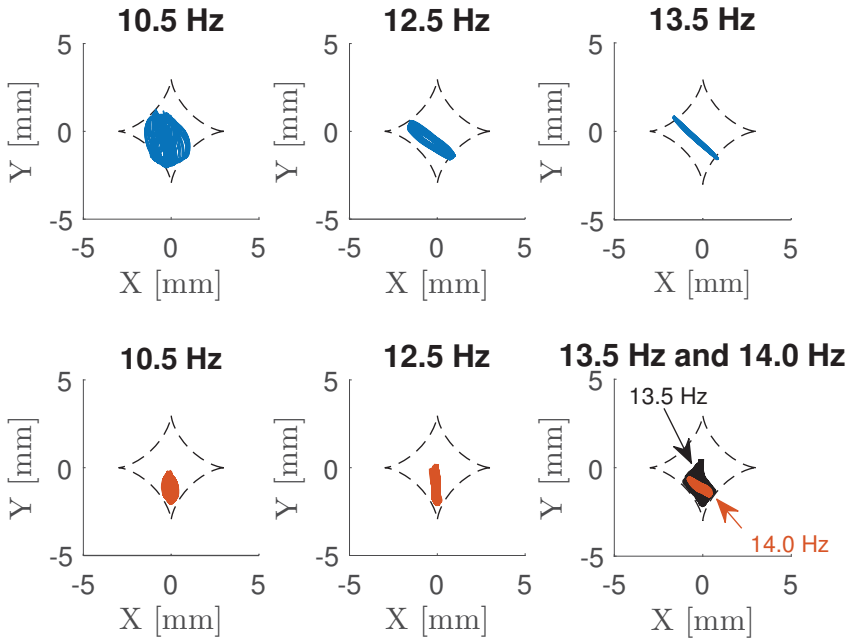

Figure 15: Comparison between experimental in blue on the top and theoretical in red below orbits for the pinned bearing case.

addressed below.

For the ball bearing case, the theoretical model reproduces with a good agreement the experimental behavior of the test rig. The nonlinear jump phenomenon is captured at the same angular velocity the rotor experimentally at 16.0 Hz, see Figure 13. The simulated trajectories of the rotor inside the clearance show some similarities with the observed ones, although they are slightly lower. The magnitudes of the impact forces are identical to the ones captured by the force transducers, while the rotor is crossing the resonance. Discrepancies here are caused by noise on the signal. Additionally, the transient period from the impact state to a contact free one is recreated by the simulated accordingly, as the rotor establishes a circular orbit in less than a second.

The pinned bearing case has also showed a good agreement between the theoretical model and the experimental behavior of the test rig. Likewise, the nonlinear jump is observed for the same experimental angular velocity at 14.0 Hz earlier than the ball bearing case. However, some other discrepancies are found and need to be mentioned. The first orbits have a similar shape,

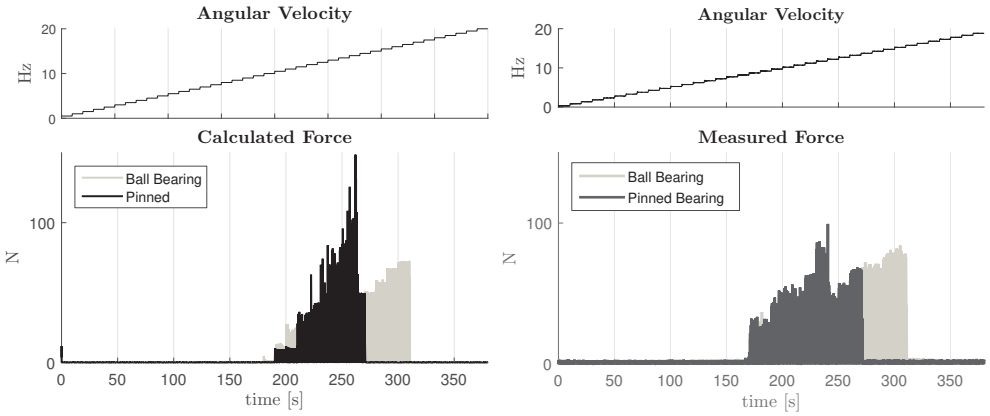

Figure 16: Force exerted on the structure for both types of bearings calculated by the simulation in time, a), and measured by the test rig, b).

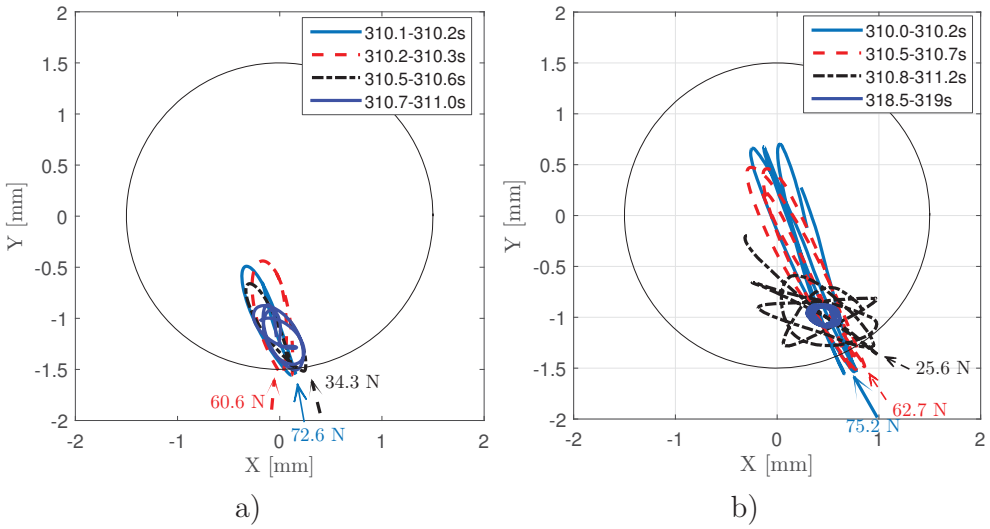

Figure 17: Ball Bearing Case: Theoretical and experimental, a) and b) respectively, transition from the impacting orbit to a safe one with the last impact forces shown at 15.5 Hz.

but for some faster ones were did not match precisely, see Figure 15. The maximum magnitude of the forces differs about 49% higher for the simulated results than the ones observed on the test rig. This is due to the fact that the forces are not measured exactly on the tips of the pins. The transient

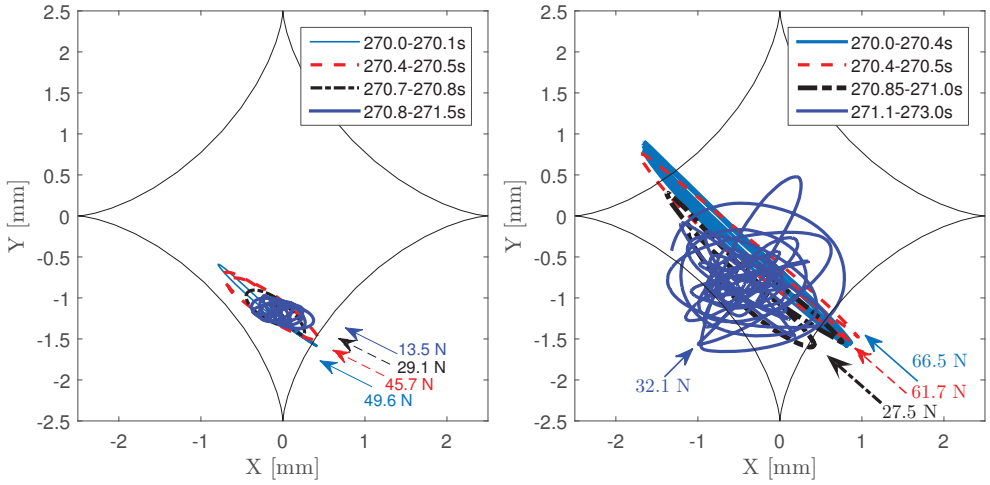

Figure 18: Pinned Bearing Case: Theoretical and experimental, a) and b) respectively, transition from the impacting orbit to a safe one with the last impact forces shown at 14.5 Hz.

time in Figure 18 takes also longer (+1.0 seconds) and is more erratic for the rotor than the simulated one, which is smoother and impacts only in one pin.

Acknowledgement

The authors express their acknowledgement to CNPq through the Science Without Borders Program with the process number: 249728/2013-3, which partially sponsored the elaboration of this paper.

References

[1] R. Gasch, R. Nordmann, and H. Pfützner. *Rotordynamik*. Springer Verlag, Berlin, 2nd ed., edition, 2002.

[2] G. Schweitzer and E. H. Maslen. *Magnetic Bearings*. Springer-Verlag Berlin Heidelberg, 1 edition, 2009.

[3] H. F. Black. Interaction of a whirling rotor with a vibrating stator across a clearance annulus. *Arch. J. Mech. Eng. Sci. 1959-1982 (vols 1-23)*, 10(1):1–12, 1968.

[4] F. K. Choy and J. Padovan. Non-linear transient analysis of rotor-casing rub events. *Journal of Sound and Vibration*, 113:529–545, 1987.

[5] J. Jiang and H. Ulbrich. The Physical Reason and the Analytical Condition for the Onset of Dry Whip in Rotor-to-Stator Contact Systems. *J. Vib. Acoust.*, 127(6):594, 2005.

[6] J. C. Pradetto and J. Schmied. Behaviour of a one ton rotor being dropped into auxiliary bearings. In *Proceeding 3rd Int. Symp. Magn. Bear.*, pages 145–156, 1992.

[7] T. Ishii and R. G. Kirk. Transient Response Technique Applied to Active Magnetic Bearing Machinery During Rotor Drop. *Transactions of the ASME*, 118(April 1996), 1996.

[8] M. A. Fumagalli. *Modelling and measurement analysis of the contact interaction between a high speed rotor and its stator*. PhD thesis, ETH - Swiss Institute of Technology Zurich, 1997.

[9] C. A. Fonseca, I. Santos, and H. I. Weber. Influence of unbalance levels on nonlinear dynamics of a rotor-backup rolling bearing system. *Journal of Sound and Vibration*, 394:482–496, 2017.

[10] H. Hertz. Über die berührung fester elastischer körper. *Journal für die reine und angewandte Mathematik*, 92:156–171, 1881.

[11] K. H. Hunt and F. R. E. Crossley. Coefficient of restitution interpreted as damping in vibroimpact. *J Appl Mech Trans ASME*, 42 Ser E(2):440–445, 1975.

[12] H. M. Lankarani and P. E. Nikravesh. A Contact Force Model With Hysteresis Damping for Impact Analysis of Multibody Systems. *J. Mech. Des.*, 112(3):369, 1990.

[13] G. Gilardi and I. Sharf. Literature survey of contact dynamics modelling. *Mechanism and Machine Theory*, 37(10):1213–1239, 2002.

[14] M. Machado, P. Moreira, P. Flores, and H.M. Lankarani. Compliant contact force models in multibody dynamics: Evolution of the hertz contact theory. *Mechanism and Machine Theory*, 53:99–121, 2012.

[15] U. Simon. *Rotor Stator Kontakt in polygonförmigen Fanglagern*. PhD thesis, Technischen Universität CaroloWilhelmina zu Braunschweig, 2001.

[16] S. Lahriri and I. F. Santos. Experimental quantification of dynamic forces and shaft motion in two different types of backup bearings under several contact conditions. *Journal Mechanical Systems and Signal Processing*, 2012.

[17] L. Ginzinger and H. Ulbrich. Control of a rubbing rotor using an active auxiliary bearing. *Journal of Mechanical Science and Technology*, 21(6):851–854, 2007.

[18] D. Zülow and R. Liebich. Ein aussenrollenlager als fanglagerkonzept für magnetgelagerte rotoren. In *SIRM 8. Internationale Tagung Schwingungen in rotierenden Maschinen, Wien, Austria, paper-ID 11*, 2009.

[19] G. Schuber, H. Walter, and D. Zülow. Safety bearing for retaining a rotor shaft of a machine, July 2014. US 8786152 B2.

[20] Hui Ma, Zhiyuan Wu, Xingyu Tai, and Bangchun Wen. Dynamic characteristics analysis of a rotor system with two types of limiters. *International Journal of Mechanical Sciences*, 88:192 – 201, 2014.

[21] O. Halminen, A. Kärkkäinen, J Sopanen, and A. Mikkola. Active magnetic bearing-supported rotor with misaligned cageless backup bearings: A dropdown event simulation model. *Mechanical Systems and Signal Processing*, 5051:692 – 705, 2015.

[22] Kärkkäinen, A., Sopanen, and A. J.and Mikkola. Dynamic simulation of a flexible rotor during drop on retainer bearings. *Journal of Sound and Vibration*, 306(35):601 – 617, 2007.

[23] M. D. Jacobsen and C. K. Christiansen. *Development of a pin-on-disk test rig*. Bachelor project, Technical University of Denmark, Department of Solid Mechanical, 2010.

Chapter 5

Conclusions and future perspectives

The present work has shown through the papers comprising Chapters 2, 3 and 4 the upsides and downsides of two types of backup bearings being tested under certain conditions. The conducted research deals with a mechanical rotatory system impacting on the surface of a backup bearing. The mechanical model derived from the laws of motion of Newton-Euler describes successfully the behavior of a rotor making intermittent contacts with a housing where the backup bearing was mounted. The parameters of the model come from an actual test bench designed for the purpose of testing backup bearings. The numerical issues regarding the extreme non-linearity of the contact are dealt with by dividing the algorithm into a non-contacting state and a contacting one. Doing so helps to correctly find the impact boundary and to substitute for an adequate solver type for stiff-related problems. Meanwhile, the test bench has been improved with a new data acquisition board, new sensors, and a linear solenoid actuator. These improvements allow the test rig to be fully automatized and adjustable to a desired purpose. It means that every test is repeatable, thus ensuring that the initial conditions are essentially the same and that the non-linearity features such as bifurcation diagrams can be plotted.

In the first paper presented in chapter 2, the theoretical results are matched with the sampled experimental data and it is shown that both appeared to be in accordance. It is shown through bifurcation diagrams, that at a power-loss scenario the characteristics of the motion of the rotor at a constant speed are sensitive to the unbalance with three distinctive levels. It is seen in Figure 5 of this Chapter, that at low unbalance, determined by Region I, the rotor performed oscillatory trajectories; however higher values of unbalance make the rotor to develop chaotic orbits at Region II or a stable forward whirl trajectory at Region III. These behaviors can be characterized by doubled-sided spectrum graphs for each level of unbalance experimentally. The conducted tests represent the consequences of a sudden increase of the unbalance together with a failure of the active magnetic bearing of a rotor, like the occurrence of high impact forces for chaotic trajectories.

Thanks to the automation added to the test rig, it permitted that the same conditions were applied to the rotor for different backup bearings. This is the main contribution

of the second paper in chapter 3, in which the pinned bearing was compared with the ball bearing. Previously, in older works, [74], the pins were made of metal, consequently, this arrangement was constantly damaging the impact surface of the rotor. Therefore, it is suggested to use a softer polymeric material. Hence the chosen material is polyoxymethylene (POM). The friction properties between POM and aluminum are determined and an adequate length of the pin was fixed for the backup bearings. The test that was made consisted of crossing the rotor's own critical speed accelerating and decelerating without an additional unbalance mass and it showed that nonlinear amplitude jumps happen for both types of bearings. Both avoided the undesired occurrence of the backward whirl and successfully recovered to impact orbit. However, the pinned had a better performance since a safe contactless orbit was achieved at a lower angular velocity at 14.0 Hz. The ball bearing case has removed from the impacting orbits at 16.0 Hz. Since the pins are made of a material much softer than the shaft, it means that they are the ones that wear. A finite-element simulation has shown evidence that the applied stresses to the pin can overcome the yield stress of POM. When an experimentally selected impact force is given as an input it caused a stress tension on the surface of the pin of 130 MPa (66 MPa above the σ_{yield}).

Moreover, the same experimental scenario from chapter 3 is simulated by a mechanical model of the rotor on a test rig and is presented in chapter 4. The impact model based on the work of Hunt and Crossley [54] is employed for both types of backup bearings and its impact parameters of this compliance model are determined from rotor drop tests. The mechanical model reproduces satisfactorily the crossing of the rotor's own critical speed constrained by a clearance. For the ball bearing case, the theoretical model reproduces with good agreement the experimental behavior of the test rig, considering that the nonlinear jump phenomenon is captured at the same angular velocity the rotor experimentally at 16.0 Hz. The simulated trajectories of the rotor inside the clearance show some similarities with the observed ones, although they are slightly lower. The magnitudes of the impact forces are identical to the ones captured by the force transducers, while the rotor is crossing the resonance. Discrepancies here are caused by noise on the signal. Additionally, the transient period from the impact state to a contact free one is recreated by the simulated one accordingly, as the rotor establishes a circular orbit in less than a second.

The pinned bearing case has also show good agreement between the theoretical model and the experimental behavior of the test rig. Likewise, the nonlinear jump is observed for the same experimental angular velocity at 14.0 Hz, earlier than the ball bearing case. However, some other discrepancies are found and need to be mentioned. The first orbits have a similar shape, but for some faster velocities they did not match as precisely. A point should be made regarding the magnitudes of the forces, though. The pinned bearing case has in fact generated higher values of impact forces than the ball bearing one. The maximum magnitude of the forces differs about 49% higher for the simulated results than the ones observed on the test rig. This is due to the fact that the forces are not measured exactly on the tips of the pins. The transient interval also takes longer (+1.0 seconds) and is more erratic for the rotor than the simulated one, which is smoother and impacts only in one pin.

Results like these add more knowledge to how the pins change the dynamics of an impacting rotor, specifically a faulty AMB, and confirm the advantages of the pinned bearing against the commonly used ones in the industry. A possible improvement can be implemented if the impact force could be measured directly by the pins with force

transducers attached to them. Also, retractable pins with embedded control techniques could be a solution for:

- the worn pin problem, because it would screw itself inside and recover the missing length;
- to advance even more the amplitude jump towards a safe orbit shortly after the critical speed passage; and
- consequently to avoid or reduce the magnitude of the impact forces on the backup bearing.

The application of smart materials for the pins and the assessment of their durability and fatigue of is also proposed for future works.

Bibliography

[1] E. Krämer. *Dynamics of Rotors and Foundations*. 1st. Springer-Verlag Berlin Heidelberg, 1993.

[2] J. S. Rao. *Rotor dynamics*. John Wiley & Sons, Inc, 1991.

[3] J. Vance, F. Zeidan and B. Murphy. *Machinery Vibration and Rotordynamics*. 1st. John Wiley & Sons, Inc.

[4] R. Gasch, R. Nordmann and H. Pfützner. *Rotordynamik*. 2nd ed. Springer Verlag, Berlin, 2002.

[5] A. Muszynska. 'Rotor-to-stationary element rub-related vibration phenomena in rotating machinery - literature survey'. *Shock and Vibration Digest* **21**(3) (1989), pp. 3–11.

[6] D. C. Johnson. 'Synchronous whirl of a vertical shaft having clearance in one bearing'. *Arch. J. Mech. Eng. Sci. 1959-1982 (vols 1-23)* **4**(1) (1962), pp. 85–93. DOI: 10.1243/JMES_JOUR_1962_004_012_02.

[7] R. A. Billet. 'Shaft whirl induced by dry friction'. *The Engineer* (1965), pp. 713–714.

[8] F. F. Ehrich and J. J. Connor. 'Stator whirl with rotors in bearing clearance'. *Journal of Engineering for Industry, ASME* (1967), pp. 381–389.

[9] H. F. Black. 'Interaction of a whirling rotor with a vibrating stator across a clearance annulus'. *Arch. J. Mech. Eng. Sci. 1959-1982 (vols 1-23)* **10**(1) (1968), pp. 1–12. DOI: 10.1243/JMES_JOUR_1968_010_003_02.

[10] A. Lingener. 'Experimental investigation of reverse whirl of a flexible rotor'. *Proceedings of the 3rd IFToMM International Conference on Rotordynamics*. 1990, pp. 13–18.

[11] S. Crandall. 'From Whirl to Whip in Rotordynamics'. *Transactions of the 3rd IFToMM International Conference on Rotordynamics*. 1990, pp. 19–26.

[12] R. F. Beatty. 'Differentiating rotor response due to radial rubbing'. *Journal of Vibration, Acoustics, Stress, and Reliability in Design* **107** (1985), pp. 151–160.

[13] W. M. Szczygielski. 'Dynamisches Verhalten eines schnell drehenden Rotors bei Anstreifvorgängen'. Doctoral dissertation. Diss. Techn.Wiss. ETH Zürich, 1986.

[14] F. K. Choy and J. Padovan. 'Non-Linear transient analysis of rotor-casing rub events'. *Journal of Sound and Vibration* **113** (1987), pp. 529–545.

[15] W. Zhang. 'The instability of multi-degree-of-freedom rotor-stator system with Coulomb friction'. *Chin. J. Vib. Eng.* **1** (1988), pp. 80–84.

[16] P. Pennacchi, N. Bachschmid and E. Tanzi. 'Light and short arc rubs in rotating machines: experimental tests and modelling'. *Mechanical Systems and Signal Processing* **23** (7 2009). DOI: 10.1016/j.ymssp.2009.03.008.

[17] S. H. Strogatz. *Nonlinear dynamics and chaos*. Ed. by W. Press. 1994, p. 498.

[18] F. Ehrich. 'Observations of subcritical superharmonic and chaotic response in rotordynamics'. *J. Vib. Acoust.* **114**(1) (1992), p. 93.

[19] P. Goldman and A. Muszynska. 'Chaotic behavior of rotor/stator systems with rubs'. *J. Eng. Gas Turbines Power* **116**(3) (1994), p. 692.

[20] P. Goldman and A. Muszynska. 'Dynamic effects in mechanical structures with gaps and impacting order and chaos'. *Journal of Vibration and Acoustics* **116** (1994), pp. 541–547.

[21] J. L. Isaksson. 'On the dynamics of a rotor interacting with non-rotating parts'. PhD Thesis. Linköping University, 1994, pp. 12+127.

[22] H. C. Piccoli and H. I. Weber. 'Experimental observation of chaotic motion in a rotor with rubbing'. *Nonlinear Dyn.* **16**(1) (1998), pp. 55–70.

[23] E. Pavlovskaia, E. Karpenko and M. Wiercigroch. 'Non-linear dynamic interactionsof a Jeffcott rotor with preloaded snubber ring'. *Journal of Sound and Vibration* **276** (2004), pp. 361–379. DOI: 10.1016/j.jsv.2003.07.033.

[24] E. V. Karpenko, M. Wiercigroch, E. E. Pavlovskaia and R. D. Neilson. 'Experimental verification of Jeffcott rotor model with preloaded snubber ring'. *Journal of Sound and Vibration* **298**(4-5) (2006), pp. 907–917. DOI: 10.1016/j.jsv.2006.05.044.

[25] V. I. Rosenblum. 'Entstehung mehrfacher Wellenbrueche nach dem Bruch einer Laufschaufel oder Radscheibe bei Dampfturbinen'. *ALLIANZ REPORT* **68**(Heft 5) (1995), pp. 176–179.

[26] S. Popprath and H. Ecker. 'Nonlinear dynamics of a rotor contacting an elastically suspended stator'. *Journal of Sound and Vibration* **308** (3-5 2007). DOI: 10.1016/j.jsv.2007.03.089.

[27] J. Paez Chavez, V. Vaziri Hamaneh and M. Wiercigroch. 'Modelling and experimental verification of an asymmetric Jeffcott rotor with radial clearance'. *Journal of Sound and Vibration* **334** (86–97 2015). DOI: 10.1016/j.jsv.2014.05.049.

[28] N. Bachschmid, P. Pennacchi, G. A. Vania A. and. Zanetta and L. Gregori. 'Identification of rub and unbalance in 320 MW turbogenerators'. *Int. Journal of Rotating Machinery* **9**(2) (2003), pp. 97–112. DOI: 10.1080/10236210390147425.

[29] N. Bachschmid, P. Pennacchi and A. Vania. 'Thermally induced vibrations due to rub in real rotors'. *Journal of Sound and Vibration* **299**(4-5) (2007), pp. 683–719. DOI: 10.1016/j.jsv.2006.04.045.

[30] P. Pennacchi and A. Vania. 'Analysis of the shaft thermal bow induced by rotor-to-stator rubs'. *IASME Transactions* **1** (2004), pp. 193–198. DOI: doi:10.1.1.540.6677.

[31] O. van Bargen. 'Simulation des Rotorverhaltens im instationaren Betrieb unter besonderer Berücksichtigung des Rotor-Stator-Kontakts'. PhD Thesis. Technischen Universität Berlin, 2011.

[32] A. R. Bartha. 'Dry friction induced backward whirl: theory and experiment'. *Proceedings of 5th IFToMM Conference on Rotordynamics*. Darmstadt, Germany, 1998, pp. 756–767.

[33] A. R. Bartha. 'Dry friction backward whirl of rotors'. PhD Thesis. ETH SWISS FEDERAL INSTITUTE OF TECHNOLOGY ZURICH, 2000.

[34] J. J. Yu, P. Goldman, D. E. Bently and A. Muzynska. 'Rotor/seal experimental and analytical study on full annular rub'. *Journal of Engineering for Gas Turbines and Power-Transactions of the Asme* **124**(2) (2002), pp. 340–350. DOI: 10.1115/1.1416691.

[35] J. Jiang and H. Ulbrich. 'The physical reason and the analytical condition for the onset of dry whip in rotor-to-stator contact systems'. *J. Vib. Acoust.* **127**(6) (2005), p. 594. DOI: 10.1115/1.1888592.

[36] Y. Chen and J. Jiang. 'Effects of forward/backward whirl mechanism on nonlinear normal modes of a rotor/stator rubbing system'. *Journal of Vibration and Acoustics* **137** (2015), p. 054503. DOI: 10.1115/1.4030347.

[37] J. J. Thomsen. 'Using fast vibrations to quench friction-induced oscillations'. *Journal of Sound and Vibration* **228** (5 1999). DOI: 10.1006/jsvi.1999.2460.

[38] D. W. Childs and A. Hattacharya. 'Prediction of dry-friction whirl and whip between a rotor and a stator'. *Journal of Vibration and Acoustics-Transactions of the Asme* **129**(3) (2007). DOI: 10.1115/1.2731412.

[39] J. C. Wilkes, D. W. Childs, B. J. Dyck and S. G. Phillips. 'The numerical and experimental characteristics of multimode dry-friction whip and whirl'. *ASME. J. Eng. Gas Turbines Power* **132**(5) (2010). DOI: 10.1115/1.3204658.

[40] T. Inoue, Y. Ishida, G. Fei and H. Zahid. 'Suppression of the forward rub in rotating machinery by an asymmetrically supported guide'. *Journal of Vibration and Acoustics* **133** (2011). DOI: 10.1115/1.4002120.

[41] J. J. Yu. 'On occurrence of reverse full annular rub'. *J. Eng. Gas Turbines Power* **134**(1) (2012). DOI: 10.1115/1.4004161.

[42] J. C. Wilkes and T. Allison. 'A general model for two-point contact dry-friction whip and whirl - further advancements and experimental test results'. *Proceedings of the Asme Turbo Expo: Turbine Technical Conference and Exposition* **7a** (2015).

[43] M. O. T. Cole and T. Wongratanaphisan. 'Synchronous whirl mode maps for rotor vibration with stator interaction across clearance annuli in multiple planes'. *Proceedings of the Institution of Mechanical Engineers Part C-Journal of Mechanical Engineering Science* **227**(C2) (2013), pp. 261–275. DOI: 10.1177/0954406212448342.

[44] M. O. T. Cole and L. Hawkins. 'Model-based analysis of friction-induced subsynchronous whirl for a rotor contacting with clearance bearings under axial load'. *Proceedings of the Asme Turbo Expo: Turbine Technical Conference and Exposition* **7a** (2015).

[45] M. O. T. Cole and L. Hawkins. 'Model-based analysis of friction-induced subsynchronous whirl for a rotor contacting with clearance bearings under axial load'. *Journal of Engineering for Gas Turbines and Power-transactions of the Asme* **138** (7 2016), p. 072507. DOI: 10.1115/1.4032343.

[46] G. Schweitzer and E. H. Maslen. *Magnetic Bearings. Theory, design, and application to rotating machinery*. Ed. by S.-V. B. Heidelberg. 1st ed. 2009. DOI: 10.1007/978-3-642-00497-1.

[47] G. Schweitzer. 'Stabilization of self-exited rotor vibration by an active damper'. *Dynamics of Rotors - IUTAM Symposium, Lyngby, Denmark* **7a** (1974).

[48] H. Ulbrich, G. Schweitzer and E. Bauser. 'A rotor supported without contact - theory and application'. *Proceedings of the Fifth World Congress on Theory of Machines and Mechanisms* (1979).

[49] J. C. Pradetto and J. Schmied. 'Behaviour of a one ton rotor being dropped into auxiliary bearings'. *Proceeding 3rd Int. Symp. Magn. Bear.* (1992), pp. 145–156.

[50] D. Bently. 'Statement on magnetic bearings'. *Orbit* **16**(1) (1995), p. 5.

[51] T. Ishii and R. G. Kirk. 'Transient response technique applied to active magnetic bearing machinery during rotor drop'. *Transactions of the ASME* **118**(April 1996) (1996).

[52] M. A. Fumagalli. 'Modelling and measurement analysis of the contact interaction between a high speed rotor and its stator'. Doctoral dissertation. ETH - Swiss Institute Of Technology Zurich, 1997.

[53] H. Hertz. 'Über die Berührung fester elastischer Körper'. *Journal für die reine und angewandte Mathematik* **92** (1881), pp. 156–171.

[54] K. H. Hunt and F. R. E. Crossley. 'Coefficient Of restitution interpreted as damping in vibroimpact.' *J Appl Mech Trans ASME* **42**(2) (1975), pp. 440–445. DOI: 10.1115/1.3423596.

[55] R. G. Kirk. 'Evaluation of AMB turbomachinery auxiliary bearings'. *Journal of Vibration and Acoustics* **121**(2) (1999), pp. 156–161.

[56] M. Aenis, E. Knopf and R. Nordmann. 'Active magnetic bearings for the identification and fault diagnosis in turbomachinery'. *IFAC Proceedings* **33**(26) (2000), pp. 1079–1084. DOI: 10.1016/S1474-6670(17)39290-X.

[57] P. S. Keogh and M. O. T. Cole. 'Rotor vibration with auxiliary bearing contact in magnetic bearing systems Part 1: synchronous dynamics'. *J. Mechanical Engineering Science* **217** (2003), pp. 377–392.

[58] P. S. Keogh and M. O. T. Cole. 'Rotor vibration with auxiliary bearing contact in magnetic bearing systems Part 2: robust synchronous control for rotor position recovery.' *J. Mechanical Engineering Science* **217** (2003), pp. 393–409.

[59] L. Hawkins, A. Filatov, S. Imani and D. Prosser. 'Test results and analytical predictions for rotor drop testing of an active magnetic bearing expander/generator'. *Journal of Engineering for Gas Turbines and Power* **129**(522-529) (2007). DOI: 10.1115/1.2436549.

[60] Y. Zhao, G. Yang, Z. Shi and L. Zhao. 'Thermal analysis and simulations of auxiliary bearings and its application in the high temperature reactor-10'. *Journal of Tribology* **138** (2016), p. 11. DOI: 10.1115/1.4031003.

[61] A. Kärkkäinen, J. Sopanen and A. Mikkola. 'Dynamic simulation of a flexible rotor during drop on retainer bearings'. *Journal of Sound and Vibration* **306** (3-5 2007), pp. 601–617.

[62] O. Halminen, A. Kärkkäinen, J. Sopanen and A. Mikkola. 'Active magnetic bearing-supported rotor with misaligned cageless backup bearings: A dropdown event simulation model'. *Mechanical Systems and Signal Processing* **50–51** (2015), pp. 692–705. DOI: https://doi.org/10.1016/j.ymssp.2014.06.001.

[63] G. Jacquet-Richardet, Torkhani, P. Cartraud, F. Thouverez, T. N. Baranger, M. Herran, C. Gibert, S. Baguet, P. Almeida and L. Peletan. 'Rotor to stator contacts in turbomachines. Review and application'. *Mechanical Systems and Signal Processing* **40**(2) (2013), pp. 401–420.

[64] P. Mcmullen, V. Vuong and L. Hawkins. 'Flywheel energy storage system with AMBand hybrid backup bearings'. *10th International Symposium on Magnetic Bearings, Martigny, Switzerland* (August 21-23, 2006). DOI: doi:10.1.1.459.4388..

[65] U. Simon. 'Rotor – Stator – Kontakt in polygonförmigen Fanglagern'. Doctoral dissertation. Von der Gemeinsamen Fakultät für Maschinenbau und Elektrotechnik der Technischen Universität Carolo Wilhelmina zu Braunschweig, 2001.

[66] L. Ginzinger, B. Heckmann and H. Ulbrich. 'Feedback control to prevent damage by rotor rubbing after an impact load'. *Proceedings of the Asme Turbo Expo, Proc. Asme Turbo Expo* **6** (2009), pp. 1003–1012. DOI: 10.1115/GT2009-60195.

[67] D. Zülow and R. Liebich. 'Ein Aussenrollenlager als Fanglagerkonzept für magnetgelagerte Rotoren'. *SIRM 8. Internationale Tagung Schwingungen in rotierenden Maschinen, Wien, Austria, paper-ID 11*. 2009.

[68] G. Schubert, H. Walter and D. Zülow. 'Safety bearing for retaining a rotor shaft of a machine'. Patent No: US 8786152 B2.

[69] P. S. Keogh. 'Contact dynamic phenomena in rotating machines: Active/passive considerations'. *Mech. Syst. Signal Process.* **29** (2012), pp. 19–33. DOI: 10.1016/j.ymssp.2011.06.024.

[70] O. Halminen, J. F. Aceituno, J. L. Escalona, J. Sopanen and A. Mikkola. 'A touchdown bearing with surface waviness: Friction loss analysis'. *Mechanism and Machine Theory* **110** (2017), pp. 73–84. DOI: 10.1016/j.mechmachtheory.2017.01.002.

[71] S. Lahriri, I. F. Santos, H. I. Weber and H. Hartmann. 'On the nonlinear dynamics of two types of backup bearings — theoretical and experimental aspects'. *J. Eng. Gas Turbines Power* **134**(11) (2012), pp. 805–818. DOI: 10.1115/1.4007166.

[72] S. Lahriri and I. F. Santos. 'Experimental quantification of dynamic forces and shaft motion in two different types of backup bearings under several contact conditions'. *Mechanical Systems and Signal Processing* **40**(1) (2013), pp. 301–312. DOI: 10.1016/j.ymssp.2013.05.013.

[73] S. Lahriri and I. F. Santos. 'Experimental quantification of contact forces with impact, friction and uncertainty analysis'. *Tribology International* **66** (2013), pp. 93–104. DOI: 10.1016/j.triboint.2013.04.016.

[74] S. Lahriri and I. F. Santos. 'Theoretical modelling, analysis and validation of the shaft motion and dynamic forces during rotor–stator contact'. *Journal of Sound and Vibration* **332**(24) (2013), pp. 6359–6376. DOI: 10.1016/j.jsv.2013.07.008.

[75] C. A. Fonseca, H. Weber, P. Fleischer and I. Santos. 'Analyzing the use of pins in safety bearings'. *J. Braz. Soc. Mech. Sci. Eng.* **37** (2015), pp. 1425–1434.

[76] C. A. Fonseca, R. R. Aguiar and H. I. Weber. 'On the non-linear behaviour and orbit patterns of rotor/stator contact with a non-conventional containment bearing'. *Int. J. of Mech. Sciences* **105** (2016), pp. 117–125. DOI: 10.1016/j.ijmecsci.2015.10.015.

[77] N. P. P. Petersen. 'Rotor drop rig – design & simulation'. Master Thesis. Department of Mechanical Engineering, Technical University of Denmark, 2011.

Conference paper C1

Influence of Unbalance Levels on Nonlinear Dynamics of a Rotor-Backup Rolling Bearing System

This paper was presented at the conference 15^{th} ISMB in 3-6 July, 2016 in Kitakyushu, Japan

ISMB15

Influence of Unbalance Levels on Nonlinear Dynamics of a Rotor-Backup Rolling Bearing System

Cesar FONSECA*, Ilmar SANTOS* and Hans WEBER**
* Dept. of Mechanical Engineering, DTU
Niels Koeppel Allé, 404, 2800, Lyngby, Denmark
E-mail: cefonse@dtu.mek.dk
** Dept. of Mechanical Eng., PUC-Rio
Rua Marquês de de São Vicente, 225, 22451-900, Rio de Janeiro, Brazil

Abstract
Rotor drops in magnetic bearing and unbalance in rotors have been objective of study for many years. The combination of these two well-known phenomena led to an interesting chaotic response, when the rotor touches the inner race of the back-up bearing. The present work explores the nonlinear rotor-backup-bearing dynamics both theoretically and experimentally using a fully instrumented test rig, where the position of shaft, its angular velocity and the contact forces between the shaft and the backup bearing are sampled at 25 kHz. The test rig is built by a removable passive magnetic bearing, which allows for simulation of magnetic bearing failure (loose of carrying capacity and rotor fall). A theoretical approach is given beforehand and supplies the basis of the study. Finally the presented results are commented on the point of view of nonlinear dynamics applied to the practical use. The theoretical and numerical analyzes are shown through Poincaré maps and double sided spectrum. The latter is important to characterize the condition at different levels of unbalance between forward of backwards whirl. Our preliminary results indicate that for small levels of unbalance the rotor oscillates at the bottom of the backup bearing. When the levels of unbalance increase, the dynamical behaviour of the rotor changes, leading to extremely harmful conditions, since the rotor can be lifted from the bottom of the bearing (contact state) and return, starting to impact on the backup inner race innumerable times without reaching a steady state.

Key words : Safety bearings, impact, friction, contact mechanics, nonlinear dynamics, magnetic bearing.

1. Introduction

The possibility to use magnetic bearing rotor in industrial applications cannot be thought correctly without the use of proper back-up bearings. Applications are many such as reaction wheels, centrifuges, energy efficiency machines, (Gasch et al., 2002), (Schweitzer and Maslen, 2009), and among others. For all these machines, a safety element has to be installed to prevent failures such as, power loss, that would cause the shaft to fall. The safety element consists normally of a rolling bearing with inner race diameter bigger than the shaft diameter, but smaller than the one at the magnetic bearing. It is designed to withstand the loads and impacts of a rotor. It also protects the whole system and prevents even more disastrous situations.

Throughout the years, several works have been published on this subject. (Muszynska, 1989) has given a good overview of the state of rotordynamics research of rub-related phenomena. In the work of (Johnson, 1962) a vertical shaft with clearance with impacts was studied . (Black, 1968) published a work of a two-degree-of-freedom rotor and stator, which is highly cited through the years. While in (Wojciech, M. S., 1986), a gyro pendulum with a piecewise linear model was investigated with a good agreement with experimental results. (Zhang, 1988) showed a multi-degree model rotor at a full annular rub using Black's model. (Choy and Padovan, 1987) showed also the interaction between the rotor and the casing on a bearing wall. By employing a proper impact model, chaos was reported by (Goldman and Muszynska, 1994). (Piccoli and Weber, 1998) investigated an application to identify chaotic motion with Lyapunov exponents and Poincaré Diagrams. In (Jiang and Ulbrich, 2005), dry friction whip investigated with an unbalanced rotor to stator contact. One of the most cited is the work from (Pradetto and Schmied, 1992), where a one-ton rotor drop is analyzed. (Fumagalli, 1997) tested the performance of a rotor sliding and tumbling while touching the auxiliary bearing.

In combination with Active Magnetic Bearings (AMB) technology, (Schweitzer, 1975), it is clear that safety bearings

are an important subject of study. (Kirk, 1996) analyzed numerically the transient response of a rotor drop. (Ginzinger et al., 2009) developed an active actuator to avoid severity of the contact. Moreover, in (Keogh, 2012), a comprehensive study of different performance on auxiliary bearings was presented. Non-conventional geometries of the back-up bearing were considered by (Simon, 2001), and later by (Zülow and Liebich, 2009) and then the new kind of bearing with pins is presented by (Lahriri and Santos, 2012) and analyzes the forces that the structure receives, where the backup is. In (Fonseca et al., 2015) it is shown that the same pins help to surpass the critical speed avoiding the backwards whirl. However, in most industrial operating machines, the safety bearing is a common rolling bearing element, and the rotor will lay down at the bottom allowing it to rotate without much damage to the system. An analysis of the rigid rotor on a safety bearing showing chaotic behavior is shown by (Wang and Noah, 1998). Later the contact between the shaft and the inner race was modeled using a finite element and was presented by (Cole et al., 2001). More recently, (Inayat-Hussain, 2010) gives an insight about the response of the rotors to different parameters with the bifurcation diagrams.

In this work, a theoretical and an experimental study of a passive magnetic bearing rotor colliding on the ball bearing inner race is presented. The failure of the rotor will be induced by the rapid removal of the passive magnetic bearing letting the rotor to fall. The tests will be compared with simulated results coming from a model of the rotor as a rigid body impacting on an compliant surface. The main contribution of this work is to show that different levels of unbalance change the dynamical behavior of the system and may lead to harmful situations, for which the backup bearing is not designed.

2. Modeling the rotor-housing kinematics

2.1. The shaft

In Figure 1a and b, the mathematical model of the rotor is built to reproduce the assembled test rig. The rotor is supported by one spherical ball bearing at point 0 and one movable passive magnetic bearing at point C. The back-up bearing is mounted between them at point B. The rotor is modeled as a rigid body and external forces from the magnets, imbalance and coupling are applied at points C, A and D respectively. The rotor is only allowed to rotate according to the following three angular degrees of freedom: $\Gamma(t)$, $\beta(t)$, $\theta(t)$ and the angular velocities:

$$ {}_I\dot{\Gamma} = \begin{bmatrix} \dot{\Gamma}(t) & 0 & 0 \end{bmatrix}^T, \quad {}_{B1}\dot{\beta} = \begin{bmatrix} 0 & \dot{\beta}(t) & 0 \end{bmatrix}^T \text{ and } \quad {}_{B2}\dot{\theta} = \begin{bmatrix} 0 & 0 & \dot{\theta}(t) \end{bmatrix}^T . \tag{1} $$

In figure 1a it is possible to see the reference frames used and the moving reference frame, $B3$, fixed to the rotating shaft and positioned at the supporting point of the rotor.

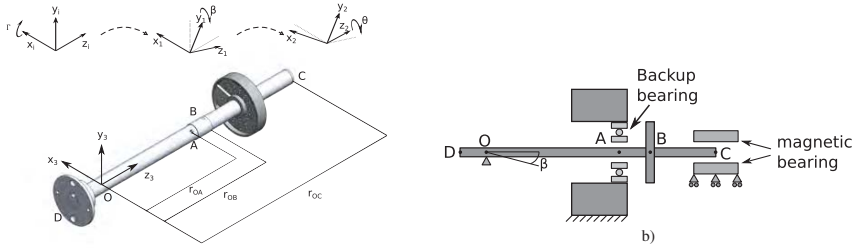

Fig. 1 The moving frame references and the points of interests, A, B and C, where forces are present.

$$ {}_I T_\Gamma = \begin{bmatrix} 1 & 0 & 0 \\ 0 & \cos\Gamma(t) & \sin\Gamma(t) \\ 0 & -\sin\Gamma(t) & \cos\Gamma(t) \end{bmatrix}, \quad {}_{B1}T_\beta = \begin{bmatrix} \cos\beta(t) & 0 & -\sin\beta(t) \\ 0 & 1 & 0 \\ \sin\beta(t) & 0 & \cos\beta(t) \end{bmatrix}, \quad {}_{B2}T_\theta = \begin{bmatrix} \cos\theta(t) & \sin\theta(t) & 0 \\ -\sin\theta(t) & \cos\theta(t) & 0 \\ 0 & 0 & 1 \end{bmatrix}. \tag{2} $$

Each external force will generate a moment with respect to O and the relevant position vector are given by:

$$ {}_{B3}r_{OA} = \begin{bmatrix} r_{OA,x} & 0 & r_{OA,z} \end{bmatrix}^T, \quad {}_{B3}r_{OB} = \begin{bmatrix} r_{OB,x} & r_{OB,y} & r_{OB,z} \end{bmatrix}^T \quad \text{and} \quad {}_{B3}r_{OC} = \begin{bmatrix} 0 & 0 & r_{OC,z} \end{bmatrix}^T . \tag{3} $$

ISMB15

The inertia tensor referred to the supporting point is:

$$ {}_{B3}I_O = \begin{bmatrix} I_{xx} & 0 & -I_{xz} \\ 0 & I_{yy} & 0 \\ -I_{zx} & 0 & I_{zz} \end{bmatrix}. \tag{4} $$

where $I_{xz} = m_u r_u l_{OD}$. The absolute angular velocity of the represented at the moving reference frame B3 (where the inertia tensor is constant) is given by:

$$ \omega_{B3} = {}_{B3}\dot{\Gamma} + {}_{B3}\dot{\beta} + {}_{B3}\dot{\theta} = \begin{bmatrix} \cos(\theta)\cos(\beta)\dot{\Gamma} + \sin(\theta)\dot{\beta} \\ -\sin(\theta)\cos(\beta)\dot{\Gamma} + \cos(\theta)\dot{\beta} \\ \sin(\beta)\dot{\Gamma} + \dot{\theta} \end{bmatrix}. \tag{5} $$

The absolute acceleration is given by:

$$ \dot{\omega}_{B3} = \begin{bmatrix} -\dot{\theta}\sin(\theta)\cos(\beta)\dot{\Gamma} - \cos(\theta)\dot{\beta}\sin(\beta)\dot{\Gamma} + \cos(\theta)\cos(\beta)\ddot{\Gamma} + \dot{\theta}\cos(\theta)\dot{\beta} + \sin(\theta)\ddot{\beta} \\ -\dot{\theta}\cos(\theta)\cos(\beta)\dot{\Gamma} + \sin(\theta)\dot{\beta}\sin(\beta)\dot{\Gamma} - \sin(\theta)\cos(\beta)\ddot{\Gamma} - \dot{\theta}\sin(\theta)\dot{\beta} + \cos(\theta)\ddot{\beta} \\ \dot{\beta}\cos(\beta)\dot{\Gamma} + \sin(\beta)\ddot{\Gamma} + \ddot{\theta} \end{bmatrix}. \tag{6} $$

2.2. The inner and outer housing

In order to determine and acquire the force between the rotor shaft and the inner race, the back-up bearing is mounted on an special casing, where there are four force transducers. The elastic elements k_{ft} represent the force transducers positioned between the bodies and the damping elements, c_h and c_v are structural damping. These damping terms are present due to the four beams that hold the inner house to slide vertically and the outer house horizontally, two for each directions. The back-up bearing is inside a block that is mounted inside a frame, called outer house. Then, the inner house is only allowed to move horizontally inside it. Subsequently, the outer house moves only vertically. Figure 2a and Figure 2b show a schematic of the complete assembly.

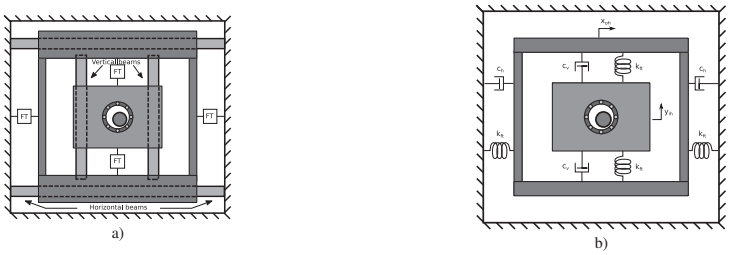

Fig. 2 Assembly of the inner housing and the outer housing.

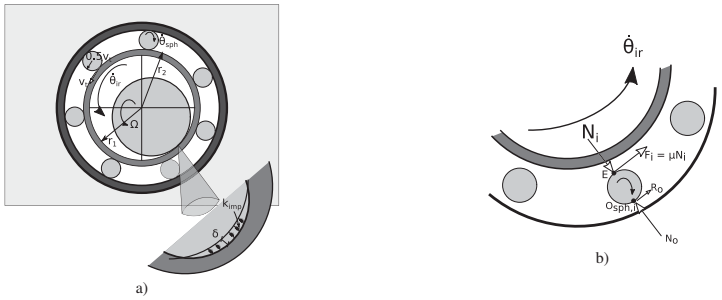

Fig. 3 Left: The shaft inside the inner bearing. Right: The forces acting at each ball of the back-up bearing.

The dynamics of both housings are included in the mechanical model. The dynamic coupling between the inner house and the rotor is introduced by the impact forces, N and the friction force F_{fric}. The beams that support the housings have the stiffness calculated as clamped-clampled beam $K_{beam} = \frac{48EI}{Fa^2(3l-4a)}$. and the damping coefficients approximated by:

$$c_h = 2\zeta\sqrt{K_{beam}\,(m_{ih}+m_{oh})} \quad \text{and} \quad \mathrm{c_v} = 2\zeta\sqrt{K_{beam}\,(m_{ih})}. \tag{7}$$

Thus the governing equations of both housings are written in Equations (8) and (9)

$$m_{ih}\ddot{y}_{ih} = -2k_{ft}y_{ih} - 2c_v y_{ih} - m_{ih}g + N\sin\alpha + F_{fric}\cos\alpha. \tag{8}$$

$$(M_{oh}+m_{ih})\,\ddot{x}_{oh} = -2k_{ft}x_{oh} - 2c_h x_{oh} + N\cos\alpha - F_{fric}\sin\alpha. \tag{9}$$

Consequently, the radial term r_r can be calculated and allows one to know whether the system is impacting or not, and it is equal to:

$$r_r = \sqrt{(\beta l_{OB} - x_{oh})^2 + (-\Gamma l_{OB}) - y_{ih})^2}. \tag{10}$$

The impact is analysed at each time step if the rotor displacement at the position of the back-up bearing is bigger or equal than the radial gap, $\delta \geq r_0 = r_1 - r_r$. The impact is modeled following a stepwise elastic model proposed by (Lankarani and Nikravesh, 1990):

$$F_{imp} = N = k_{imp}\delta^{3/2}\left(1 + \frac{3(1-e^2)}{4}\frac{\dot{\delta}}{\dot{\delta}^-}\right), \quad \text{if} \quad \delta \geq 0, \tag{11}$$

in which the stiffness coefficient is given as:

$$k_{imp} = \frac{4}{3\left(\frac{1-\nu_s^2}{E_s} + \frac{1-\nu_i^2}{E_i}\right)}\left(\frac{r_s r_1}{r_1 - r_s}\right)^{1/2}. \tag{12}$$

Therefore, the forces acting on the mechanical model are the rotor's own weight, the magnetic force and the damping force plus the impact forces

$${}_I\mathbf{F}_g = \begin{bmatrix} 0 \\ -mg \\ 0 \end{bmatrix},\ {}_I\mathbf{F}_{mag} = \begin{bmatrix} -K\cos\alpha \\ -K\sin\alpha \\ 0 \end{bmatrix},\ {}_I\mathbf{F}_{damp} = \begin{bmatrix} -c\cos\rho \\ -c\sin\rho \\ 0 \end{bmatrix},\ {}_I\mathbf{F}_{imp} = \begin{bmatrix} N\cos\alpha \\ N\sin\alpha \\ 0 \end{bmatrix} \text{ and } {}_I\mathbf{F}_{fric} = \begin{bmatrix} F_{fric}\sin\alpha \\ F_{imp}\cos\alpha \\ 0 \end{bmatrix}. \tag{13}$$

Finally one writes Euler's equation with respect to the supporting point O

$$\sum{}_{B3}\text{Force Moments}_O = {}_{B3}\,I_O\left(\frac{\mathrm{d}}{\mathrm{dt}}\omega_{B3}\right) + {}_{B3}\,\omega \times ({}_{B3}I_O \cdot_{B3}\,\omega) \tag{14}$$

and solves the set of equation considering the angles Γ and β small. The motor has an independent control and is capable to deliver the necessary torque to keep the angular velocity to $\dot{\theta}$. The differential equations are highly nonlinear with many coupled terms and the solution is found using the symbolic program Maple®. However, we are more interested in the position of the center of shaft at the backup bearing plane and using the transformation matrices, the coordinates are written as:

$$\begin{bmatrix} X \\ Y \\ Z \end{bmatrix} = \left({}_I T_\Gamma^T(t) \cdot_{B1} T_\beta^T(t) - {}_I T_\Gamma^T(0) \cdot_{B1} T_\beta^T(0)\right) \cdot_{B2} r_{OC}, \tag{15}$$

where the initial conditions are taken into consideration, $t = 0$, $\Gamma(0) = 0$ and $\beta(0) = 0$.

2.3. The back-up bearing

When the rotor falls and hits the rolling back-up bearing, Figure 3, the friction force accelerates the inner race and the spheres.The angular position of the inner race, θ_{Ir}, is also a degree of freedom. Figure 3a illustrates a schematic view of balls and inner race and their velocities. Since the outer race is not moving and the spheres are not sliding on the touching point with it, point O_{sph}, the tangential velocity is half of the one on the edge between the sphere and the inner

race, point E. The force acting on one rolling bearing ball is shown in Figure 3b the following equations for one isolated ball are written in (16)-(18):

$$\sum \text{Moment}_{O_{sph}} = I_{sph}\ddot{\theta}_{sph} \tag{16}$$

$$2r_{sph}F_i = I_{sph}\ddot{\theta}_{sph}, \quad \text{since, } v_t = \dot{\theta}_{ir}r_2 = \dot{\theta}_{sph}r_{sph}, \tag{17}$$

$$2r_{sph}F_i = I_{sph}\ddot{\theta}_{ir}\frac{r_2}{r_{sph}}, \tag{18}$$

where $I_{sph} = 2/5\left(\pi r_{sph}^2\right) + m_{sph}r_{sph}^2$. Newton equation for the tangential direction leads to:

$$F_i + R_o = m_{sph}a_t. \quad \text{From (17) and (18), } R_o + I_{sph}\ddot{\theta}_{ir}\frac{r_2}{2\left(r_{sph}\right)^2} = m_{sph}\ddot{\theta}_{ir}r_2. \tag{19}$$

Therefore the angular acceleration of the inner race, $\ddot{\theta}_{ir}$ can be obtained taking into account the influence of all rolling spheres j.

$$\ddot{\theta}_{ir}I_{ir} = fr_1 - r_2\sum_{j=1}^{N_{sph}}\left(F_{i,j}\right), \tag{20}$$

$$\ddot{\theta}_{ir}I_{ir} = fr_1 - r_2N_{sph}\left(\ddot{\theta}_{ir}\frac{I_{sph}r_2}{2\left(r_{sph}\right)^2}\right) \rightarrow \ddot{\theta}_{ir}\left(I_{ir} + N_{sph}\frac{I_{sph}}{2}\left(\frac{r_2}{r_{sph}}\right)^2\right) = fr_1. \tag{21}$$

3. Simulation and nonlinear analysis

3.1. Integration in time

The governing equations (14), (20), (8), and (9) are integrated in time using a combined Matlab differential equation solver *ode45* and a dedicated Runge-Kutta algorithm. The former is employed together with an *Event* function in order to find the exact moment of the impact. The latter is applied during the short period of impact. It was done so, because it is a highly stiff problem and demands an enormous time with very tight integration tolerances of the algorithm. Therefore a test of convergence was performed and the adequate step time was set to 10^{-6} s. During the impact the relative velocity between the shaft and the inner race, v_{rel}, plays an important role. The friction force is dependent on it. If the velocities match, there is no friction. Otherwise, the friction force is modeled as $F = \mu N\text{sign}\left(v_{rel}\right)$. The model parameters are shown in table 1.

Table 1 Parameters set applied to the simulation.

Parameter of the shaft	
Mass without unbalance	$m = 1.28$ kg
Length to magnetic bearing	$r_{OC} = [0,\ 0,\ 0.384\text{m}]$
Length to rolling bearing	$r_{OB} = [r_r\cos(\alpha),\ r_r\sin(\alpha),\ 0.211\text{m}]$
Shaft diameter	$d_r = 25$ mm
Parameter of the rolling bearing	
Inner diameter	$d_1 = 2r_1 = 28$ mm
Inner race outer diameter	$d_2 = 2r_2 = 37$ mm
Sphere radius	$r_{sph} = 5.0$ mm
Impact stiffness	$k_n = 2.5 \cdot 10^{10}$ N/m$^{3/2}$
Friction coefficient	$\mu = 0.20$
Restituition coefficient	$e = 0.90$
Parameter of the inner and outer house	
Mass from inner house	$m_{ih} = 1.70$ kg
Damping 1	$c_h = 7.04 \cdot 10^2$ Ns/m
Mass from outer housing	$M_{oh} = 8.87$ kg
Damping	$c_v = 2.28 \cdot 10^2$ Ns/m

3.2. Simulated results and experimental comparison.

As mentioned before, the test rig is a rotor suspended at one end by a removable passive bearing. From the moment that the magnetic force is removed, there are three distinct stages: a) the rotor free fall inside the bearing; b) contact

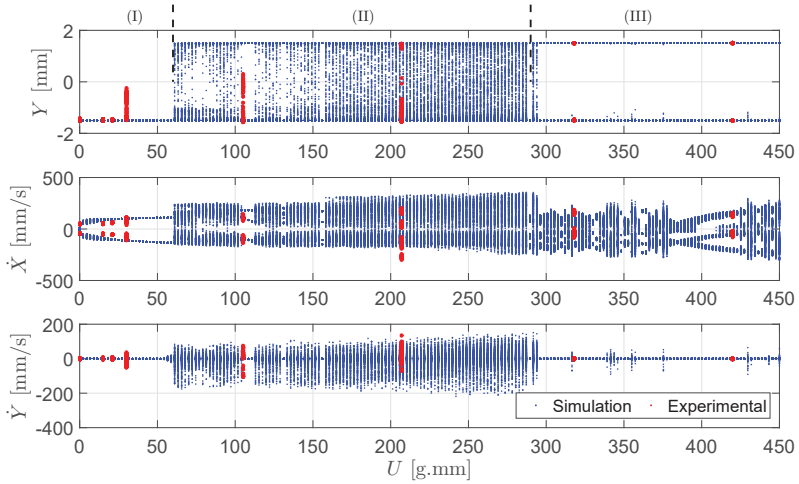

Fig. 4 10 Hz simulated bifurcation for different unbalance levels together with 8 different experimental tests with unbalance levels of: U_1 = 0.0 g.mm, U_2 = 15 g.mm, U_3 = 21 g.mm, U_4 = 30 g.mm, U_5 = 105 g.mm, U_6 = 207 g.mm, U_7 = 318 g.mm and U_8 = 420 g.mm.

between rotor and inner ring surfaces occurs leading to the deformation of the compliant and surface and angular acceleration of the inner race; and finally c) the relative velocities between the inner race and shaft surfaces almost vanish and the rotor fins a steady state condition at the bottom of the backup bearing. In fact, since the rotor keeps executing small translational movement around the equilibrium and rarely the relative velocity will coincide.Though this steady-state general dynamic behavior of the rotor changes significantly according to the unbalance level. After removing the magnetic force, the rotor falls and impacts several times on the surface of the inner race. The energy will be dissipated by the damping from the coupling between the inner and outer housing and from the impact with the compliant surface.

The changes in the steady-state behavior can be evaluated more explicitly with a Poincaré Map, Figure 4. The variables Y, $\dot{X}$ and $\dot{Y}$ are sampled every time the center of the shaft crosses the vertical line, in other words, when $X = 0$. The first plot on the top of Figure 4 shows the vertical position, Y, through which the rotor crosses the vertical line as a function of the control variable i.e. the unbalance, U.

Overall the phenomena are captured by both experiments and simulation. We can divide the bifurcation diagram into three specific regions. First the rotor center is always crossing at the bottom of the shaft at $Y = -1.5$ mm in region (I). Suddenly there is a change and more crossings at the vertical line occur. This can be seen in the region (II) of figure 4. The more unbalance the more evident that the center of the shaft performs chaotic trajectories. In the simulation it is expected to see the rotor crossing from the bottom to the top of the bearing, but the mechanical set up shows a gradual increase in the vertical crossing as the unbalance gets bigger until the rotor is able to perform a full whirl. In the right end of the plot, region III, the rotor is only executing a full whirl so the rotor is crossing the vertical line in the extremes, $Y = -1.5$ to $Y = 1.5$ mm. In the following plots, the horizontal and the vertical crossing velocity, $\dot{X}$ and $\dot{Y}$, are plotted against the unbalance and, once again, the experimental and the simulation tend to agree to each other.

To visualize the existence of chaotic trajectories performed by the rotor center, a double-sided spectrum is displayed in Figure 5a and b. Two levels of unblance are chosen: $U = 207$ g.mm from region (II) and $U = 420$ g.mm from region (III). The noise is significantly raised and several other peaks appear. This is a clear indication that chaos is happening. Higher unbalance levels show clearly higher peaks at $\Omega = -10.0$ Hz than its opposite pair, confirming the predominance of a full whirl at the same directions of the rotor spinning. Negative values of ω means the same spinning direction of the rotor.

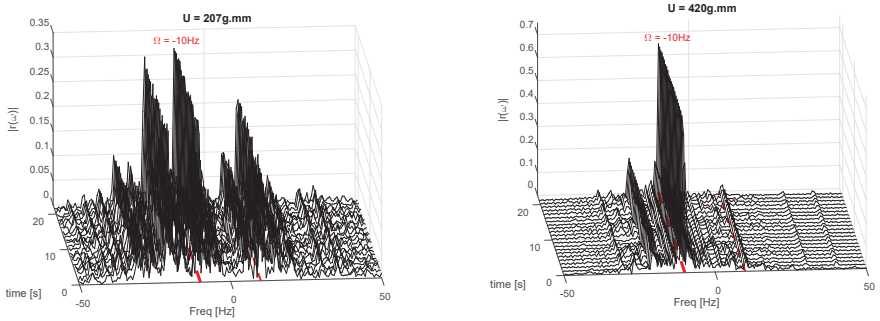

Fig. 5 Experimental 10 Hz double sided spectrum of the radial displacement, the unbalance corresponding to 0.27 kg.mm a) belongs to region II. For the unbalance corresponding to 0.42kg.mm b) A clear dominance of one peak at $\Omega = -10$ Hz indicates the full whirl in the same direction the shaft rotates stays in the region III.

4. Conclusion and Future Aspects

From the theoretical and experimental nonlinear analysis carried out in the paper, one can conclude that the rotor -backup bearing system has three distinguished dynamical behaviors depended on the level of rotor unbalance. Zone (I), characterized by low unbalance level from (0, 60] g.mm, simple oscillatory movementes of the rotor center at the bottom of the backup bearing are see. Zone (II) by unbalance levels from (60 to 280] g.mm, chaotic motions followed by impacts between rotor and backup inner race surface. Finally, zone (III) characterized by high unbalance levels, full forward whirl of the rotor center takes place.

There is much more to explore in this problem. The magnitude of the forces at the three different zones changes and supports the idea that it may damage the backup bearing. The relationship between the radii of the rotor and the inner race may also affect the magnitude of the forces and should be investigated in the next future. Different material properties and angular velocities shall contribute a lot to the response of the system and further results shall point in that direction.

5. Acknowledgement

The authors express their acknowledgement to CNPq through the Science Without Borders Program with the process number: 249728/2013-3, which sponsored the elaboration of this paper.

References

H. F. Black. Interaction of a whirling rotor with a vibrating stator across a clearance annulus. *Arch. J. Mech. Eng. Sci. 1959-1982 (vols 1-23)*, 10(1):1–12, 1968. ISSN 0022-2542. doi: 10.1243/JMES_JOUR_1968_010_003_02.

F. K. Choy and J. Padovan. Non-linear transient analysis of rotor-casing rub events. *Journal of Sound and Vibration*, 113: 529–545, 1987.

M. T. Cole, P. S. Keogh, and C. R. Burrows. The dynamic behavior of a rolling element auxiliary bearing following rotor impact. *ASME. J. Tribol.*, 2(124):406–413, 2001.

C. A. L. L. Fonseca, H.I. Weber, P.F. Fleischer, and I.F. Santos. Analyzing the use of pins in safety bearings. *J. Braz. Soc. Mech. Sci. Eng.*, 37:1425–1434, 2015.

M. A. Fumagalli. *Modelling and measurement analysis of the contact interaction between a high speed rotor and its stator*. PhD thesis, ETH - Swiss Institute Of Technology Zurich, 1997.

ISMB15

R. Gasch, R. Nordmann, and H. Pfützner. *Rotordynamik*. Springer Verlag, Berlin, 2nd ed., edition, 2002.

L. Ginzinger, B. Heckmann, and H. Ulbrich. Feedback control to prevent damage by rotor rubbing after an impact load. *Proceedings of the Asme Turbo Expo, Proc. Asme Turbo Expo*, 6:1003–1012, 2009. doi: 10.1115/GT2009-60195.

P. Goldman and A. Muszynska. Chaotic Behavior of Rotor/Stator Systems With Rubs. *J. Eng. Gas Turbines Power*, 116 (3):692, 1994.

J. I. Inayat-Hussain. Nonlinear dynamics of a magnetically supported rigid rotor in auxiliary bearings. *Mechanism and Machine Theory*, 45(11):1651–1667, 2010.

J. Jiang and H. Ulbrich. The Physical Reason and the Analytical Condition for the Onset of Dry Whip in Rotor-to-Stator Contact Systems. *J. Vib. Acoust.*, 127(6):594, 2005. ISSN 07393717. doi: 10.1115/1.1888592.

D. C. Johnson. Synchronous whirl of a vertical shaft having clearance in one bearing. *Arch. J. Mech. Eng. Sci. 1959-1982 (vols 1-23)*, 4(1):85–93, 1962. ISSN 0022-2542. doi: 10.1243/JMES_JOUR_1962_004_012_02.

P. S. Keogh. Contact dynamic phenomena in rotating machines: Active/passive considerations. *Mech. Syst. Signal Process.*, 29:19–33, may 2012. ISSN 08883270. doi: 10.1016/j.ymssp.2011.06.024.

R. G. Kirk. Transient Response Technique Applied to Active Magnetic Bearing Machinery During Rotor Drop. *Transactions of the ASME*, 118(April 1996), 1996.

S. Lahriri and I. F. Santos. Experimental quantification of dynamic forces and shaft motion in two different types of backup bearings under several contact conditions. *Journal Mechanical Systems and Signal Processing*, 2012.

H. M. Lankarani and P. E. Nikravesh. A Contact Force Model With Hysteresis Damping for Impact Analysis of Multibody Systems. *J. Mech. Des.*, 112(3):369, 1990.

A. Muszynska. Rotor-to-stationary element rub-related vibration phenomena in rotating machinery - literature survey. *Shock and Vibration Digest*, 21(3):3–11, 1989. ISSN 05831024, 17413184.

H. C. Piccoli and H. I. Weber. Experimental observation of chaotic motion in a rotor with rubbing. *Nonlinear Dyn.*, 16 (1):55–70, 1998.

J. C. Pradetto and J. Schmied. Behaviour of a one ton rotor being dropped into auxiliary bearings. In *Proceeding 3rd Int. Symp. Magn. Bear.*, pages 145–156, 1992.

G. Schweitzer. Stabilization of self-excited rotor vibrations by an active damper. *Dynamics of rotors*, pages 472–493, 1975.

G. Schweitzer and E. H. Maslen. *Magnetic Bearings*. Springer-Verlag Berlin Heidelberg, 1 edition, 2009.

U. Simon. *Rotor Stator Kontakt in polygonförmigen Fanglagern*. PhD thesis, Technischen Universität CaroloWilhelmina zu Braunschweig, 2001.

X. X. Wang and S. S. Noah. Nonlinear dynamics of a magnetically supported rotor on safety auxiliary bearings. *ASME. J. Vib. Acoust.*, 2(120):596–606, 1998.

Wojciech, M. S. *Dynamisches Verhalten eines schnell drehenden Rotors bei Anstreifvorgangen*. PhD thesis, TU Karlsruhe, 1986.

W Zhang. Dynamic instability of multi-degree-of-freedom flexible rotor systems due to full annular rub. *IMechE C252/88*, pages 305–308, 1988.

D. Zülow and R. Liebich. Ein aussenrollenlager als fanglagerkonzept für magnetgelagerte rotoren. In *SIRM 8. Internationale Tagung Schwingungen in rotierenden Maschinen, Wien, Austria, paper-ID 11*, 2009.

DTU Mechanical Engineering
Section of Solid Mechanics
Technical University of Denmark

Nils Koppels Allé, Bld. 404
DK-2800 Kgs. Lyngby
Denmark
Phone (+45) 4525 4250
Fax (+45) 4593 1475
www.mek.dtu.dk
ISBN: 978-87-7475-500-5

DCAMM
Danish Center for Applied Mathematics and Mechanics

Nils Koppels Allé, Bld. 404
DK-2800 Kgs. Lyngby
Denmark
Phone (+45) 4525 4250
Fax (+45) 4593 1475
www.dcamm.dk
ISSN: 0903-1685